


12-2010

## **AGROBACTERIUM VIRB10 CONTRIBUTIONS TO TYPE IV SUBSTRATE SECRETION, T-PILUS BIOGENESIS, AND OUTER MEMBRANE PORE FORMATION**

Isaac Garza

Follow this and additional works at: [https://digitalcommons.library.tmc.edu/utgsbs\\_dissertations](https://digitalcommons.library.tmc.edu/utgsbs_dissertations)

 Part of the [Biochemistry, Biophysics, and Structural Biology Commons](#), [Microbiology Commons](#), and the [Molecular Genetics Commons](#)

### **Recommended Citation**

Garza, Isaac, "AGROBACTERIUM VIRB10 CONTRIBUTIONS TO TYPE IV SUBSTRATE SECRETION, T-PILUS BIOGENESIS, AND OUTER MEMBRANE PORE FORMATION" (2010). *The University of Texas MD Anderson Cancer Center UTHealth Graduate School of Biomedical Sciences Dissertations and Theses (Open Access)*. 99.

[https://digitalcommons.library.tmc.edu/utgsbs\\_dissertations/99](https://digitalcommons.library.tmc.edu/utgsbs_dissertations/99)

This Thesis (MS) is brought to you for free and open access by the The University of Texas MD Anderson Cancer Center UTHealth Graduate School of Biomedical Sciences at DigitalCommons@TMC. It has been accepted for inclusion in The University of Texas MD Anderson Cancer Center UTHealth Graduate School of Biomedical Sciences Dissertations and Theses (Open Access) by an authorized administrator of DigitalCommons@TMC. For more information, please contact [digitalcommons@library.tmc.edu](mailto:digitalcommons@library.tmc.edu).

**AGROBACTERIUM VIRB10 CONTRIBUTIONS TO TYPE IV SUBSTRATE SECRETION,  
T-PILUS BIOGENESIS, AND OUTER MEMBRANE PORE FORMATION**

by

**Isaac Garza, B.S.**

**APPROVED:**

---

**Peter J. Christie, Ph.D., Supervisory Professor**

---

**William Margolin, Ph.D.**

---

**Ambro van Hoof, Ph.D.**

---

**Renhao Li, Ph.D.**

---

**Hung Ton-That, Ph.D.**

**APPROVED:**

---

**George M. Stancel, Ph.D. Dean, The University of Texas  
Graduate School of Biomedical Sciences at Houston**

***AGROBACTERIUM* VIRB10 CONTRIBUTIONS TO TYPE IV SUBSTRATE SECRETION,  
T-PILUS BIOGENESIS, AND OUTER MEMBRANE PORE FORMATION**

**A  
Thesis**

Presented to the Faculty of  
The University of Texas Health Science Center at Houston and  
the University of Texas M.D. Anderson Cancer Center  
Graduate School of Biomedical Sciences  
In Partial Fulfillment of the Requirements  
For the Degree of

**MASTER OF SCIENCE**

by

**Isaac Garza, B.S.**

Houston, Texas  
December 2010

## **Acknowledgements**

The completion of these studies is largely due to the patience, encouragement, and mentoring of Dr. Peter J. Christie. I also express gratitude to the members of the Christie laboratory whom provided one-on-one guidance and training. I am also grateful to the members of my supervisory committee for providing expert advice and useful suggestions.

I am appreciative of the Microbiology and Molecular Genetics (MMG) department for creating an environment that promotes development of critical thinking and research related skills. Further, I am grateful to the Graduate School of Biomedical Sciences (GSBS) and the University of Texas Health Science Center (UTHSC) for providing me the opportunity to study in a leading research institution with access to state-of-the art facilities and resources.

Overall I express gratitude to my parents and loved ones who provided financial and emotional support.

# **AGROBACTERIUM VIRB10 CONTRIBUTIONS TO TYPE IV SUBSTRATE SECRETION, T-PILUS BIOGENESIS, AND OUTER MEMBRANE PORE FORMATION**

Publication No. \_\_\_\_\_

Isaac Garza

Supervisory Professor: Peter J. Christie, Ph.D.

The VirB/D4 type IV secretion system (T4SS) of *Agrobacterium tumefaciens* functions to transfer substrates to infected plant cells through assembly of a translocation channel and a surface structure termed a T-pilus. This thesis is focused on identifying contributions of VirB10 to substrate transfer and T-pilus formation through a mutational analysis. VirB10 is a bitopic protein with several domains, including a: (i) cytoplasmic N-terminus, (ii) single transmembrane (TM)  $\alpha$ -helix, (iii) proline-rich region (PRR), and (iv) large C-terminal modified  $\beta$ -barrel. I introduced cysteine insertion and substitution mutations throughout the length of VirB10 in order to: (i) test a predicted transmembrane topology, (ii) identify residues/domains contributing to VirB10 stability, oligomerization, and function, and (iii) monitor structural changes accompanying energy activation or substrate translocation. These studies were aided by recent structural resolution of a periplasmic domain of a VirB10 homolog and a 'core' complex composed of homologs of VirB10 and two outer membrane associated subunits, VirB7 and VirB9. By use of the substituted cysteine accessibility method (SCAM), I confirmed the bitopic topology of VirB10. Through phenotypic studies of Ala-Cys insertion mutations, I identified "uncoupling" mutations in the TM and  $\beta$ -barrel domains that blocked T-pilus assembly but permitted substrate transfer. I showed that cysteine replacements in the C-terminal periplasmic domain yielded a variety of phenotypes in relation to protein accumulation, oligomerization, substrate transfer, and T-pilus formation. By SCAM, I also gained further evidence that VirB10 adopts different structural states during machine biogenesis. Finally, I showed that VirB10 supports substrate transfer even when its TM domain is extensively mutagenized or substituted with heterologous TM domains. By contrast, specific residues most probably involved in oligomerization of the TM domain are required for biogenesis of the T-pilus.

## Table of Contents

Acknowledgements.....	iii
Table of Contents .....	v
List of Illustrations .....	vii
List of Tables .....	ix
Chapter 1. Introduction to <i>Agrobacterium tumefaciens</i> VirB/D4 Type IV Secretion System ...	ii
Introduction .....	2
Type 4 secretion systems (T4SS) are dynamic and multifunctional transport devices .....	2
VirB10 is a multifunctional dynamic core subunit of the VirB/D4 T4SS .....	6
Assembly of VirB7, VirB9, and VirB10 homologs as a ‘core’ complex.....	6
Significance.....	11
Chapter 2. Materials and Methods.....	12
Bacterial strains and growth/induction conditions .....	13
Construction of <i>virB10</i> insertions, substitutions, and transmembrane domain swaps .....	13
Protein analysis by western blotting.....	19
T-pilus isolation (shear assay) .....	19
VirB2 pilin surface assay.....	20
Virulence assays .....	20
Conjugation assays.....	20
MPB labeling .....	21
Isolation and detection of MPB-labeled VirB10.....	21
TOXCAT experimental procedures .....	22
Construction of profinity-VirB10 .....	23
Outer membrane channel gating assay through detection of substrate (FLAG-VirE2) release.....	23
Chapter 3. Cysteine-based Mutagenesis of VirB10: Applications for Topology Modeling, Studies of Conformational Dynamics, and Assignments of Domain Functions .....	24
Introduction .....	25
Results .....	26
Ala-Cys insertion mutations in the putative TM domain do not affect substrate transfer but block T-pilus formation .....	26

Confirmation of a VirB10 bitopic topology by SCAM <sup>TM</sup> .....	32
Cys mutations in the proline rich region (PRR) and $\beta$ -barrel domains exert effects on protein stability, oligomerization, and substrate transfer .....	35
MPB labeling studies aimed at probing the VirB10 conformational status .....	44
Further characterization of the AP domain by cysteine mutational analysis .....	48
Discussion .....	52
Roles of the N-terminal cytoplasmic and transmembrane domains on protein function .....	52
Role of the PRR and $\alpha$ 1 helix on protein function and complex formation .....	54
VirB10, the T4SS outer membrane pore .....	55
 Chapter 4. VirB10 TM Domain: A Leucine Interaction Motif is Necessary for T-pilus Formation but not for Substrate Transfer.....	58
Introduction .....	59
Results .....	61
The GA <sub>4</sub> dimer motif is dispensable for VirB10 function .....	61
VirB10 TM domain substitutions: an FtsN TM domain swap .....	74
VirB10 TM domain substitutions: poly Leu-Ala TM domain swaps .....	78
Introduction of conserved residues in the VirB10 poly-LA TM domain restores T-pilus production.....	81
VirB10 TM domain weakly self-associates.....	84
VirB10 TM domain mutations do not disrupt outer membrane channel gating .....	93
Discussion .....	96
 Chapter 5. Summary and Perspectives .....	103
Summary .....	103
Future experiments .....	108
Do the VirB10 TM or AP domains mediate subunit contacts with VirB2 pilin?.....	108
Do VirB10 and VirB4 interact? .....	108
Complex isolation through the use of an N-terminal profinity-VirB10.....	109
 Final Acknowledgements.....	112
 References .....	113
 Vita.....	122

## List of Illustrations

Figure 1-1 Location of VirB/D4 T4SS subunits within the gram-negative cell wall .....	4
Figure 1-2 T4SS outer membrane complex; outer membrane pore .....	9
Figure 3-1 VirB10 domain organization and mutation positions .....	28
Figure 3-2 Effects of Ala-Cys insertion mutations on protein function .....	30
Figure 3-3 Results of MPB labeling accessibility .....	33
Figure 3-4 Effects of Cys mutations on protein function .....	38
Figure 3-5 Mobility of VirB10 Cys mutant proteins .....	40
Figure 3-6 Location of Cys mutations in the TraF X-ray structure .....	42
Figure 3-7 MPB Labeling profiles for VirB10 Cys mutant proteins expressed in a $\Delta virB10$ versus a $\Delta virB1-B11$ ( $\Delta virB$ operon) strain background.....	46
Figure 3-8 Effects of VirB10 AP Cys mutations on protein function .....	50
Figure 4-1 VirB10 TM aligned with GA <sub>4</sub> consensus motif and Pro Dom analysis.....	63
Figure 4-2 Effects of GA <sub>4</sub> point mutations on protein function.....	65
Figure 4-3 VirB10 TM aligned in a heptad repeat to identify possible Leu zippers.....	68
Figure 4-4 Effects of Ala substitutions in the putative LZ1 motif (L33, L40, L47) .....	70
Figure 4-5 Effects of Ala substitutions in the putative LZ2 motif (V35, L42, L49) .....	72
Figure 4-6 FtsN TM domain substitutions.....	76
Figure 4-7 poly-LA (poly Leu-Ala) TM substitutions.....	79
Figure 4-8 Introduction of conserved residues into a poly-LA TM domain restores T-pilus production .....	82
Figure 4-9 Growth of MM39 cells expressing ToxR-B10 <sub>TM</sub> -MBP proteins on maltose minimal media .....	87
Figure 4-10 Quantification of CAT activity from cell lysates expressing ToxR-B10 <sub>TM</sub> -MBP fusion proteins.....	89
Figure 4-11 TOXCAT with poly-LA sequences.....	91



Figure 4-12 Outer membrane gating defect assay (release of FLAG-VirE2 substrate)..... 94

Figure 4-13 Model depicting VirB10 helical TM packing..... 101

Figure 5-1 Models depicting contributions of VirB10 TM helices to entry of VirB2 pilin  
subunits into the core complex ..... 106

Figure 5-2 Effects of profinity-VirB10 fusion on protein function..... 110

## List of Tables

Table 2.1 Bacterial strains and plasmids .....	15
Table 2.2 Oligonucleotides used for construction of VirB10 residue replacements, and transmembrane (TM) domain substitutions .....	17

**Chapter 1.    Introduction to *Agrobacterium tumefaciens* VirB/D4 Type IV Secretion  
System**

## Introduction

### **Type 4 secretion systems (T4SS) are dynamic and multifunctional transport devices**

The translocation of macromolecules across the bacterial cell envelope is an important element in the establishment or progression of pathogenic relationships. Substrate translocation is achieved through specialized secretion systems. This thesis is centered on a group of ancestrally related translocation systems termed the Type IV Secretion Systems (T4SS) (1). These systems carry out a diverse array of functions and are classified into three subfamilies as: (i) conjugation machines, (ii) effector translocation systems, and (iii) DNA uptake and release systems (1). The VirB/VirD4 T4SS of *Agrobacterium tumefaciens* is a model system capable of transferring both DNA and protein substrates across the cell envelope and into the host cytoplasm. *A. tumefaciens* is a phytopathogen that uses the VirB/D4 T4SS to infect and genetically transform multiple species of plants (2). During the course of infection, the bacterium delivers a DNA-protein complex, called the transfer DNA or T-DNA, as well as protein substrates to plant cells with the outcome of infection resulting in the formation of plant tumors called Crown Galls (3). Although the overall infection process is highly complex and beyond the scope of this thesis, work described in this thesis sheds light into the mechanism of action of the VirB/VirD4 T4SS and phylogenetically related systems in mediating intercellular substrate transfer.

The virulence (*vir*) genes encode the VirB/D4 T4SS subunits, named VirB1 through VirB11 and VirD4 (4). The VirB subunits can be separated into three categories according to known or predicted functions and subcellular locations at the cell envelope: (i) energetic subunits, (ii) channel subunits, (iii) T-pilus or other subunits (1) (Figure 1-1) (5). Three ATPases VirB4, VirB11, and VirD4, comprise the energetic subunits (1, 6). All three ATPases are associated with the inner membrane and required for substrate transfer (7-10), but only VirB4 and VirB11 are required for the formation of the T-pilus (6). The channel subunits include bitopic proteins VirB8 and VirB10, polytopic VirB6, and the outer membrane proteins VirB7 and VirB9 (10). The T-pilus subunits include VirB2 and VirB5 (1), in which VirB2 assembles as the T-pilus and VirB5 is thought to localize at the T-pilus tip (11) (Figure 1-1). Although the VirB proteins are classified into different groups, they are all required to build a functional secretion channel and the extracellular T-pilus.

As mentioned above, many T4SS can be loosely categorized based on ancestral lineage and function into three distinct areas, e.g. conjugation, protein translocation, and DNA

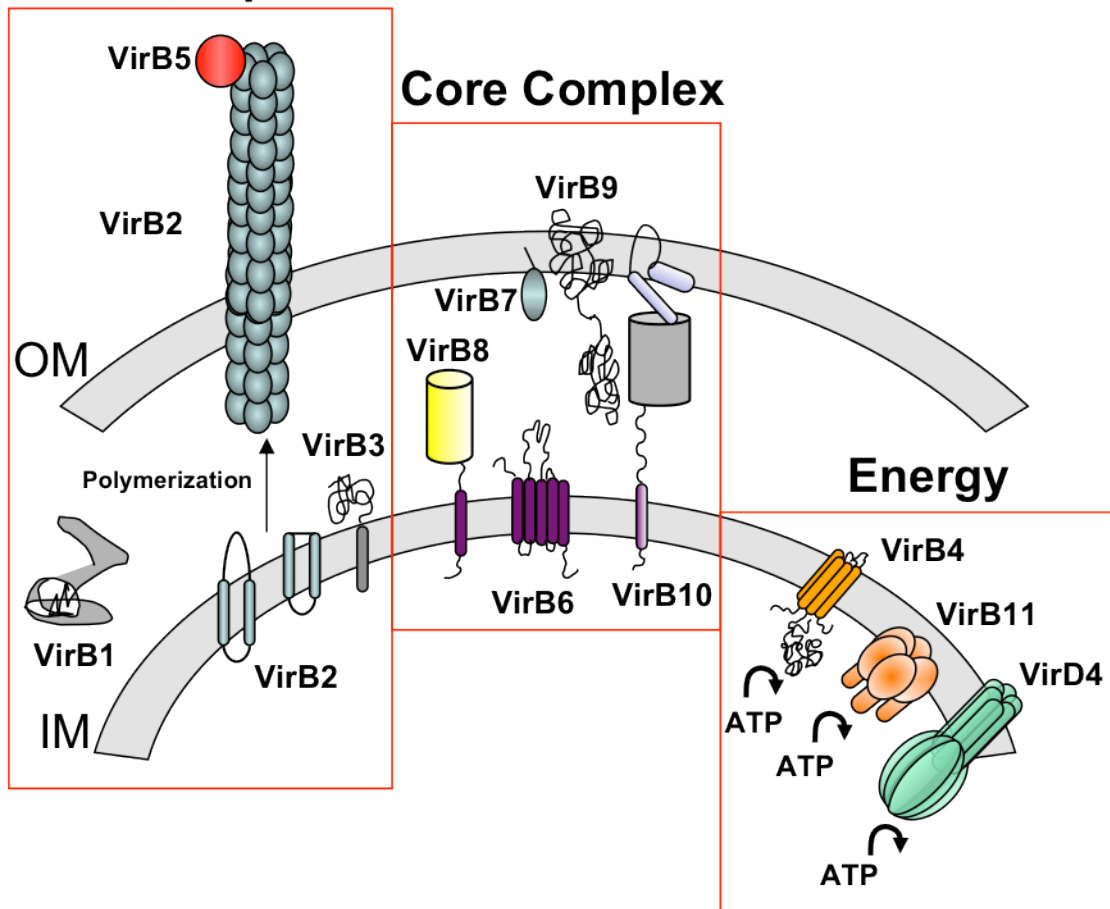
release/uptake (1). Across the bacteria and archaea, the different T4SS can vary widely in terms of their subunit compositions, but among the Gram-negative bacteria the T4SS invariably possess homologs of the VirB core subunits (VirB6 – VirB10), and at least two of the three ATPases (VirD4, VirB4) (12-14). In view of this conservation in sequence and probably also function, results of studies of individual T4SS subunits can have a broad importance. My studies of VirB10 have supplied new mechanistic information about the role of this subunit in machine assembly and function. In addition, the Waksman laboratory recently published results of ultrastructural studies of a T4SS encoded by the conjugative IncN plasmid pKM101 from *Escherichia coli* (15, 16). These structural findings have led to predictions regarding VirB10 function and have therefore guided some of my experiments. The combination of structural and functional data presented in this thesis provides a better understanding of how T4SS assemble and function.

An exciting development in the Christie laboratory was the determination of the T-DNA substrate route during channel translocation. This study utilized a formaldehyde (FA)-based crosslinking assay termed transfer DNA immunoprecipitation or TrIP (17). With TrIP, the translocation process was ordered spatially across the bacterial cell envelope through identification of FA-crosslinkable contacts between the translocating T-DNA substrate and VirB channel subunits. Specifically, the T-DNA substrate first forms a close contact at the cytoplasmic face of the channel with the VirD4 ATPase, also termed the substrate receptor or coupling protein, and then the VirB11 ATPase (17). Next, the T-DNA forms close contacts with the inner membrane channel subunits VirB6 and VirB8, and finally with VirB2 and VirB9 within the periplasm and possibly across the outer membrane. Of interest for the present studies, the T-DNA did not form close contacts with bitopic VirB10, although VirB10 was required for the T-DNA transfer from the inner membrane VirB6/VirB9 to the periplasmic/outer membrane VirB2/VirB9 subunits (17).

**Figure 1-1 Location of VirB/D4 T4SS subunits within the gram-negative cell wall**

Represented are the subcellular locations and topologies of the VirB (VirB1-VirB11) and VirD4 subunits. Subunits are categorized based on reported or putative functions: energy, core complex, and other/T-pilus. Energetic subunits include the three ATPases VirD4, VirB4, and VirB11. The core channel components VirB6, VirB7, VirB8, VirB9, VirB10 are believed to form a transenvelope complex that acts as a scaffold for the secretion channel or the T-pilus. The T-pilus components include VirB2 and VirB5. The biogenesis of the T-pilus first includes maturation of VirB2 subunits at the inner membrane followed by polymerization of these subunits across the cell envelope to the cell exterior. IM, inner membrane, OM, outer membrane.

## Other; T-pilus



## **VirB10 is a multifunctional dynamic core subunit of the VirB/D4 T4SS**

This thesis focuses on defining the contributions of the bitopic subunit VirB10 to substrate transfer and T-pilus biogenesis. Based on sequence analysis, the VirB10 domain architecture is thought to consist of an N-terminal cytoplasmic domain,  $\alpha$ -helix transmembrane (TM) domain, periplasmic proline-rich region (PRR), and a C-terminal periplasmic domain (12). An X-ray crystal structure is available for a portion of the VirB10 homolog, ComB10, from the *Helicobacter pylori* T4SS system (18). This structure shows that the C-terminal periplasmic domain of ComB10 adopts a modified  $\beta$ -barrel with two unusual  $\alpha$ -helical extensions. An  $\alpha$ 1-helix is positioned on the side of the  $\beta$ -barrel and extends perpendicular to the  $\beta$ -barrel strands. Another helical element, a helix-loop-helix ( $\alpha$ 2, $\alpha$ 3), projects from the top of the  $\beta$ -barrel. Part of the  $\alpha$ 2, $\alpha$ 3 extension (termed the antennae projection or AP) was structurally unresolved, which could be an indicator of a flexible region. The  $\beta$ -barrel itself was unusual in the presence of a groove or depression on the  $\beta$ -barrel surface. In the crystal structure the  $\beta$ -barrels of two monomers of ComB10 aligned in head-to-tail fashion and the  $\beta$ -barrel grooves formed the packing interface (18). This overall structure conveyed useful predictions for the VirB10 protein family.

As noted above, VirB10 is required for both substrate transfer and T-pilus formation (19). Previously, the Christie laboratory presented evidence that VirB10 senses ATP utilization by the inner membrane ATPases VirD4 and VirB11 and, in turn, undergoes a conformational change (20). This conformational change is necessary for substrate transfer, and deduced from the findings that the translocating T-DNA failed to form close contacts with VirB2 and VirB9 in ATP-depleted wild-type cells or strains lacking VirB10 or the inner membrane ATPases (20). The energy induced conformational switch was identified as a change in protease susceptibility. These findings led to a working model that ATP hydrolysis combined with VirB10 energy sensing together act as a molecular switch to regulate substrate translocation through the distal portion of the translocation channel (20).

## **Assembly of VirB7, VirB9, and VirB10 homologs as a 'core' complex**

Besides its role in energy sensing, recent structural data indicate that VirB10 assembles with two other subunits, the VirB7 lipoprotein and VirB9, as a higher-order structure termed a 'core' complex. This core complex is believed to form part of the secretion channel that spans across the inner membrane, periplasm, and outer membrane. The argument for a core complex is supported by results of protein-protein interaction studies (21, 22) and further reinforced by the available structural information. The ultrastructural data were generated for a



'core' complex comprised of homologs of VirB7, VirB9, and VirB10 from the conjugation T4SS encoded by the *E. coli* plasmid pKM101. Initially, a structure obtained by cryoelectron microscopy (cryo-EM) showed that 14 copies each of the VirB7, VirB9, and VirB10 homologs (TraN, TraO, and TraF, respectively) assemble as a large, 1.05 megadalton (mDa), ring-shaped complex (16). Further, the core channel complex is divided into two parts: (i) the O layer predicted to embed in the outer membrane, and (ii) I layer, believed to insert in the inner membrane. The O and I layer both have hollow chambers and thus the whole structure is cylindrical. The O layer is a complex of TraN, TraO, and TraF and creates a cap domain that possibly functions as the outer membrane pore (16). In contrast, the I layer appears to be largely composed of VirB10-like TraF. The dimensions of the core channel are such that the cap domain of the O layer resolved with a 10 Å diameter opening whereas the base of the channel made by the I layer resolved with a 55 Å diameter opening (16). These features therefore create a channel structure with a narrow opening at the cap or pore domain and large opening at the base of the channel. Due to the small diameter of the channel opening at the OM, it was proposed that the cap domain undergoes conformational changes in order to accommodate passage of large macromolecules such as DNA and protein substrates, or extrusion of the T-pilus (15, 16).

Very recently, an X-ray-crystal structure of a portion of the pKM101 core complex was determined (15) (Figure 1-2). This structure corresponds to the O layer of the core complex. A surprising finding was that the OM channel and cap domain consists not of VirB9-like TraO, as had been previously predicted, but of the VirB10-like TraF. This pore is composed of 14  $\alpha$ -helical projections from VirB10, specifically the  $\alpha 2, \alpha 3$  helix-loop-helix or antennae projections (AP) (15) (Figure 1-2). These findings suggest that VirB10 is a scaffold for the core complex and also that the AP comprises the outer membrane pore. If this model is correct, VirB10 would be the first described bacterial protein shown to span the entire Gram-negative bacterial cell envelope (23). As a result of these new structural developments, many questions have surfaced concerning the requirements for pore opening and closing. Overall, the combined structural and functional studies are providing valuable insights into how large macromolecular complexes assemble across the bacterial cell envelope. Our working model for T4SS machine morphogenesis posits that the VirB7, VirB9, and VirB10 subunits first assemble to form an intrinsically stable core complex. Next, the core complex recruits the other VirB subunits for further assembly of the secretion channel or, alternatively, the T-pilus.

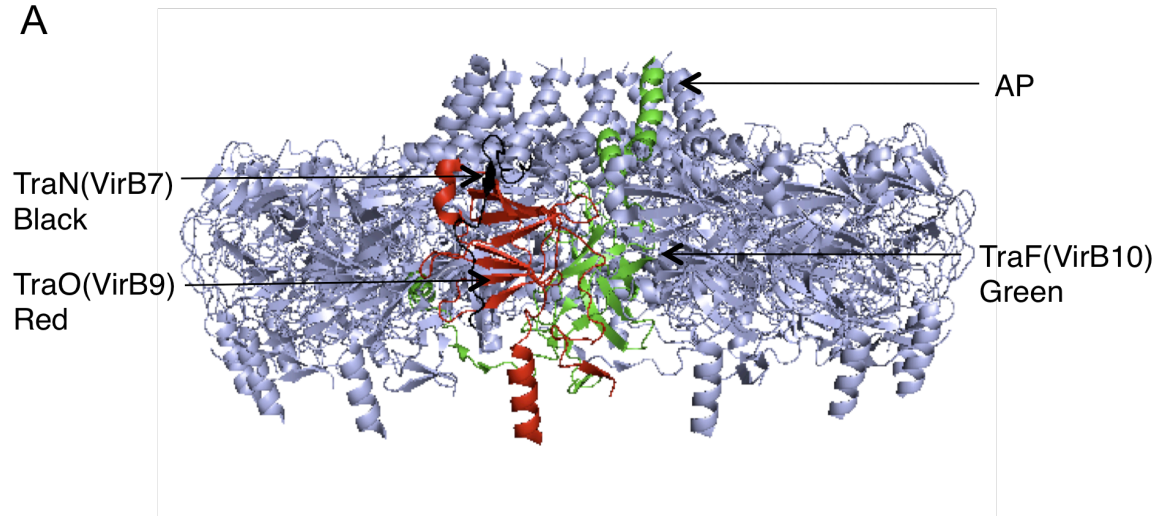
In summary VirB10, a required subunit for T4SS-mediated substrate transfer and T-pilus biogenesis possesses several novel and intriguing features. It is an ATP energy sensor, a structural scaffold for a large macromolecular machine, and a putative outer membrane pore.

**Figure 1-2 T4SS outer membrane complex; outer membrane pore**

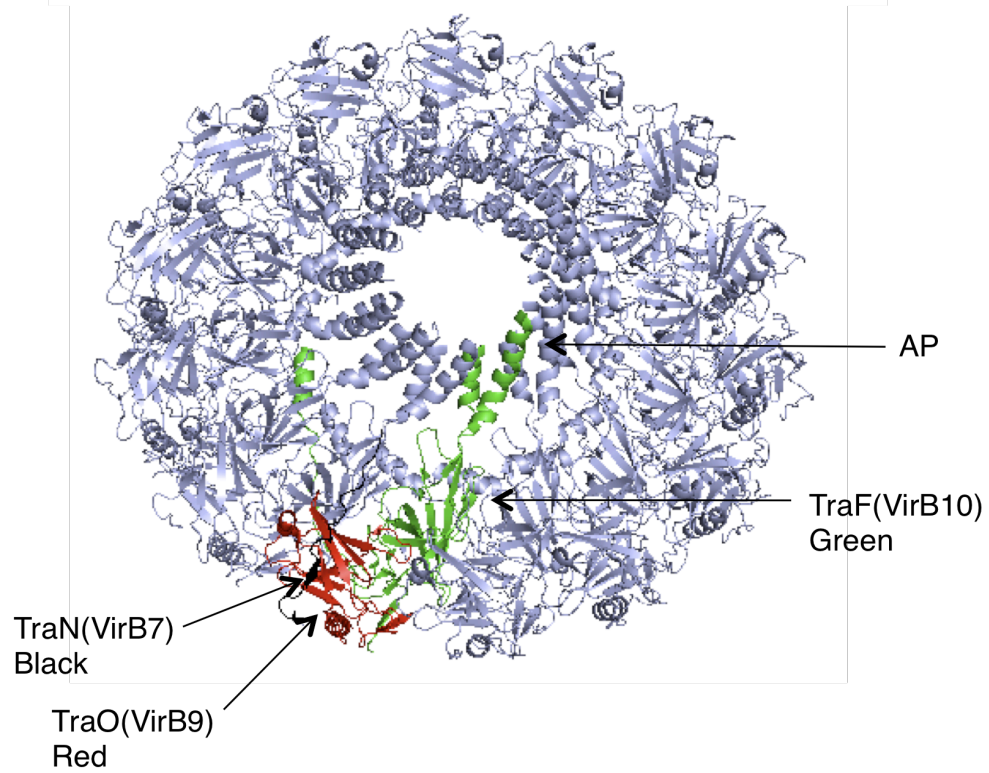
- A. Ribbon diagram of the pKM101 X-ray crystal structure of the outer membrane complex (O layer).
- B. The structure tilted (Top view). The core complex is shown as light blue. The Tra subunit fragments are color-coded: TraF (VirB10) is green, TraO (VirB9) is red, TraN (VirB7) is black. The antennae projection (AP) of TraF (VirB10) is indicated with an arrow.

This structure was resolved and published by (15). I used the coordinates from the published structure in the protein data bank (<http://www.pdb.org>) (accession code; 3JQO) along with the MacPyMOL visualization tool to create this figure. I have an educational (Academic) subscription to use MacPyMOL (PyMOL Molecular Graphics System, 2006, Delano scientific, LLC., <http://www.pymol.org>).

A



B



## Significance

The ability of bacteria to transfer macromolecules to diverse cell types is an important adaptation of special importance for infection processes. This work seeks to extend previous studies concerned with understanding how T4SS are architecturally arranged and how they mediate substrate transfer across the bacterial cell envelope. Specifically, this thesis seeks to define the contributions of VirB10 to substrate transfer and T-pilus biogenesis through phenotypic characterization of mutations introduced into specific domains.

In chapter 3, I collaborated with a technician (Vidhya Krishnamoorthy), graduate student (Jennifer E. Kerr), and postdoctoral fellow (Simon J. Jakubowski) (24). I present my specific contributions to this project. I used the substituted cysteine accessibility method or SCAM (25) to: (i) to determine VirB10 topology, (ii) refine our understanding of VirB10 conformational dynamics, and (iii) explore VirB10 domain contributions to protein function. One interesting finding from this study is that a partial deletion of the  $\alpha 2, \alpha 3$  antennae projection results in a block in T-pilus formation while maintaining substrate transfer. Moreover, the AP deletion mutation results in the release of VirB2 pilin into the milieu (24).

In chapter 4, I focused on the VirB10 TM domain, seeking to define the underlying mechanism for my initial observation that Ala-Cys (i2) insertions in this domain selectively block T-pilus production without affecting substrate transfer. Mutations were introduced into two putative TM helix-helix interaction motifs and assayed for effects on oligomerization and protein function. I determined that a leucine-based motif— a possible Leu zipper - is important for T-pilus formation but not for substrate transfer. By TOXCAT, a bacterial reporter system designed to measure self-association of TM helices in membranes (26), I showed that VirB10 weakly self-associates and that the capacities of VirB10 mutant TM domains to self-associate generally correlated with T-pilus production.

## **Chapter 2. Materials and Methods**

### **Bacterial strains and growth/induction conditions**

*Agrobacterium tumefaciens* A348 served as the wild-type strain for these studies (27). A348 deleted of the *virB* operon and *virB10* are strains PC1000 and PC1010, respectively (19, 28) (Table 2-1). Conditions for growth of *A. tumefaciens* cells and induction of *vir* genes have been previously described (29). Briefly, strains were taken from frozen glycerol stocks (-80°C) and streaked on MG/L plates (Luria Bertani (LB) plates supplemented with mannitol and glutamate) (30, 31). After 2-3 days growth at room temperature (~25°C; RT) fresh colonies from MG/L plates were inoculated into 5 ml MG/L broth media and grown overnight at RT on a shaker. To maintain plasmids in *A. tumefaciens*, appropriate antibiotics were added to the media at the following concentrations (in µg/ml): carbenicillin (100), tetracycline (5), kanamycin (100), gentamicin (100), spectinomycin (500) (24, 28). For induction of the virulence genes, 1 ml of cells grown in MG/L to mid-exponential phase (OD<sub>600</sub> of ~0.6-0.8) were harvested by centrifugation (3 min at 11,200 x g). Optical density readings were taken on a Beckman DU 530 UV/VIS spectrophotometer. Harvested cells were re-suspended in 5 ml of *vir* induction media (ABIM; AB 5.5 minimal media containing 200 µl acetosyringone (100 mM) (32)). ABIM cultures were incubated while shaking at RT for 14-18 h and subsequently used for protein analysis.

### **Construction of *virB10* insertions, substitutions, and transmembrane domain swaps**

The oligo-directed mutagenesis method of Kunkel and McClary was utilized to generate codon insertions and substitutions in *virB10* (33). In this method, a single stranded template is first created by transformation of the template plasmid into *E. coli* strain CJ236 (*dut*, *ung*) cells. These cells lack functional activity of dUTPase (*dut*) and uracil N-glycosylase (*ung*). Therefore, during plasmid replication uracils are incorporated as a substitute for thymines. The CJ236 cells are infected with the *E. coli* bacteriophage M13K07, which packages plasmid strands as single-stranded DNA into viral particles. Uracil-containing single stranded DNA is purified from these viral particles through a series of phenol chloroform extractions and used for subsequent oligo-directed mutagenesis. Oligonucleotides containing mutations of interest are annealed to the single-stranded template; the annealed oligonucleotides then serve as primers for complementary strand synthesis with T4 DNA polymerase. The *in vitro*-synthesized double-stranded plasmids are transformed into *E. coli* DH5α cells. In this background, the uracil-containing strand is degraded while the mutant strand lacking uracils is replicated (33). In my experiments, pKVD10, encoding P<sub>lac</sub>-*virB10*, served as the template for construction of all residue insertions (Ala-Cys; GCA TGC), and residue replacements (cysteine; TGC, alanine; GCA, isoleucine; ATT). These Kunkel reactions utilized oligonucleotides with 12-15 base pair

sequence complementary to regions both upstream and downstream of the mutation. In addition, the mutations incorporated sequence changes that introduced an SphI or PstI restriction site, thus enabling diagnosis of the introduced mutations by restriction enzyme digestion (Table 2-2). Plasmids with mutations were identified by restriction enzyme analysis and verified through DNA sequencing (MMG core facility). Lastly, these ColE1 plasmids, which do not replicate in *A. tumefaciens*, were ligated to a broad-host-range (BHR) plasmid, pSW172 (34) or pXZ151 (35), and the resulting cointegrate plasmids were introduced into *A. tumefaciens* cells by electroporation (36).

Plasmids encoding VirB10 with heterologous TM sequences were created by PCR amplification of the N-terminus containing the respective TM sequence change (FtsN or pLA derivatives). PCR reactions utilized pKVD10 (carries  $P_{lac}$ -*virB10*) as template and primers listed in Table 2-2. PCR products incorporated an N-terminal NdeI (CAT ATG) site and an SphI (GCA TGC) site inserted at the 50<sup>th</sup> codon position. The PCR products were digested with NdeI and SphI and the resulting fragments were introduced into similarly digested pIG50, a plasmid containing a phenotypically-silent SphI (GCA TGC) restriction site at codon position 50 (24). Resulting plasmids encoded full-length VirB10 with the variant TM sequence. DNA constructs were verified through sequencing and then introduced into *A. tumefaciens* by ligation to a BHR plasmid and electroporation.



**Table 2.1 Bacterial strains and plasmids**

Strains or plasmids	Relevant Characteristics	Source
<i>E. coli</i>		
DH5 $\alpha$	Genotype; $\lambda$ - $\phi$ 80d/lacZ $\Delta$ M15 $\Delta$ (lacZYA-argF) U169 recA1 endA1 hsdR17 ( $r_k^-$ , $m_k^+$ ) supE44 thi-1 gyrA relA1	Gibco-BRL / Invitrogen
CJ236	Genotype; <i>dut ung thi relA</i> ; pCJ105(Cam <sup>r</sup> )	(37)
S17-1	Tra genes encoded by the broad-host-range plasmid RP4 incorporated in the chromosome for conjugal transfer of RSF1010 derivative (pML122 $\Delta$ km)	(38, 39)
MM39	<i>malE</i> ; TOXCAT strain	(26)
<i>A. tumefaciens</i>		
A348	<i>A. tumefaciens</i> containing the octopine-type Tumor-inducing (Ti) plasmid pTiA6NC	(40)
A348Spc <sup>r</sup>	Spc <sup>r</sup> : A348 recipient for conjugation	(38)
PC1010	A348 pTiA6NC with a nonpolar $\Delta virB10$	(19)
PC1000	A348 pTiA6NC deleted of $\Delta virB(1-11)$ operon	(28)
Plasmids		
pSW172	Tet <sup>r</sup> ; broad-host-range IncP plasmid	(34)
pXZ151	Kan <sup>r</sup> ; derivative of pSW172 encoding a Kan <sup>r</sup> cassette replacing Tet <sup>r</sup>	(35)
pML122 $\Delta$ Km	Gen <sup>r</sup> ; mobilizable IncQ derivative (RSF1010)	(41)
pKVD10	Crb <sup>r</sup> ; pBSIISK <sup>+</sup> NdeI expressing P <sub>lac</sub> - <i>virB10</i> ; parental plasmid for site-directed mutagenesis.	(24)
pIGXX <sup>a</sup> series	Crb <sup>r</sup> ; pKVD10 carrying in-frame Ala-Cys (GCA TGC) codon insertions at positions following the residue indicated.	(24)
pIG011-022 <sup>a</sup> series	Crb <sup>r</sup> ; pKVD10 carrying single cysteine substitutions (TGC) in the PRR and $\beta$ -barrel regions.	(24)
pIG043-049 <sup>b</sup> series	Crb <sup>r</sup> ; pKVD10 carrying single cysteine substitutions (TGC) along the $\beta$ -barrel antennae projection or AP	This Study
pIG024-025 <sup>b</sup> series	Crb <sup>r</sup> ; pKVD10 carrying transmembrane Isoleucine replacements in the GA <sub>4</sub> motif	This Study
pIG026-033 <sup>b</sup> series	Crb <sup>r</sup> ; pKVD10 carrying single and triple transmembrane leucine to alanine replacements in atypical leucine zipper motifs	This Study
pIG034-036 <sup>a,b</sup>	Crb <sup>r</sup> ; pKVD10 encoding various FtsN TM domain substitutions	This Study
pIG037-041 <sup>b</sup>	Crb <sup>r</sup> ; pKVD10 encoding various poly-Leucine Alanine (pLA) TM domain substitutions	This Study

pIG042 <sup>b</sup>	Crb <sup>r</sup> ; pKVD10 carrying a replacement of conserved tryptophan 48 with alanine	This Study
pccKan	Crb <sup>r</sup> , Kan <sup>r</sup> ; TOXCAT cloning vector	(26)
pccGpA	Crb <sup>r</sup> ; TM domain of glycoporphin A encoded in pccKan	(26)
pccGpA G83I	Crb <sup>r</sup> ; nondimerizing TM domain of glycoporphin A encoded in pccKan	(26)
pccB10XX	Crb <sup>r</sup> ; TM domain sequences from native and mutant VirB10 encoded in pccKan	This Study
pCM50	Crb <sup>r</sup> ; Encodes E1 FLAG-E2 from a ColE1 plasmid.	This Study
pIG051	Crb <sup>r</sup> ; Encodes N-terminal profinity-tagged <i>virB10</i>	This Study

For expression in *A. tumefaciens* all listed ColE1 plasmids were ligated to either pSW172<sup>a</sup> or pXZ151<sup>b</sup>, and introduced into competent cells by electroporation.

**Table 2.2 Oligonucleotides used for construction of VirB10 residue replacements, and transmembrane (TM) domain substitutions**

<b>α-helical Antennae (AP) Cysteine Replacements</b>	
M289C	5'-AACAGCACTCAAGAG <b>GCATGC</b> <sup>1</sup> TCCGCTAAAACG-3'
F298C	5'-GGTGCTAGCTGCCTG <b>GCATGC</b> <sup>1</sup> GCCTTGAACAGC-3'
S302C	5'-GCCAGCGTAGGT <b>GCATGC</b> <sup>1</sup> TGCCTGGAAGGCGCC-3'
N315C	5'-GTTATTTTGAAG <b>CTGCAG</b> <sup>2</sup> AAGCTCATCCCGCC-3'
F317C	5'-TTGTTACACGTTATTTTGG <b>CAGCTG</b> <sup>3</sup> TTGAAGCTCAT-3'
L329C	5'-GATGGTCGCCTT <b>GCATGC</b> <sup>1</sup> TGTCTCAGTTGTTTG-3'
T332C	5'-CGGTATGTTGAT <b>GCATGC</b> <sup>1</sup> CTTAAGGGCTGTCTC-3'
<b>Transmembrane (TM) Residue Substitutions</b>	
G37I	5'-CGCGAGAACGACAATTCCGACGATA <b>AAGCTT</b> <sup>4</sup> CTGAGACCC-3'
A41I	5'-TAGC <b>CATATG</b> <sup>5</sup> AGGCTTAACGATAAAATGAGAACGACACC-3'
L33A	5'-ACCTCCGACGATCGCTTTCTG <b>GGATCC</b> <sup>6</sup> CGAAAGACGCCG-3'
V35A	5'-GAACGACACCTCCGGCGATA <b>AAGCTT</b> <sup>4</sup> CTGAGACCC-3'
L40A	5'-CTAGC <b>CATATG</b> <sup>5</sup> AGGCTTAACGATAACGCGGCAACGACACC-3'
L42A	5'-CCAAATGAGGCTTA <b>AGCTAGC</b> <sup>7</sup> CGCGAGAACGACACC-3'
I47A	5'-CACCTTCTTTTGG <b>GCGGCCGC</b> <sup>8</sup> CTAGCCAAGCGAGGCTTAAC-3'
L49A	5'-CACCTTCTTTTGG <b>GCGGCCGC</b> <sup>8</sup> CTGCCCAAATGAGGCT-3'
L33A, L40A, I47A	5'-CCCACCTAGCCAAGCGAGGCTTAACGATAACGCGGCAACGACACCTCCGACGATCGCTTTCTG <b>GGATCC</b> <sup>6</sup> CGAAAGACG-3'
V35A, L42A, L49A	5'-GACGCCCACCTGCCCAAATGAGGCTTA <b>AGCTAGC</b> <sup>7</sup> CGCGAGAACGACACCTCCGGCGATCAATTTCTG-3'
<b>TOXCAT PCR Primers</b>	
FP-TM33	5'-GGGTCTCAGAAAT <b>CTAGA</b> <sup>9</sup> TTGATCGTCGGAGGT-3'
RP-TM50	5'-CTTTTGACGCCCC <b>GGATCC</b> <sup>6</sup> CTAGCCAATGAG-3'
FP-TM33-(L33A)	5'-GGGTCTCAGAAAT <b>CTAGA</b> <sup>9</sup> GCGATCGTCGGAGGT-3'
FP-TM33-(V35A)	5'-GGGTCTCAGAAAT <b>CTAGA</b> <sup>9</sup> TTGATCGCCGGAGGT-3'
RP-TM50-(I47A)	5'-CTTTTGACGCCCC <b>GGATCC</b> <sup>6</sup> CTAGCCAAGCGAG-3'
RP-TM50-(L49A)	5'-CTTTTGACGCCCC <b>GGATCC</b> <sup>6</sup> CTGCCCAAATGAG-3'
FP-TM33-(35AC)	5'-CGTCTTTCGGGGTCTCAGAAAT <b>CTAGA</b> <sup>9</sup> TTGATCGTC-3'
<b>Transmembrane (TM) domain substitutions</b>	
B10-Nterminal-S	5'- <b>CATATG</b> <sup>5</sup> AATAACGATAGTCAGCAAGCGGC-3'
B10PtN-Termi-Ndel	5'-AATTTACACAGGAAACAC <b>CATATG</b> <sup>5</sup> AATAACGATAGTCAG-3'
FtsN(35-50)	5'- <b>GCATGC</b> <sup>1</sup> AATGAAGTACAGACCACCGATAAAGGTCACAA GAACGGCGGCAGCGACGATAAGCTTCTGAGACCCCGAAAG-3'
FtsN-L47A	5'-CACCTTCTTTTGACGCCCC <b>GCATGC</b> <sup>1</sup> AATGAAGTATGCAC CACCGATAAAGGTCACAAGAAC-3'
FtsN-L33A,L40A,L47A	5'-CACCTTCTTTTGACGCCCC <b>GCATGC</b> <sup>1</sup> AATGAAGTATGCACCAC CGATAAAGGTCACTGCAACGGCGGCAGCGACGATAGCCTT CTGAGACCC-3'

pLA (33-50, W48)	5'- <b>GCATGC</b> <sup>1</sup> CGCCAGCCACAGCGCCAGCGCCAGCGCCAGCGC CAGCGCCAGCGCCAGCGCCAGTTTCTGAGACCCCGAAAGACG CCG-3'
pLA (33-50)	5'- <b>GCATGC</b> <sup>1</sup> CGCCAGCGCCAGCGCCAGCGCCAGCGCCAGCG CCAGCGCCAGCGCCAGCGCCAATTTCTGAGACCCCGAAAGAC GCCG-3'
pLA (27-50)	5'- <b>GCATGC</b> <sup>1</sup> CGCCAGCGCCAGCGCCAGCGCCAGCGCCAGC GCCAGCGCCAGCGCCAGCGCCAGCGCCAGCGCCAGCGCAA GACGCCGGCGATGTTTGTCTGGAGACCAGGGATCC-3'
W48A	5'-CTTCTTTT <b>GTCTGAC</b> <sup>10</sup> CACCTAGCGCAATGAGGCTTAAC-3'
pLA (33-50, W48, VL/SL)	5'-CTTCTTTTGACGCCC <b>GCATGC</b> <sup>1</sup> CGCCAGCCACAGCGCCA GTAACGACGCCAGGAGAACCGCCAGCGCCAGCGCCAATTTCT GAGACCCCGAAAGACGCCG-3'
pLA (33-50, W48, L40)	5'-CTTCTTTTGACGCCC <b>GCATGC</b> <sup>1</sup> CGCCAGCCACAGCGCCAGC GCCAGCGCCAGCAGCAGCGCCAGCGCCAGCGCCAATTTCTGA GACCCCGAAAGACGCCG-3'

Bases in bold identify silent restriction sites: <sup>1</sup>SphI (GCATGC), <sup>2</sup>PstI (CTGCAG), <sup>3</sup>PvuII (CAGCTG), <sup>4</sup>HindIII (AAGCTT), <sup>5</sup>NdeI (CATATG), <sup>6</sup>BamHI (GGATCC), <sup>7</sup>NheI (GCTAGC), <sup>8</sup>NotI (GCGGCCGC), <sup>9</sup>XbaI (TCTAGA), <sup>10</sup>Sall (GTCGAC).

### **Protein analysis by western blotting**

To assay for accumulation of VirB subunits, *vir*-induced cells were harvested, cell numbers were normalized by adjusting to equivalent optical densities (OD<sub>600</sub>), and cells were re-suspended in Laemmli's buffer (50 mM Tris-HCl, 4% SDS, 20% glycerol, 20 mM dithiothreitol (DTT), 1%  $\beta$ -mercaptoethanol ( $\beta$ -ME), 0.1% bromophenol blue, pH 6.8) and boiled for 10 min. When assaying for possible Cys-mediated intermolecular crosslinks, cells were suspended in Laemmli's buffer lacking reducing agents  $\beta$ -mercaptoethanol and dithiothreitol. The boiled cell extracts were resolved by sodium dodecyl sulfate (SDS) polyacrylamide gel electrophoresis (SDS-PAGE) or a tricine-SDS-PAGE as previously described (19). Separated proteins were then transferred to nitrocellulose membranes and incubated overnight with anti-VirB antibodies and then for 3 h with goat anti-rabbit antibodies conjugated to alkaline phosphatase (AP) or horseradish peroxidase (HRP) (New England Biolabs) for immunodetection. For TOXCAT, the steady state levels of the ToxR-B10<sub>TM</sub>-MBP proteins were assessed using an anti-MBP monoclonal antibody conjugated to horseradish peroxidase (HRP). AP activity was detected by the addition of the chemical reagents 5-Bromo-4-Chloro-3-Indolyl (BCIP) and Nitrotetrazolium blue chloride (NBT). Detection of HRP was done using an enhanced chemiluminescence (ECL) kit (Thermo Scientific) and blue lite autoradiography film (ISCBioExpress, Kaysville, UT).

### **T-pilus isolation (shear assay)**

T-pili were isolated by mechanical shearing and ultracentrifugation as previously described (24, 38). Briefly, a 500  $\mu$ l aliquot of *vir*-induced *A. tumefaciens* cells prepared as described above were spread on ABIM agar plates, followed by incubation for 3-5 days at 18°C. Cells were gently scraped from ABIM plates and collected in 1 ml KPO<sub>4</sub> buffer (50mM, pH 5.5). To recover T-pili from the cell surfaces, the cell suspension was repeatedly passed through a 25-gauge needle. Sheared cells were separated from T-pili by centrifugation at 14,000 x *g* for 30 min at 4°C, followed by filtration of the supernatant through a cellulose acetate membrane (0.22- $\mu$ m-pore-size; VWR sterile syringe filter). T-pili were then pelleted by ultracentrifugation at 100,000 x *g* for 1 h at 4°C. The pellet was re-suspended in Laemmli's buffer and electrophoresed through a tricine-SDS-polyacrylamide gel. The presence of pilin, monitored by western transfer of proteins to nitrocellulose and immunostaining with anti-VirB2 antibodies, served as a diagnostic for T-pilus production (38, 42).

### **VirB2 pilin surface assay**

T-pilus production was also monitored with a surface colony blot assay (24). One milliliter cultures of *vir*-induced cells with equivalent optical densities (OD<sub>600</sub>), were pelleted by centrifugation and cells were re-suspended in 100 µl of ABIM liquid media. This suspension was then spotted in 25 µl aliquots on an ABIM agar plate and incubated at 18°C for 3 days. Cells were then transferred to a nitrocellulose membrane and the resulting membrane was subjected to immunostaining with anti-VirB2 antibodies for detection of surface-exposed pilin.

### **Virulence assays**

The capacities of *A. tumefaciens* strains to transfer DNA and protein substrates through the VirB/VirD4 T4SS were assessed with a plant tumor formation assay (19, 43). Briefly, glycerol stocks were streaked on MG/L agar plates and strains were grown for 2-3 days at RT. These fresh cells were inoculated onto wounded leaves of the succulent plant, *Kalanchoe daigremontiana*. Wounding was accomplished by scratching the leaf with a sterile wooden applicator. Each leaf was co-inoculated with A348 (wild-type; positive control) and  $\Delta virB10$  (avirulent mutant strain; negative control), and virulence of a given strain was affirmed by inoculation of at least 3 different leaves. Inoculated leaves were observed for tumor formation over a 4-6 week period.

### **Conjugation assays**

The capacities of *A. tumefaciens* strains to transfer DNA through the VirB/VirD4 T4SS were also tested with an interbacterial conjugation assay (24, 41). First, the mobilizable IncQ plasmid pML122ΔKm (an RSF1010 derivative) was introduced into *A. tumefaciens* strains of interest by conjugative transfer using *E. coli* S17-1 (pML122ΔKm) as a donor strain. *E. coli* S17-1 efficiently delivers IncQ plasmids to *A. tumefaciens* cells due to the presence of the plasmid RP4 (IncP) transfer region in its chromosome (38, 39). Next, *A. tumefaciens* strains carrying pML122ΔKm served as donors in mating experiments with a  $Spc^r$  A348 derivative (24, 41). Briefly, *A. tumefaciens* donor and recipient cells were induced for expression of the *vir* genes for 6-8 h by shaking at RT. Cells were harvested and mixed in a 1: 5 ratio of donors to recipients. Five microliters of these mixtures were spotted on sterile nitrocellulose filters placed on top of an ABIM agar plate and incubated for 4-5 days at 18°C. The mating mixtures were re-suspended in MG/L media, serially diluted, and plated on antibiotic-containing media to select for transconjugants and donors. Transfer frequencies were reported as the number of transconjugants per donor cell. For each strain, mating experiments were carried out in triplicate and results of a representative experiment are reported.

## **MPB labeling**

MPB labeling of Cys-substituted VirB10 mutants were carried out as previously described (24). Briefly, *A. tumefaciens* strains grown in MG/L were used to inoculate 25 ml ABIM media in 125 ml flasks. These flasks were incubated in a RT shaker (~ 200 rpm) for 14-18 h to an optical density (OD<sub>600</sub>) of ~0.5. Cells were pelleted and re-suspended at an OD<sub>600</sub> of 12 in 500 µl of buffer A (100 mM HEPES, 250 mM sucrose, 25 mM MgCl<sub>2</sub>, 0.1 mM KCl, pH 7.5) with or without the thiol blocking reagent 4-acetamido-40-maleimidylstilbene-2, 20-disulphonic acid (AMS; Molecular Probes) at a final concentration of 5 mM. AMS-exposed cells were incubated at RT for 30 min, and then AMS was removed by pelleting the cells with centrifugation and aspirating the AMS containing buffer A. These cells were washed with 10 ml of fresh buffer A. AMS-pretreated and untreated cells were exposed to 3-(N-maleimidylpropionyl) biocytin (MPB; Molecular Probes). MPB and cells were gently mixed in a final concentration of 100 µM MPB and incubated at RT for 5 min. To quench the reaction, cells were washed with buffer A containing 20 mM β-mercaptoethanol. To determine accessibility of cysteine residues introduced in the putative cytoplasmic and transmembrane regions, cells were lysed by sonication prior to MPB labeling.

## **Isolation and detection of MPB-labeled VirB10**

MPB labeled cells were re-suspended in 200 µl of TES (10 mM Tris, 5 mM EDTA, 2% SDS, pH 7.5) and vortexed for 30 min at 37°C. Next 250 µl of buffer C (150 mM Tris, 0.5 M sucrose, 10 mM EDTA, pH 8.0) was added. These samples were then incubated with lysozyme at a final concentration of 1 mg ml<sup>-1</sup> on ice for 1 h. The samples were vortexed for 15 min at 37°C. To each of these samples, 20 µl of Triton X-100 were added, as well as 30 µl of an EDTA-free protease inhibitor cocktail (Pierce Biochemicals) and 13 µl from a 1 M MgCl<sub>2</sub> stock solution. These samples were then vortexed for 10 min at 25°C, followed by incubation for 3 h at 4°C with gentle rocking. The detergent-solubilized cell extracts were diluted with 900 µl of buffer C, and clarified by centrifugation at 14,000 x g for 15 min. The supernatant was incubated with protein A-sepharose CL4B beads (Pharmacia) (30 µl bed volume) for 60 min at RT. The supernatant and protein A-sepharose with non-specifically bound proteins were separated by centrifugation for 5 min at 5,000 x g. The supernatant was incubated with protein A-sepharose beads previously coupled to anti-VirB10 antibodies, and then the mixture was incubated with gentle rocking overnight at 4°C. The beads were washed twice in 1% Triton X-100 solution for 10 min, and once in a 0.1% Triton X-100 solution. To these beads, Laemmli's buffer was added and samples were analyzed by western blotting as previously described (24).

## TOXCAT experimental procedures

For the TOXCAT experiments, constructs expressing ToxR-B10<sub>TM</sub>-MBP were made as follows. The *Escherichia coli malE* strain MM39 and vectors, pccKan, pccGpA-WT, and pccGpA-G83I were obtained from Dr. Donald Engelman (Yale, New Haven, CT). Plasmids encoding the native TM sequence as well as TM sequences with mutations served as templates for PCR reactions to amplify the TM sequence of interest with the addition of 5' and 3' flanking XbaI and BamHI sites, respectively. Next, PCR products and pccKan were similarly digested, ligated, and the products pccB10XX were constructed (Table 2.1 and Table 2.2). Native and mutant TM sequences in the TOXCAT vector were confirmed by DNA sequencing.

The pccB10 and derivative plasmids were introduced into MM39 cells and tested for protein synthesis, and ability to complement maltose metabolism to confirm correct orientation of the bitopic protein at the inner membrane. To quantify TM-mediated dimerization of ToxR, cell lysates were assayed for chloramphenicol acetyltransferase (CAT) activity (44). Briefly, to test for maltose utilization of MM39 cells expressing ToxR-B10<sub>TM</sub>-MBP, cells were grown overnight in 0.4% glucose M9 minimal broth media while shaking. The cells were harvested, washed, and streaked on a 0.4% maltose M9 minimal media plate. These plates were incubated for 2 days at 37°C after which strains were monitored for growth. Cells expressing MBP in the periplasm (pMal -p2) and cytoplasm (pMal -c2) (New England Biolabs) were also included as positive and negative controls, respectively (26).

To quantify chloramphenicol acetyltransferase (CAT) activity, cells expressing ToxR-B10<sub>TM</sub>-MBP were first grown overnight in a 37°C shaking incubator in LB broth media containing 100 µg/ml of carbenicillin. This culture was used to inoculate a fresh 5 ml LB culture, which was then incubated at 37°C to an OD<sub>420</sub> of ~1.0. Cells numbers were normalized to the same OD<sub>420</sub> value, harvested, washed, and re-suspended in 2 ml sonication buffer (25 mM Tris, 2 mM EDTA, pH 8.0). Cells were sonicated on ice for 4 min (Branson 250 Analog sonicator, output= 2, duty cycle= 50%). A sample of the whole cell lysate was saved and used for western blot analysis. The remainder was centrifuged at 13,000 x g for 20 min and the supernatant was saved on ice for CAT assays. For detection of CAT activity, an enzymatic reaction was traced for absorbance at 412 nm for 5 min in a reaction mixture consisting of 10 µl cell lysate, 10 µl of 2.5 mM chloramphenicol, and 250 µl of reaction buffer (100 µM acetyl-CoA, 0.4 mg/ml of DNTB or 5,5'-dithiobis(2-nitrobenzoic acid), 100 µM Tris-HCl, pH 7.8) (44). A blank reaction mix, lacking chloramphenicol, was traced to determine the background absorbance. The kinetic trace data with chloramphenicol was revised to account for



background absorbance and was subsequently used to calculate the CAT enzyme activity. Reported CAT activities are mean values from three separate experiments and all kinetic traces were performed on a Beckman DU 530 UV/VIS spectrophotometer.

### **Construction of profinity-VirB10**

The profinity tag was PCR amplified from the pPal expression vector (Bio-Rad; obtained from Dr. Kevin Ridge, Biochemistry Dept., UT Houston Medical School) with the addition of 5' and 3' flanking NcoI and NdeI-linker-BamHI sites, respectively. This PCR product and pBluescriptIIKS (pBSIIKS-NcoI) were both digested with NcoI and BamHI and ligated together. The resultant plasmid, pBSIIKS-profinity, was digested with NdeI and SacI and the *virB10* gene flanked by NdeI and SacI sites was inserted, generating the profinity-tagged *virB10* gene fusion. This plasmid was verified through automated DNA sequencing and later introduced into *A. tumefaciens* for phenotypic and biochemical studies.

### **Outer membrane channel gating assay through detection of substrate (FLAG-VirE2) release**

To assay for outer membrane channel gating defects, I tested for release of T4SS substrates (FLAG-VirE2) to the cell surface by use of an assay developed by Dr. L. Banta at Williams College. All *A. tumefaciens* strains used in these studies produced native or mutant forms of VirB10 as well as FLAG-VirE2. VirB10 carrying a G272R mutation served as a positive control for leaking of FLAG-VirE2, as this has been shown to confer leakage of the VirB/VirD4 channel (L. Banta, personal communication). Briefly this assay is identical to the colony blot assay described above for the detection of T-pilus; however, here the anti-FLAG monoclonal or anti-VirE2 polyclonal antibodies were used for immunodetection.

### **Chapter 3. Cysteine-based Mutagenesis of VirB10: Applications for Topology Modeling, Studies of Conformational Dynamics, and Assignments of Domain Functions**

*Note: Data presented in this section were used in a published manuscript: “Agrobacterium VirB10 domain requirements for type IV secretion and T pilus biogenesis.” Molecular Microbiology (2009) 71(3), 779-794. This study was done in close collaboration with other laboratory members, Simon J. Jakubowski, Jennifer E. Kerr, and Vidhya Krishnamoorthy. Here, I present my contributions to the finished manuscript. Permission was given to reproduce and/or modify content for the purpose of this thesis. I have a license agreement (license number; 2501481389405) with the publisher John Wiley and Sons provided by the Copyright Clearance Center (CCC).*

## Introduction

The *A. tumefaciens* VirB/D4 T4SS consists of a channel that conveys DNA and protein substrates to infected plant cells and a filamentous surface structure termed the T-pilus that functions to initiate contacts between the bacterium and host target cells (45-47). Recent studies suggest that VirB10-like proteins contribute in at least three important ways to the assembly and function of cognate T4SS's. First, VirB10 is a component of a 'core' complex that spans the entire cell envelope and is required for stabilization of other VirB subunits during machine biogenesis. Current structural models depict VirB10 as a scaffold subunit of the core complex. These models are based on an X-ray crystal structure of the *Helicobacter pylori* ComB10 (18), a cryoelectron microscopy (Cryo-EM) structure of the pKM101 core complex composed of homologs of VirB7, VirB9, and VirB10 (16), and an X-ray structure of a portion of the pKM101 core complex (15).

Second, VirB10 undergoes a conformational switch upon sensing of ATP energy consumption by the inner membrane associated ATPases VirB11 and VirD4 (20). These ATPases, plus the VirB4 ATPase, are thought to supply power through conversion of chemical energy derived from ATP hydrolysis to a mechanical force to promote machine assembly and/or substrate transfer through the T4SS apparatus (4, 20). The conformational switch in VirB10 was detected as a change in protease susceptibility between wild-type cells and ATP-depleted cells or strains lacking VirB11 or VirD4 (20). The conformational switch was required for stable interaction of VirB10 with the outer membrane subunits VirB9 and VirB7 and for T-DNA translocation through the distal portion of the translocation channel as shown by a substrate-trapping assay (17, 20). VirB10 interacts with all three ATPases either directly or indirectly, as shown by co-immunoprecipitation (48) or affinity chromatography with a functional glutathione-S-transferase (GST) tagged derivative of VirB10 (S. J. Jakubowski, unpublished data).

Finally, the structural data suggest that an  $\alpha$ -helical domain of VirB10 termed the antennae projection (AP) forms a pore at the outer membrane. This is a surprising finding given that such a pore is composed of alpha helices. In all but one other documented case, the *E. coli* Wza protein, outer membrane proteins insert as  $\beta$ -barrels, not as  $\alpha$ -helices (49). The presumptive VirB10 AP pore is proposed to be the conduit for passage of T4SS substrates and possibly also the T-pilus across the outer membrane. However, this model remains to be rigorously tested.

At the outset of this study, we proposed that VirB10 forms a number of intersubunit contacts along its length that are required for core complex assembly, sensing of ATP energy use by the inner membrane ATPases, and substrate transfer. Prior studies supplied evidence for homomeric and heteromeric interactions (20, 21, 30, 48, 50). As noted above, VirB10 extensively interacts with VirB9 and VirB7 to form the core complex. Additionally, there is evidence from the Christie laboratory and other laboratories that VirB10 interacts directly with the VirD4 ATPase, and indirectly or directly with the VirB4 and VirB11 ATPases (48). VirB10 was also shown to interact in a two-hybrid screen with bitopic VirB8 and likely also interacts with the polytopic subunit VirB6 (21, 51). The contacts identified in the pKM101 core complex X-ray structure guide our predictions for VirB7, VirB9, and VirB10 interactions; however, the nature of other VirB10 heteromeric interactions and the importance of these interactions for machine function are not known.

To explore the role of distinct domains of VirB10 to binding partner interactions and protein function, I initiated a structure-function study based in part on the ComB10 and TraF X-ray crystal structures. Phenotypic studies of 2-residue insertion mutations as well as Cys substitution mutations confirmed a predicted bitopic topology for VirB10, identified discrete contributions of the transmembrane (TM) domain and AP to substrate transfer and T-pilus biogenesis, and supplied further evidence for structural flexibility of the VirB10 AP. A concluding section of this chapter focused on the AP domain through phenotypic analyses of cysteine substitution mutations. I examined whether these mutant alleles complement a *virB10* gene deletion and whether the engineered cysteine residues are surface displayed as predicted for a loop domain of the AP (15).

## Results

### **Ala-Cys insertion mutations in the putative TM domain do not affect substrate transfer but block T-pilus formation**

VirB10 homologs in several conjugative systems have been reported to interact with cognate VirD4-like ATPases (52, 53). In the Christie laboratory, a former postdoctoral fellow, K. Atmakuri supplied evidence that VirD4 and VirB10 form immunoprecipitable complexes in detergent solubilized cell extracts (48). VirB10 also has a unique ability to sense ATP energy use by the VirD4 or VirB11 ATPases that ultimately triggers a conformational change of probable importance for protein function. In view of these findings, I sought to explore the possibility that the N-terminal cytoplasmic and  $\alpha$ -helical TM domain could be responsible for mediating interaction with VirD4 and energy sensing. To test this hypothesis, I created ten Ala-

Cys insertion mutations at five residue intervals along the N-terminus (Figure 3-1). The goal was to determine whether these insertion mutations would disrupt VirB10 function and, if so, attempt to identify an underlying mechanism by assaying for formation of VirB10 – VirD4 complexes by co-immunoprecipitation. Full phenotypic characterization of all Ala-Cys mutant proteins is described in Jakubowski et. al. (24). Here, I will present my contributions to this larger study.

I found that nearly all 10 of the i2 mutant proteins accumulated at abundant levels. The one exception, a mutant with an i2 mutation at residue 35 within the presumptive TM domain was less abundant than the other mutants, suggestive of a perturbing effect on protein stability (Figure 3-2). In addition, all of the i2 derivatives supported DNA transfer as shown by the capacity of the corresponding mutant strains to incite tumor formation on plant leaves (Figure 3-2). The functionality of the VirB10.i2 mutant proteins with respect to T-DNA transfer supported the notion that the mutants retained the capacity to interact with and sense ATP energy use by the inner membrane ATPases. Another lab member, V. Krishnamoorthy, assayed for VirB10.i2 complex formation with the VirD4 ATPase by co-immunoprecipitation. She found that all of the mutant proteins co-precipitated with VirD4, whereas a mutant deleted of the first 46 residues of VirB10 (spanning the cytoplasmic and TM domains) did not form a complex with VirD4 (24). Together, the functionality of the VirB10.i2 mutant proteins and their capacity to interact – directly or indirectly – with VirD4 suggests the mutant proteins support machine biogenesis and retain the capacity to sense ATP energy use by the inner membrane ATPases.

Interestingly, when another graduate student, J. Kerr, assayed for the capacity of strains producing the VirB10.i2 mutant proteins to elaborate T-pili, three strains made little or no detectable T-pilus. Strains with insertions at residues 35 and 45 of VirB10 elaborated low levels of T-pilus and a strain with an insertion at residue 40 elaborated no detectable T-pilus (24). Therefore, derivatives with i2 mutations in the presumptive TM domain supported substrate transfer but blocked T-pilus formation. Note that a deletion of the TM domain renders cells transfer-minus (Tra<sup>-</sup>). Therefore, although the TM domain is essential for VirB10 function, i2 mutations that would be predicted to shift the register of the transmembrane  $\alpha$ -helix selectively disrupt T-pilus biogenesis. These initial findings formed the basis for further studies described in Chapter 4 to decipher the contribution of the TM domain to T-pilus production.

### **Figure 3-1 VirB10 domain organization and mutation positions**

Domain diagram of VirB10 indicating locations of all Ala-Cys (i2) insertions and cysteine substitution mutations.

Schematic of VirB10 was taken from (24). This figure was modified to include Cys residue replacements located in the antennae projection (AP) in the  $\beta$ -barrel domain. I have a license agreement between the publisher, John Wiley and Sons, to include this content in my thesis (license number; 2501481389405). I isolated and introduced all mutations into *A.tumefaciens* except those indicated with an asterisk (\*); these were constructed by Ms. V. Krishnamoorthy.

Black dots represent sites of i2 mutations. Cyto, cytoplasm; TM, transmembrane domain; PRR, proline rich region;  $\alpha 1$ ,  $\alpha$ -helical extension or level arm from the  $\beta$ -barrel domain,  $\alpha 2$ - $\alpha 3$  (AP) helix-loop-helix extension or antennae projection (AP) from the  $\beta$ -barrel domain.

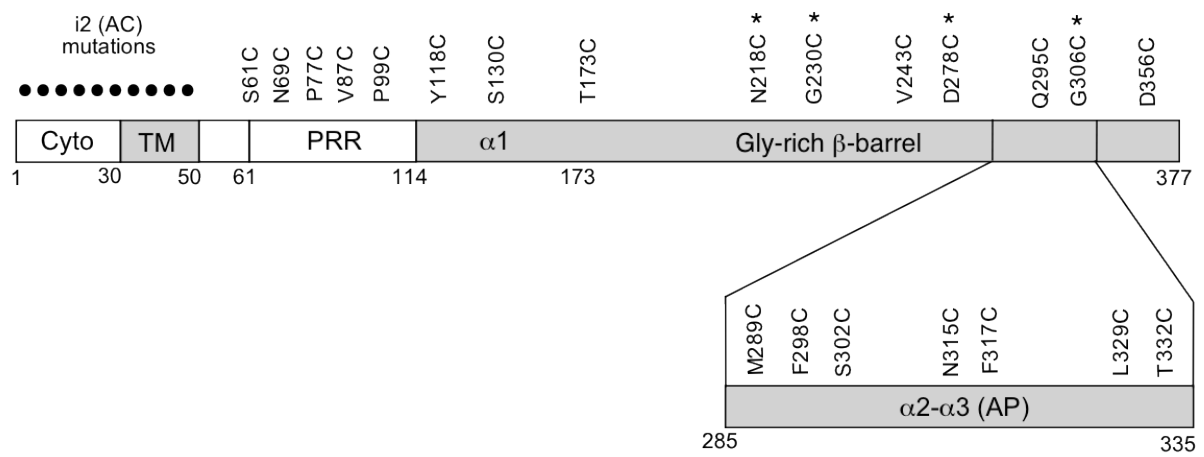


### **Figure 3-2 Effects of Ala-Cys insertion mutations on protein function**

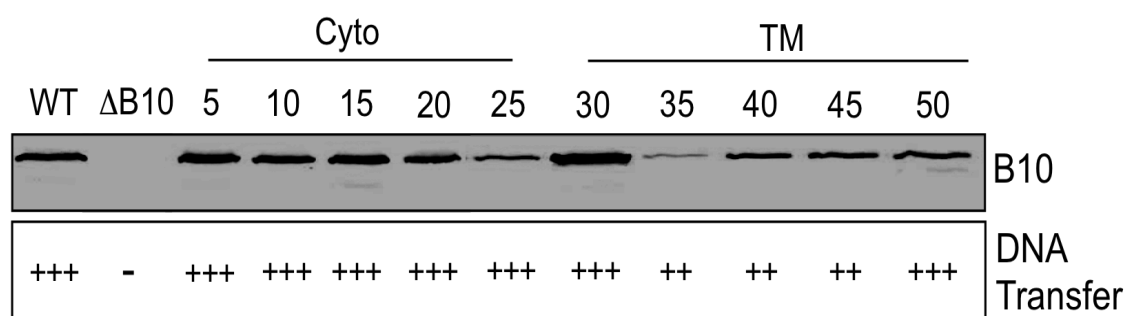
Western blot analysis of total cell extracts for all 10 Ala-Cys insertions introduced along the cytoplasmic and transmembrane domains of VirB10. Equivalent optical densities of induced cells were used for protein analysis by western blotting. Cells re-suspended in Laemmli's buffer, boiled for 10 min, and loaded on 12.5% SDS-polyacrylamide gels. Relative levels of VirB10 derivatives were visualized by western blotting and immunostaining with anti-VirB10 antibodies.

Strains: A348, WT *A. tumefaciens*;  $\Delta$ B10, PC1010; Ala-Cys mutations synthesized in a PC1010 strain background.

Ability to transfer DNA substrates was determined through plant virulence assays. *K. daigremontiana* plant leaves were co-inoculated with A348,  $\Delta$ B10, and the VirB10 Cys mutants, and monitored after 4-5 weeks for the presence (+) or absence of tumors (-). A348 (WT) and  $\Delta$ B10 served as positive and negative controls, respectively. Virulence assays were repeated 3 times.

These data were taken and modified from (24). I have a license agreement between the publisher, John Wiley and Sons, to include this content in my thesis (license number; 2501481389405).





## Confirmation of a VirB10 bitopic topology by SCAM<sup>TM</sup>

I next utilized the substituted cysteine accessibility method (SCAM<sup>TM</sup>) to test the prediction that VirB10 stably integrates as a bitopic protein into the inner membrane (25). In SCAM, natural or engineered cysteine residues are assayed for accessibility to a membrane-impermeable, thiol-specific reagent, in this case 3-maleimidylpropionyl biocytin (MPB, Molecular Probes). MPB is a maleimide derivative linked to biotin and due to its molecular size (~500 daltons, Da) readily diffuses through outer membrane pores. MPB only inefficiently crosses the inner membrane under the experimental conditions used in our studies (25). MPB labeling of Cys residues that do not disrupt protein function thus are indicative of a periplasmic or more distal location, whereas MPB inaccessibility is suggestive of cytoplasmic or inner membrane localization. This is an attractive method to determine residue disposition relative to the inner membrane. MPB labeling also can be used to assess whether a protein associates dynamically with the inner membrane in different genetic contexts or experimental conditions. This question is relevant for VirB10, because a 'shuttling' mechanism from the inner to outer membrane has been proposed for another energy transducer, TonB, on the basis of MPB labeling of Cys residues in an N-terminal cytoplasmic domain of this bitopic protein (54).

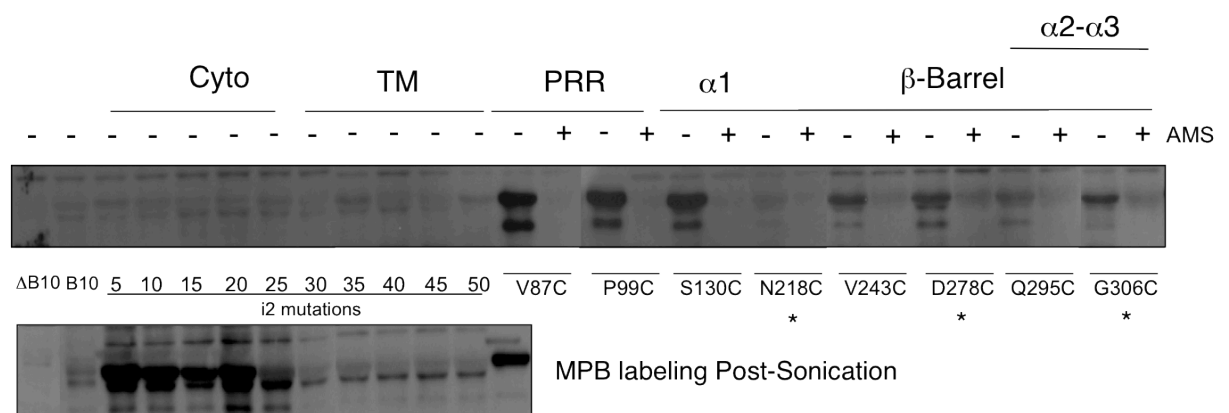
In my study, none of the N-terminal Cys insertions deriving from the Ala-Cys insertions was MPB labeled in whole cells, consistent with a cytoplasmic and transmembrane localization (Figure 3-3). By contrast, Cys substitutions positioned more C-terminally were efficiently labeled, consistent with the predicted locations of the PRR,  $\alpha$ 1 helix, and  $\beta$ -barrel domains in the periplasm. Sonication of cells prior to MPB labeling renders cytoplasmic Cys residues accessible to MPB and here resulted in strong labeling of Cys residues inserted at positions 5, 10, 15, and 20 relative to the N-terminus of the protein. Residue 25 labeled weakly, whereas residues 30, 35, 40, 45 and 50 did not label. For all residues in which MPB labeling was detected in whole cells, pretreatment with a nonbiotinylated maleimide derivative (AMS) effectively blocked subsequent MPB labeling. Together, these results support a topology model in which residues 1 to 25 are cytoplasmic, residues 30 to 50 insert in the inner membrane, and more C-terminal domains are periplasmic. These results also indicate that VirB10 does not dissociate from the inner membrane and shuttle to the outer membrane upon energy activation.

### **Figure 3-3 Results of MPB labeling accessibility**

Top panel: MPB labeling of whole cells and bottom panel is labeling of lysates. Strains synthesizing C-terminal cysteine mutant proteins were labeled in the presence (+) and absence (-) of a blocking reagent AMS. Labeled proteins were resolved on a 12.5% polyacrylamide gel, and blots were incubated with avidin-HRP and developed with commercial enhanced chemiluminescence (ECL) reagents. Strains:  $\Delta$ B10, PC1010; B10, PC1010 (pKVD10) expressing wild-type VirB10; PC1010 (pIGXX) expressing mutant alleles shown.

VirB10 mutations with an asterisk (\*) were constructed and introduced into *A. tumefaciens* by V. Krishnamoorthy.

These data were taken and modified from (24). I have a license agreement between the publisher, John Wiley and Sons, to include this in my thesis (license number; 2501481389405).



## **Cys mutations in the proline rich region (PRR) and $\beta$ -barrel domains exert effects on protein stability, oligomerization, and substrate transfer**

Structural models for the C-terminal domain (CTD) of VirB10 can be derived from X-ray structures of the *H. pylori* ComB10 and the *E. coli* pKM101 TraF proteins (15, 18). The two structures are comprised mainly of a  $\beta$ -barrel with a surface groove and both have two  $\alpha$ -helical projections, although the sequence compositions and the overall structures of these projections display important differences. For example, in the ComB10 X-ray structure, two monomers are aligned in a head-to-tail fashion such that the AP of one monomer sits in the groove formed by the  $\beta$ -barrel of the second (18). By contrast, in the TraF structure, 14 copies of TraF align such that the  $\beta$ -barrels form a network of interactions with each other and with homologs of VirB7 (TraN) and VirB9 (TraO) (15). In this structure, the AP domains from the 14 TraF subunits assemble together as an outer membrane  $\alpha$ -helical pore (15). Although the ComB10 structure is informative, we believe the TraF structure more accurately depicts the structure of the VirB10 protein family in complex with its partner proteins VirB7 and VirB9. Here, I sought to test for effects of Cys substitution mutations in the  $\beta$ -barrel domain and  $\alpha$ -helical projections on protein function and capacity to form higher-order dimers or multimers. No structural information is available for the PRR domain; therefore, to examine the contributions of this domain to oligomerization and protein function, I also introduced cysteine mutations along its length (Figure 3-1). Overall, I introduced 11 single cysteine replacements along the PRR, and  $\beta$ -barrel (groove and helical projections) (Figure 3-1).

In our original paper describing the phenotypic consequences of the VirB10 mutations, the available structural model based on ComB10 (18) guided our experiments as well as data interpretation (24). The availability of the new TraF structure (15) allows for some reinterpretation of the data. Therefore, when warranted I will highlight our revised views about some of the earlier findings.

The PRR, which extends from residues 61 – 114, contains 14 Pro residues within this 53 residue domain, many of which are strongly conserved among VirB10 homologs. In this region, I generated 5 Cys substitutions of highly conserved (S61, N69, P77) and nonconserved (V87, P99) residues. Large deletions of this region ( $\Delta$ 70-92,  $\Delta$ 93-114,  $\Delta$ 70-114) were constructed and analyzed by V. Krishnamoorthy. Only the N69C mutant accumulated at low levels relative to the native protein or the other mutants, suggesting that this mutation could disrupt a stabilizing fold or protein-protein contact (Figure 3-4). Substitutions of any of the three highly conserved residues (S61, N69, P77) abolished substrate transfer and T-pilus

production, whereas substitutions of the weakly conserved V87 and P99 had no apparent effect on VirB10 function (Figure 3-4).

PRR's of proteins are implicated in mediating protein – protein interactions (55). Therefore, we analyzed effects of the PRR mutations on VirB10 oligomerization. We assessed the capacity of VirB10 to form higher-order disulfide crosslinked dimers/multimers and also to form precipitable complexes with the other core components VirB7 and VirB9. When electrophoresed under nonreducing conditions, all of the Cys-substituted PRR mutants formed a higher-order species of ~105-kDa, the expected size of a VirB10 dimer (Figure 3-5). I analyzed whether other VirB proteins might be part of this higher-order complex, but none of our VirB antibodies reacted with this species. These findings suggest that the higher-order disulfide crosslinked species are VirB10 homodimers, which is in agreement with the recent cryoelectron images of the pKM101 core complex showing extensive packing of TraF (VirB10) monomers with each other along the length of the protein (16). S. Jakubowski determined that all of the Cys-substituted mutants except for the unstable N69C mutant co-precipitated with VirB7 and VirB9; apparently, the individual PRR substitutions did not abolish either the capacity of VirB10 to interact with itself or with the other core subunits (24). However, S. Jakubowski also showed that the  $\Delta 70-92$ ,  $\Delta 93-114$ , and  $\Delta 70-114$  mutant proteins failed to form precipitable complexes with VirB7 and VirB9 (24). These findings suggest that the PRR plays a critical role in assembly of the VirB7/VirB9/VirB10 core complex. Further studies in the laboratory are currently examining the role of the PRR in assembly of the ring-shaped core complex.

In our publication of this work, we referred to the region spanning residues 114 -173 as a linker region. However, the TraF crystal structure shows this region as an  $\alpha$ -helix that makes extensive contacts with  $\beta$ -barrel domains of adjacent TraF monomers. Therefore we now designate this region as helix  $\alpha 1$  or the 'lever arm' following nomenclature proposed by Waksman and his colleagues (15). We characterized only a couple mutations in this helix. Tyr118 is highly conserved among VirB10 homologs and, correspondingly, a Y118C mutation was destabilizing. Tyr118 is in a cluster of highly conserved residues ( $E_{107}PRPEETPIFAY_{118}$ ) at the end of the PRR. This region is enriched in charged and aromatic residues, which I predict to be important for adopting a functionally important tertiary or quaternary structure. Consistent with this prediction, the Y118C mutant protein did not form the ~105-kDa disulfide crosslinked species detected for other Cys mutant proteins (Figure 3-5). S. Jakubowski determined that the Y118C mutant protein also did not form a precipitable complex with VirB7

and VirB9 (24). However, it is not possible to draw strong conclusions regarding the functional importance of Y118 because the Y118C mutant protein is unstable (Figure 3-4). By contrast, S130 is not conserved among homologs and the S130C mutation did not affect protein accumulation or substrate transfer (Figure 3-4). J. Kerr showed that this mutation did not affect T-pilus biogenesis and S. Jakubowski showed that this mutation did not affect formation of a precipitable VirB7/VirB9/VirB10 complex (24). Together, the limited analyses of the  $\alpha$ 1 helix domain allow for a general proposal that the conserved residues in this domain might play an important role in promoting protein – protein contacts required for machine function. This prediction is consistent with X-ray structural information for TraF (15).

In the  $\beta$ -barrel, four additional regions were targeted for Cys mutational analysis, including: (i) the groove (V243C), (ii) the base of the barrel (T173C, N218C, D356C), (iii) a region we now designate as a bridging domain (D278C), (iv) the  $\alpha$ 2 $\alpha$ 3 helix-loop-helix (G306C, Q295C) (Figures 3-1 and 3-6). Cysteine mutations in the groove and base yielded reduced protein accumulation and disrupted or abolished substrate transfer and T-pilus assembly (Figure 3-4). Cysteine mutations in the  $\alpha$ -helical AP and the bridging domain did not affect protein stability or function (Figure 3-4). Correspondingly, S. Jakubowski and J. Kerr showed that partial deletions of the AP and the bridging domain did not abolish protein function with respect to substrate transfer (24). Finally, the Cys substitutions in the AP and bridging domain formed higher-order disulfide crosslinked species; those in the  $\beta$ -barrel groove, base/flap regions did not form such species (Figure 3-5). The  $\beta$ -barrel most likely forms extensive homo- and heteromultimeric interactions as suggested by the recent cryoEM and X-ray structures of the pKM101 core complex (15, 16). However, a more extensive Cys mutational analysis is needed to confirm such interactions through a biochemical approach. My data do suggest that the bridge and AP domains of adjacent VirB10 monomers extensively interact, which is in agreement with predictions based on the pKM101 core complex X-ray structure (15).

### **Figure 3-4 Effects of Cys mutations on protein function**

Detection of 14 mutant proteins bearing Cys substitution mutations in the PRR,  $\alpha$ 1helix, and  $\beta$ -barrel domains. Equivalent optical densities of induced cells were harvested and analyzed by SDS-PAGE and immunostaining with anti-VirB10 antibodies (Top panels). Strains: A348 (WT);  $\Delta$ B10, PC1010;  $\Delta$ B10 strains producing the Cys-substituted mutant proteins shown. DNA transfer was assessed by plant virulence assays. Plant leaves, *K. daigremontiana*, were co-inoculated with cysteine mutant strains, A348, and  $\Delta$ B10, and monitored after 4-5 weeks for the presence (+) or absence of tumors (-). A348 (WT) and  $\Delta$ B10 served as positive and negative control, respectively. Virulence assays were repeated 3 times.

VirB10 mutations with an asterisk (\*) were constructed and introduced into *A. tumefaciens* by V. Krishnamoorthy.

These data were taken and modified from (24). I have a license agreement between the publisher, John Wiley and Sons, to include this in my thesis (license number; 2501481389405).



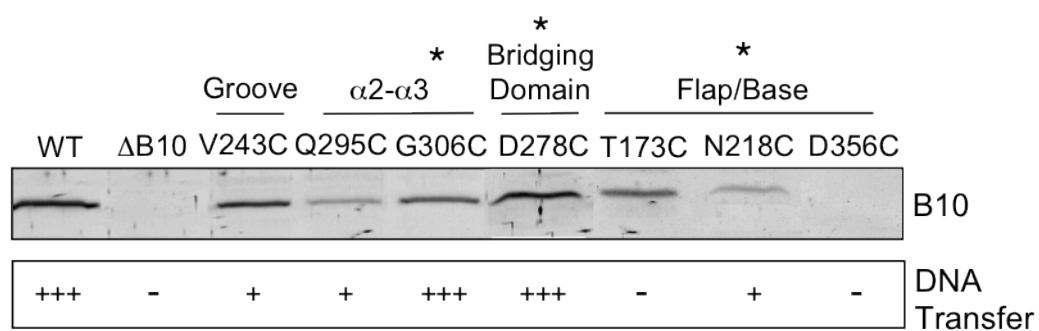
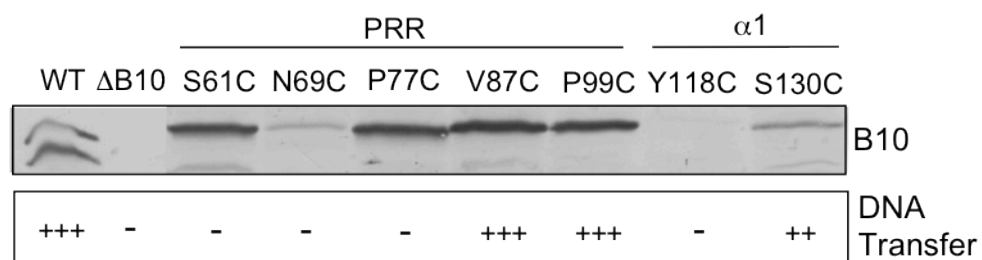


### **Figure 3-5 Mobility of VirB10 Cys mutant proteins**

Equivalent amounts of induced cells were harvested and cell extracts were resolved by electrophoresis through a 10% polyacrylamide gel. Cell extracts were re-suspended in Laemmli's buffer with (reducing; bottom panel) and without (nonreducing; top panel)  $\beta$ -mercaptoethanol ( $\beta$ -ME) and dithiothreitol (DTT). Protein standards (Bio-Rad) are listed at left.

Strains:  $\Delta$ B10, PC1010; B10, PC1010 expressing wild-type *virB10*; PC1010 expressing alleles encoding the Cys-substituted mutant proteins as shown. VirB10 mutations with an asterisk (\*) were constructed and introduced into *A. tumefaciens* by V. Krishnamoorthy.

These data were taken and modified from (24). I have a license agreement between the publisher, John Wiley and Sons, to include this in my thesis (license number; 2501481389405).

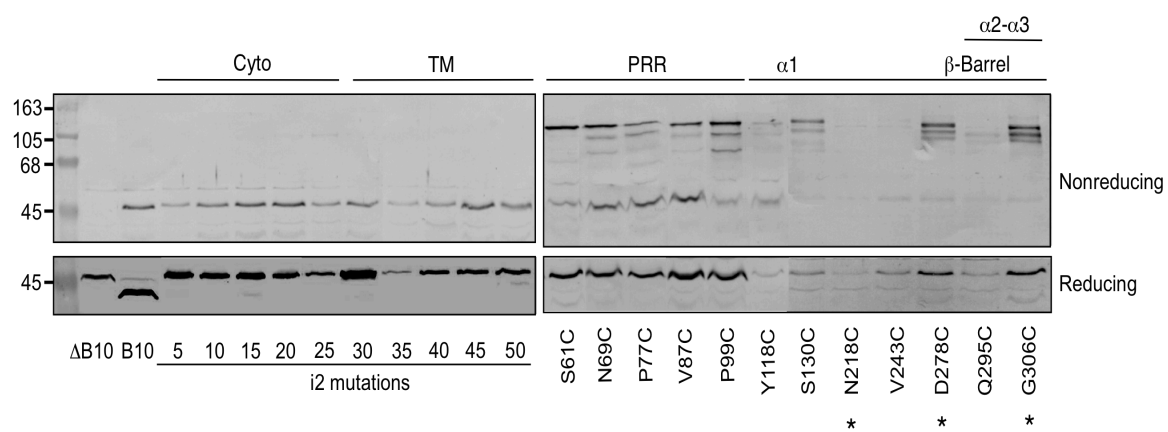
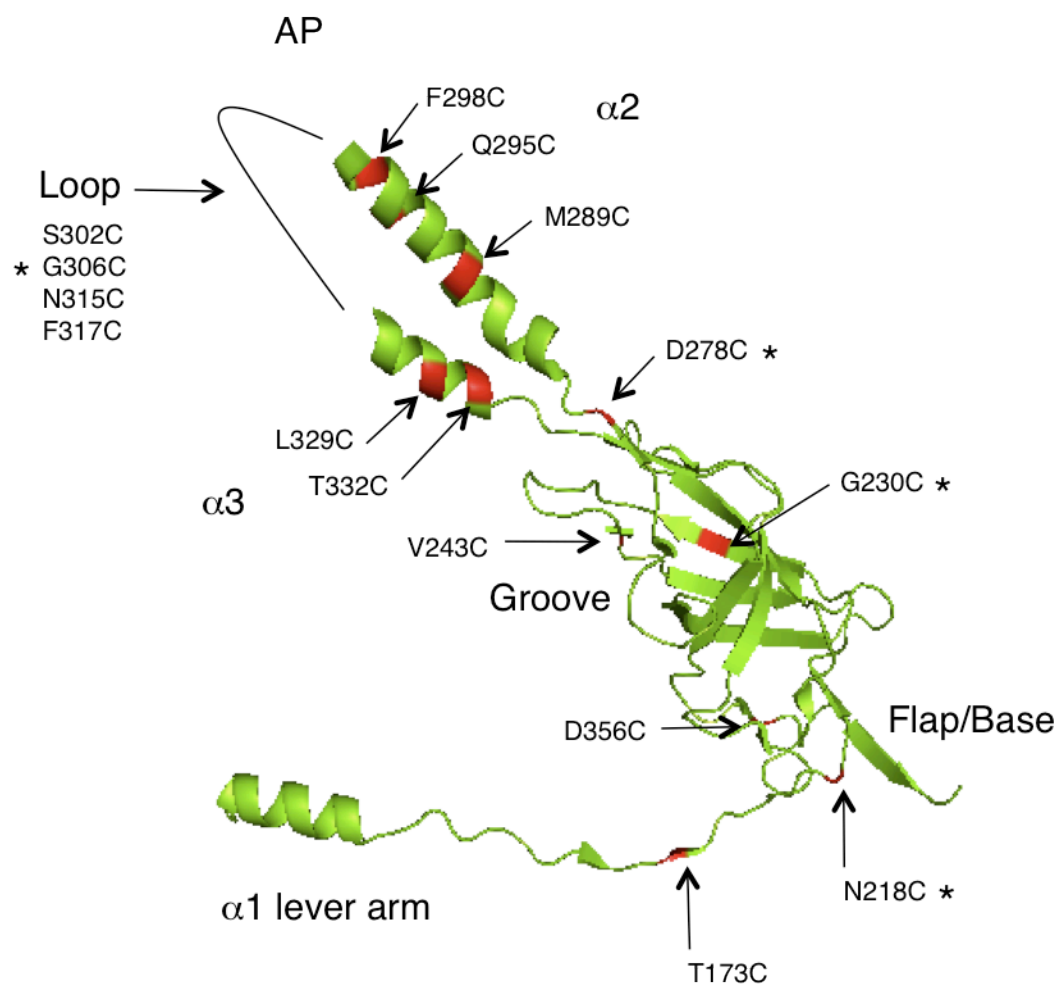


### **Figure 3-6 Location of Cys mutations in the TraF X-ray structure**

Ribbon diagram of the TraF (VirB10 homolog) from the pKM101 X-ray crystal structure of the outer membrane complex (O layer). The antennae projection (AP;  $\alpha 2\alpha 3$ ), groove,  $\alpha 1$  lever arm, and flap/base regions are labeled. Cys substitution mutations are indicated in red with arrows.

The TraF outer membrane structure was resolved and published by the G. Waksman laboratory (15). Coordinates from the published structure were accessed from the protein data bank (<http://www.pdb.org>) (accession code; 3JQO) and used with the MacPyMOL visualization tool to create this figure. I have an educational (Academic) subscription to use MacPyMOL (PyMOL Molecular Graphics System, 2006, Delano scientific, LLC., <http://www.pymol.org>).

Mutations indicated with an asterisk (\*) were constructed by Ms. V. Krishnamoorthy.



## **MPB labeling studies aimed at probing the VirB10 conformational status**

Prior studies with VirB10 identified a conformational switch upon sensing of ATP hydrolysis from inner membrane associated VirB11 and VirD4 (20). This conformational switch was detected as a change in susceptibility to the *Streptomyces griseus* protease such that VirB10 (48-kDa) was degraded to a (40-kDa) species when produced in wild-type cells but was not degraded when produced in ATP-depleted cells or *virD4* or *virB11* null mutant strains (20). The conformational switch was postulated to be required for stable interaction or productive channel formation with the outer membrane subunits VirB7 and VirB9 (20). To gain further evidence for the proposed energy dependent conformational switch, I assayed for changes in accessibility of Cys residues introduced along the length of VirB10 in different mutant strains. This study utilized the single Cys residue replacements introduced throughout the periplasmic domains of VirB10 (described above). Initially, I compared the Cys accessibility profiles of the Cys-substituted VirB10 derivatives when synthesized in a non-polar *virB10* deletion mutant PC1010 (19) (produces all of the VirB proteins) and a  $\Delta virB$  operon mutant PC1000 (28) (lacks the other VirB subunits).

An important caveat to this analysis was that native VirB10 as well as the Cys-substituted VirB10 derivatives accumulated at lower levels in the  $\Delta virB$  operon mutant compared with the  $\Delta virB10$  mutant. This was most likely due to the absence of stabilizing interactions in the absence of other channel subunits. When normalized for VirB10 levels, however, some potentially interesting differences in MPB labeling were observed. Specifically, among all of the Cys-substituted derivatives examined, only those with mutations in (D278C, G306C, Q295C) or near (V243C) the AP domain were more strongly labeled in the  $\Delta virB10$  background as compared with the  $\Delta virB$  background (Figure 3-7). Residue substitutions in the PRR and  $\alpha 1$  domains, as well as a few residue substitutions in the  $\beta$ -barrel, showed similar levels of labeling in both genetic backgrounds. These results are compatible with predictions from the TraF structural studies (15) that the outer membrane pore formed by the AP domain of VirB10-like TraF undergoes conformational transitions during substrate translocation or T-pilus biogenesis.

At this time, we do not know whether the observed differences in MPB labeling of the AP Cys mutations are due to a lack of energy activation or improper folding of VirB10 in the absence of partner channel subunits. Further investigations of the proposed energy-mediated dynamic activity of the AP will require parallel MPB labeling studies of the Cys-substituted VirB10 mutants produced in strains lacking one or more of the VirB4, VirB11 or VirD4

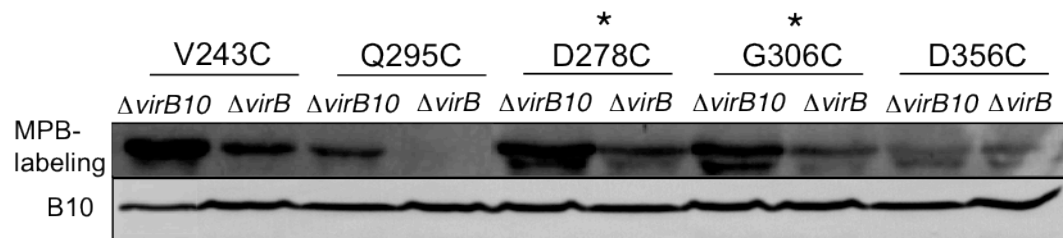
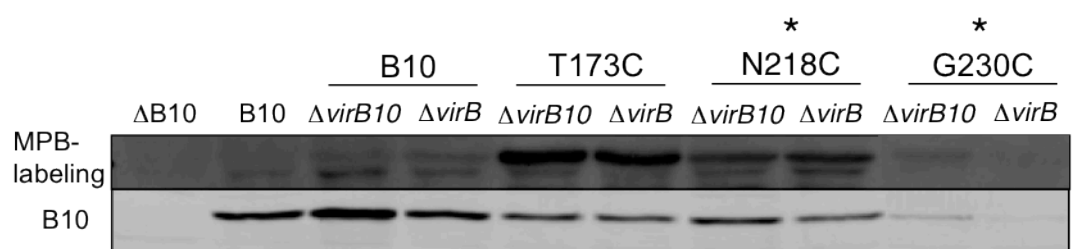
ATPases. This will require construction of additional strains, e.g., the appropriate nonpolar deletion mutants (e.g.,  $\Delta virB10/\Delta virD4$ ,  $\Delta virB10/\Delta virB4$ ,  $\Delta virB10/\Delta virB11$ ) expressing *virB10* alleles encoding the VirB10 Cys mutants without or with wild-type or mutant ATPases.

**Figure 3-7 MPB Labeling profiles for VirB10 Cys mutant proteins expressed in a  $\Delta virB10$  versus a  $\Delta virB1-B11$  ( $\Delta virB$  operon) strain background**

Top panel: MPB labeled proteins separated on a 12.5% polyacrylamide gel followed by transfer to nitrocellulose membranes and incubated with an avidin-HRP antibody, developed with enhanced chemiluminescence reagents. Bottom panel: total cell extracts from listed strains showing the relative steady state protein levels in the different strain backgrounds.

Strains: WT, A348;  $\Delta B10$ , PC1010 (19);  $\Delta virB$ , PC1000 (28). VirB10 mutations with an asterisk (\*) were constructed by V. Krishnamoorthy.





### Further characterization of the AP domain by cysteine mutational analysis

Two intriguing observations prompted us to initiate a further study of the VirB10 AP domain. First, the X-ray crystal structure of a homolog of VirB10, TraF, of the pKM101 conjugation T4SS identified the AP domain as forming a presumptive outer membrane pore (15). Recall that the overall X-ray structure of the pKM101 core complex presented as a heterotrimeric complex in a 1:1:1 ratio of TraF (VirB10), TraO (VirB9), and TraN (VirB7) with 14 copies of each subunit (15). The TraF AP is postulated to span between two conserved residues, Arg306 and I355, which for VirB10 correspond to residues Arg284 and I335. If the VirB10 AP forms an outer membrane pore, it might form close contacts with translocating substrates, the T-pilus, or both. Additionally, a flexible loop domain positioned between the two membrane spanning  $\alpha$ -helices should be surface-exposed. To test these predictions, I introduced 7 Cys substitution mutations along the length of the VirB10 AP with a goal of assaying for intra- and intermolecular disulfide crosslinks and accessibility of the engineered Cys residues to membrane-impermeable, thiol-reactive reagents. As with the other Cys mutational analyses, these studies were carried out in collaboration with another graduate student, J. Kerr, and a postdoctoral fellow, S. Jakubowski.

The positions of the 7 Cys residues as well as two Cys substitution mutations that V. Krishnamoorthy previously constructed in the AP (Q295C and G306C) are shown in Figures 3-1 and 3-6. Three Cys mutations (M289C, Q295C, F298C) were in the putative membrane-spanning  $\alpha$ 2-helix, 4 mutations (S302C, G306C, N315C, F317C) were in the intervening loop, and 2 mutations (L329C, T332C) were in the putative membrane-spanning  $\alpha$ 3-helix (Figure 3-6).

The initial studies assayed for effects of Cys mutations on protein stability, substrate transfer and T-pilus biogenesis. The 7 Cys mutant proteins accumulated at abundant levels, comparable to the level of the native protein when produced in *trans* from an IncP replicon (Figure 3-8). Nearly all of the mutant proteins supported efficient levels of substrate transfer as well as T-pilus biogenesis, as monitored by T-pilus colony and shear assays (Figure 3-8). The one exception, T332C, supported efficient substrate transfer, but only low levels of T-pilus compared with the other mutant proteins. Effects of the Q295C and G306C mutations were reported previously (24); these mutations phenocopied the other 7 Cys AP mutations with respect to effects on protein stability and function.

The functionality of the Cys mutant proteins enabled further studies aimed at testing for interactions with other channel subunits or translocating substrate. I first assayed for formation of disulfide crosslinked complexes by maintaining proteins under nonreducing conditions during cell lysis and gel electrophoresis. Interestingly, all Cys mutant proteins formed high-molecular weight species of estimated sizes (~100 to 105-kDa) expected of a VirB10 homodimer (Figure 3-8). Antibodies to other VirB subunits and to the protein substrate VirE2 did not react with the higher-order species. Further studies are being carried out by S. Jakubowski and J. Kerr to test for disulfide crosslinking with secretion substrates such as VirF and VirD2. However, in view of the pKM101 X-ray structure showing close packing of the TraF AP domains in the presumptive outer membrane pore (15), it seems most probable that Cys residues of juxtaposed AP domains form disulfide bridges to generate crosslinked homodimers.

Next, I tested for surface accessibility of the AP Cys residues by assaying for reactivity with the thiol reactive compound MPEG. MPEG (5-kDa) is a sulfhydryl reactive maleimide that is too large to pass through outer membrane pores and therefore covalently reacts with accessible thiol groups located on the cell surface (25, 56, 57). Chemical reactivity with MPEG results in a 5-kDa shift in the apparent molecular size of a protein upon electrophoresis through a SDS-polyacrylamide gel. Interestingly, I was unable to detect reactivity of any AP Cys residue with MPEG. Previously, our laboratory used MPEG to gain evidence for surface accessibility of a domain of VirB9 (56). It is possible the Cys residues of the VirB10 AP are buried in the pore or another protein – protein interface, and further tests for AP surface accessibility are in progress.

**Figure 3-8 Effects of VirB10 AP Cys mutations on protein function**

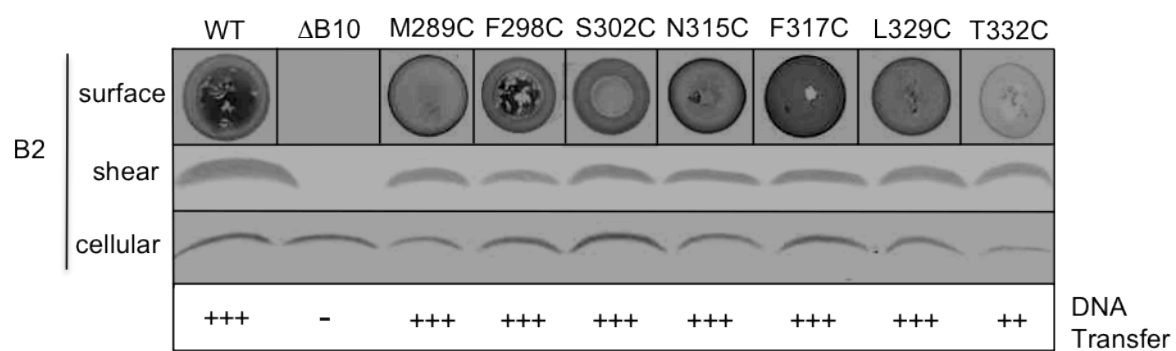
A. T-pilus production was affirmed through surface and shear assays. Protein accumulation was determined by western blot analysis with anti-VirB2 and anti-VirB10 antibodies, as listed. DNA substrate transfer was assessed by the ability of strains to incite production of tumors (+) or no tumors (-) on *K. daigremontiana* plant leaves. Virulence is reported in relation to WT (+++; WT virulence) and  $\Delta$ B10 ( - ; avirulent).

B. Migration of VirB10 Cys mutants in 10% polyacrylamide gels under nonreducing conditions, monitored by immunoblotting with anti-VirB10 antibodies.

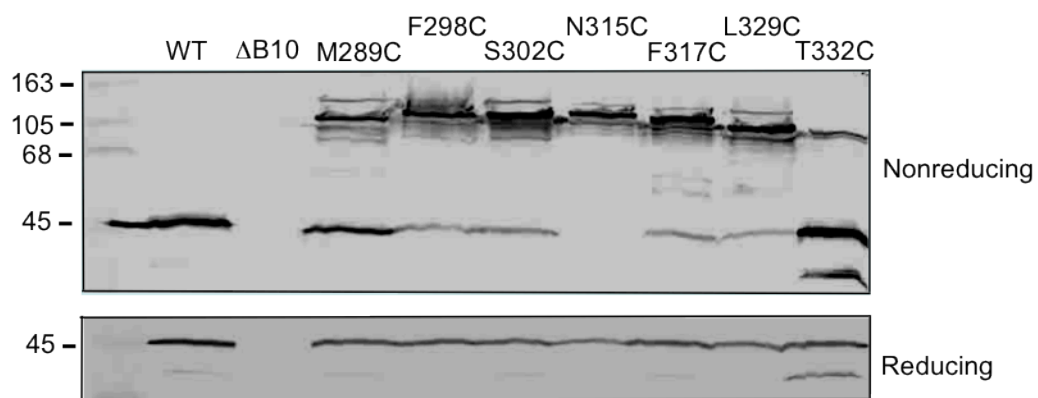
Strains: WT, A348;  $\Delta$ B10, PC1010;  $\Delta$ B10 strains producing Cys mutant proteins as listed.

Colony (surface) assays for strains producing VirB10 derivatives with Cys substitutions in the AP domain were replicated by graduate student Jennifer E. Kerr.

A



B



## Discussion

### Roles of the N-terminal cytoplasmic and transmembrane domains on protein function

The VirB proteins assemble as a transenvelope secretion channel and an attachment organelle called the T-pilus (4). This study was aimed at defining the contributions of various domains of VirB10 to assembly of these surface organelles. I constructed and characterized Ala-Cys insertion mutations along the N-terminal cytoplasmic and putative transmembrane domains of VirB10, and Cys substitution mutations of conserved and nonconserved residues in the periplasmic domains. As these studies were proceeding, structures of the VirB10 homologs ComB10 and TraF in complex with other core components were solved by X-ray crystallography and cryoelectron microscopy (15, 16, 18). These structures guided further experimentation and also enabled refined interpretations of our existing data.

Our mutational analyses confirmed the importance of the N-terminal domains for VirB10 function. Although VirB10 accommodated i2 mutations at 5-residue intervals along the cytoplasmic domain, deletion of the N-terminal 18 residues disrupted protein function at least to some extent (24). V. Krishnamoorthy constructed a larger deletion mutation of the first 46 residues, this mutant protein did accumulate, however, did not support substrate transfer, T-pilus biogenesis, and interaction with VirD4 (24). The N-termini of VirB10 homologs in *A. tumefaciens* and related species in the family *Rhizobaceae* are highly conserved (see below; Figure 4-1). It seems reasonable that the cytoplasmic domain contributes to the establishment of productive contacts with other channel subunits. Although the i2 insertions apparently did not disrupt critical contacts, it is noteworthy that a swap of the N-terminal cytoplasmic and TM domains of the cell division protein FtsN for the corresponding region of VirB10 abolished protein function (Figure 4-6). By contrast, as discussed further in Chapter 4, a swap of just the FtsN TM domain for that of VirB10 did not abolish activity. These findings provide further evidence for the importance of the N-terminal cytoplasmic domain for VirB10 function.

With respect to the TM domain, the i2 mutations did not disrupt substrate transfer or formation of a precipitable complex with the VirD4 ATPase (24). These findings suggest that the mutant proteins retained the capacity to sense ATP energy use by VirD4 and VirB11 and support substrate transfer. By contrast, i2 mutations at residues 35, 40, 45, had either reduced or no observable T-pili (24). These mutations were designated “uncoupling” mutations because they selectively blocked T-pilus biogenesis without affecting substrate transfer.

The isolation of VirB10 “uncoupling” mutations adds to a list of such mutations isolated in other VirB subunits, including the VirB11 ATPase (38, 58), polytopic VirB6 (59), outer-membrane-associated VirB9 (60), and VirB2 pilin (61). Although the identification of such mutations has led to a proposal that the VirB subunits alternatively assemble as a secretion channel or the T-pilus, the underlying mechanism of action(s) of “uncoupling” mutations remains unknown. For “uncoupling” mutations in the other VirB subunits, it has not been possible to predict effects on protein structure or oligomerization. By contrast, the isolation of “uncoupling” mutations in the VirB10 TM domain allows for the first time the development of testable models regarding the contributions of a discrete domain specifically for T-pilus biogenesis. For example, the i2 mutations are predicted to generate a shift in the register of the TM helix; this in turn could disrupt helix – helix interactions that are required for T-pilus assembly but not for elaboration of a functional secretion channel.

The T-pilus is a polymer assembled from VirB2 pilin (4). Our working model is that mature VirB2 pilin accumulates in the inner membrane as a pool for polymerization upon receipt of an unspecified signal. For polymerization, VirB2 must first be extracted from the inner membrane, presumably through an energy dependent process involving ATP energy and/or an electrochemical gradient. The VirB10 TM mutations could exert a direct block in the T-pilus assembly pathway by impeding the early pilin dislocation or polymerization reactions. In view of the CryoEM structure of the pKM101TraF(VirB10)/TraN(VirB7)/TraO(VirB9) core complex, it is reasonable to suggest that a VirB10/VirB7/VirB9 complex serves as a scaffold for T-pilus assembly. If so, an early step in polymerization of the T-pilus might involve translocation of VirB2 pilin through the inner membrane into the core chamber. Accordingly, VirB10 TM helix-helix interactions - either homo- or heterospecific - might directly impact the passage of the pilin into the core chamber. An alternative model is that VirB10 TM helix – helix interactions influence the overall structure or dynamic activity of the T-pilus assembly platform. According to this model, the helix-helix contacts might act indirectly by modulating the activities of other domains or subunits involved in T-pilus biogenesis. In Chapter 4, I summarize results of my studies further exploring the role of the VirB10 TM domain in T-pilus biogenesis.

Besides mediating protein – protein contacts required for machine assembly or function, the TM domain likely anchors VirB10 in the inner membrane. However, the question of whether VirB10 stably or transiently associates with the inner membrane is raised through investigations of the energy transducer TonB. In early studies of TonB mutants, Cys residues engineered in the putative cytoplasmic domain were MPB-labeled upon treatment of intact

cells (54). These findings led to formulation of the 'shuttling' model, whereby the energy-activated form of TonB resulting from sensing of the proton motive force was dislocated from the inner membrane and subsequently delivered to the outer membrane where it activates translocation of small molecules through cognate transporters (54). More recent studies appear to have discounted this early 'shuttling' model for TonB (62), but the idea prompted me to assay for a stable vs transient association of the VirB10 energy sensor with the inner membrane. I was unable to detect any labeling of Cys residues engineered into the cytoplasmic or TM domains of VirB10 upon treatment of intact cells. By contrast, Cys residues in the cytoplasmic domain were labeled upon treatment of cell lysates, whereas Cys residues in the putative TM domain failed to label under any condition, strongly indicating that these residues are buried in the hydrophobic lipid bilayer and inaccessible to thiol-reactive reagent. Together, these data confirm a bitopic membrane topology for VirB10 and also argue against a possible energy-mediated 'shuttling' mechanism. Our topology model indicates that the TM domain spanning residues ~30-50 stably anchors VirB10 in the inner membrane and the bulk of the rest of the protein is periplasmic.

### **Role of the PRR and $\alpha 1$ helix on protein function and complex formation**

Prolines in protein domains can impart unique conformational restrictions and can result in extended protein structures (63, 64). This property is accredited to the unusual bond between the proline side-chain and the backbone amide position (55). Proline-rich regions (PRR's) also can mediate protein – protein interactions (55, 65). We postulated that the VirB10 PRR is required for extension of the protein from the inner to outer membranes and also that PRR's of adjacent subunits interact in the assembled core complex. Consistent with these predicted functions, V. Krishnamoorthy and S. Jakubowski determined through characterization of deletion mutations that the VirB10 PRR is essential for VirB10 function and also for a VirB10 interaction with the VirB7/VirB9 heterodimer (24). My broad goal was to introduce Cys residues along the PRR to assay for disulfide crosslinking with partner proteins. Since we also had determined that VirB10 undergoes a conformational switch in response to sensing of ATP energy use by inner membrane ATPases, I also sought to determine whether PRR Cys residues display changes in MPB labeling in different mutant strain backgrounds.

The VirB10 PRR (residues ~ 61-114) is ~ 28 % Pro, and also has two Pro-Pro dipeptides (Pro<sub>81</sub>-Pro<sub>82</sub>, Pro<sub>98</sub>-Pro<sub>99</sub>) which tend to restrict flexibility even more than individual prolines (55). As might be expected, Cys substitutions of conserved residues in the PRR abrogated protein function, whereas substitutions of nonconserved residues did not affect



function. Regardless, all of the Cys substitutions in the PRR and newly-designated 'lever arm' formed disulfide-crosslinked species of similar molecular size (~105 kDa) when cell extracts were electrophoresed under nonreducing conditions (Figure 3-5). The estimated molecular size of the crosslinked species and apparent absence of other VirB proteins migrating at this position in the nonreducing gels suggests the Cys-substituted VirB10 derivatives crosslinked to form homodimers. The propensity of both the PRR and the lever arm to mediate self-association of adjacent VirB10 monomers fits with the structural predictions derived from the pKM101 crystallography and cryoelectron microscopy images (15, 16).

A couple of mutations were also introduced into the  $\alpha$ 1 helical lever arm of VirB10, a region spanning residues 114 – 173. As mentioned above, this region was originally thought to join the PRR with the  $\beta$ -barrel identified in the ComB10 X-ray structure. In the recent TraF X-ray structure, this region comprises an essential feature of the core complex. It extends laterally from the  $\beta$ -barrel of one monomer to establish contacts not only with the adjacent  $\beta$ -barrel but also with the next  $\beta$ -barrel in the complex (15). The lever arms thus overlap laterally to form a structural 'belt' surrounding the core complex. If this structure is correct, one might anticipate that Cys residues in the lever arm would form intermolecular disulfide crosslinks.

Interestingly, the Cys substitutions in the PRR and lever arm were MPB-labeled to similar extents when the mutant proteins were produced in the presence or absence of other VirB proteins. These observations allow only for a limited conclusion that the positions marked by these Cys substitutions are not buried in a structural fold or protein – protein interface in these two genetic contexts. Further studies are needed to determine whether Cys substitutions of other residues in the PRR or lever arm would display differences in MPB labeling in other *virB* mutant backgrounds.

### **VirB10, the T4SS outer membrane pore**

The X-ray structure of the pKM101 core complex highlights the structural importance of the  $\beta$ -barrel, as well as the TraF (VirB10) AP domain which appears to assemble as an outer membrane  $\alpha$ -helical pore (15). In view of the extensive network of intersubunit contacts, it is not surprising that Cys substitutions of  $\beta$ -barrel residues did not label efficiently with MPB and also did not form higher order species when the mutant proteins were subjected to nonreducing gel electrophoresis (Figure 3-3 and 3-5). Moreover, Cys substitutions of  $\beta$ -barrel residues tended to abrogate protein function, consistent with the notion that native residues at

these positions contribute to folding of the  $\beta$ -barrel domain or oligomerization. By contrast, Cys substitutions in the AP did not disrupt protein function (Figure 3-4). These residues also were readily labeled by MPB and formed higher order disulfide crosslinked species when maintained under nonreducing conditions (Figure 3-3 and 3-5). These findings are compatible with the crystallographic data indicating that the AP extends from the  $\beta$ -barrel and that AP's of adjacent monomers in the core complex form close contacts in the presumptive outer membrane pore (15). Also of considerable interest, the AP Cys residues were efficiently MPB-labeled when the mutant proteins were synthesized in the presence of other VirB subunits, but only weakly labeled in the absence of other VirB subunits (Figure 3-7). These observations suggest that VirB10 complex formation with other VirB partner proteins is required for proper folding of the AP and, possibly, assembly of the outer membrane pore.

Our early finding that VirB10 undergoes a conformational switch upon sensing of ATP energy consumption by the VirD4 and VirB11 ATPases led to a model that energy activation serves to induce formation or opening of the outer membrane pore (20). Results of these initial MPB labeling studies are compatible with this model, but further MPB-labeling studies are needed to explore the contributions of the inner membrane ATPases to the overall structure of the VirB10 AP domain.

A central question emerging from the pKM101 core crystal structure is whether the VirB10 AP extends entirely across the outer membrane. Since the structure was generated for a complex of only 3 of the 11 T4SS subunits, it is conceivable that the AP is very differently configured in the fully assembled channel. I attempted to detect surface accessibility of the VirB10 AP by treatment of intact cells with the thiol reactive reagent MPEG. However, I was unable to detect a ~5-kDa shift of the AP Cys mutants, suggesting that the AP does not extend entirely across the outer membrane or that the AP was buried by another protein, e.g., VirB2, VirB5, or some unspecified surface molecule, e.g., LPS, cellulose. Another possibility is that the AP is transiently surface-exposed or exposed only upon establishment of stable mating junctions with target cells. Besides the two Cys substitutions originally introduced in the AP region (D278C, G306C), I have recently constructed an additional 7 Cys replacements. My initial studies have shown that none of the mutations affect protein function and all of them form higher-order crosslinked species in nonreducing conditions (Figure 3-8). This collection of AP mutations will allow for expanded tests of AP domain interactions, structural flexibility, and surface accessibility.

In summary, my findings support a general model that VirB10 forms a structural scaffold for assembly of the secretion channel or T-pilus. Of most interest, the VirB10 TM domain appears to play a critical role in T-pilus biogenesis, and further studies focused on exploring this function are described in more detail in the following chapter. Results of the mutational, MPB labeling, and crosslinking studies support a model that VirB10 stably associates with the inner membrane and extends across the outer membrane to make critical contacts with outer membrane subunits VirB7 and VirB9. The initial studies of AP Cys mutations also are consistent with a model that this domain is structurally dynamic. Ongoing studies are exploring the surface accessibility of the AP region to test the hypothesis that this region functions as an outer membrane pore.

**Chapter 4. VirB10 TM Domain: A Leucine Interaction Motif is Necessary for T-pilus Formation but not for Substrate Transfer**

## Introduction

The VirB/VirD4 type IV secretion system (T4SS) of *Agrobacterium tumefaciens* translocates DNA and protein substrates to plant and other eukaryotic cells by a process requiring direct cell-cell contact (1). The eleven VirB proteins and the VirD4 substrate receptor direct assembly of the T4SS channel that spans the Gram-negative cell envelope as well as an extracellular filamentous structure termed the T-pilus. All of the VirB proteins are required for channel and T-pilus formation, and their general functions can be subclassified as: i) energetic components (VirD4, VirB4, VirB11 ATPases), ii) core channel subunits (VirB6, VirB7, VirB8, VirB9, VirB10), and iii) T-pilus or other structural components (VirB1, VirB2, VirB3, VirB5) (4). Early studies of this system defined pairwise contacts and subcellular localizations of the VirB subunits, supplying a general view of the VirB/VirD4 channel architecture. Very recently, however, a core complex from a related T4SS encoded by the conjugative plasmid pKM101 was resolved by cryoelectron microscopy (Cryo-EM) and X-ray crystallography (15, 16). Most notably, the emerging structural information highlights the importance of three subunits, bitopic protein VirB10 and two outer membrane-associated subunits VirB7 lipoprotein and VirB9. Fourteen copies each of the pKM101-encoded homologs of VirB7, VirB9, and VirB10 interact to form a large (~1.5-MDa) ring-shaped complex that spans the entire cell envelope (16). The complex has a central chamber of sufficient size to accommodate other VirB subunits. These structural features, in addition to observed stabilizing functions of these core subunits on other machine components, have prompted a model in which the VirB7/VirB9/VirB10 core complex serves as a scaffold for assembly of the translocation channel and the T-pilus.

A particularly interesting feature of the core complex is that VirB10-like TraF spans the entire cell envelope (23). As discussed earlier, VirB10 has several discrete domains that localize in different cellular compartments: i) an N-terminal cytoplasmic domain (residues ~1-30), ii) a transmembrane TM domain (residues ~30-50), iii) a periplasmic proline-rich region (PRR, ~61-114), iv) a periplasmic  $\beta$ -barrel (~115-377), positioned in the periplasm near the outer membrane, with 2  $\alpha$ -helical extensions termed the lever arm (~114-173) and the antennae projection (AP, ~285-335) (15, 24). In the TraF structure, the AP is depicted as forming an  $\alpha$ -helical pore at the outer membrane (15).

Mutational studies in our laboratory supplied evidence that the two membrane-spanning domains, the inner membrane TM domain and the presumptive outer-membrane-spanning AP, are critical for VirB10 function (24). While our deletion analyses have

established that both domains are essential for both substrate transfer and T-pilus production, certain mutations in these domains selectively abolished T-pilus biogenesis without blocking substrate transfer. V. Krishnamoorthy showed that a partial AP deletion conferred this phenotype, and I showed that an Ala-Cys insertion (i2) at residue 40 corresponding to the middle of the TM domain abolished T-pilus production (24). Moreover, i2 mutations at residues 35 and 45 conferred reduced levels of T-pilus without affecting substrate transfer (24). Our ability to isolate transfer-positive, pilus-minus ( $\text{Tra}^+, \text{Pil}^-$ ) “uncoupling” mutations is of considerable interest in that it establishes that this T4SS system mediates substrate transfer in the absence of detectable T-pili. More specifically, however, their isolation in the TM and AP domains suggests that both of these putative membrane-spanning regions of VirB10 contribute in distinct ways to channel and T-pilus assembly.

In this study, I focused on defining the mechanism of action of the VirB10 TM domain in mediating T-pilus biogenesis. My overarching hypothesis is that the VirB10 TM helix interacts with one or more TM helices and that such helix-helix contact(s) are critical for T-pilus assembly but not for substrate transfer. VirB10 TM helices might self-associate, forming homodimers or multimers, or form stable or transient interactions with membrane helices of other channel subunits. My proposal that the VirB10 TM domain multimerizes is supported by several observations. First, the recently published images of the pKM101 core complex obtained by cryoelectron microscopy and X-ray crystallography present evidence that 14 copies of TraF form the outer wall of the core channel (15, 16). Whereas the core complex X-ray structure identifies extensive contacts among  $\beta$ -barrel domains of adjacent TraF subunits, the cryoEM images also suggest that the PRR's and, possibly, the TM helices of adjacent TraF subunits interact (16). As discussed in Chapter 3, results of my disulfide crosslinking experiments support the idea that adjacent PRR's dimerize. The association of VirB10 TM helices might be important for stabilization of the core complex ring structure at the inner membrane.

Second, in the pKM101 core complex structure resolved by CryoEM, the diameter of the chamber interior at the inner membrane is  $\sim 55$  Å, a dimension of sufficient size to accommodate other VirB channel subunits (16). By use of a substrate trapping assay, our laboratory previously reported that two other inner membrane subunits, polytopic VirB6 and bitopic VirB8, form close contacts with translocating DNA substrates (17). If our model that the core complex houses the translocase is correct, both VirB6 and VirB8 should assemble within the core chamber at the inner membrane. It is reasonable to predict that the VirB10 helices

would interact with one or both of these subunits. As discussed further below, the VirB10 helices might also interact dynamically with the VirB2 pilin, or with other subunits, during early stages of T-pilus biogenesis.

Finally, on examination of the VirB10 TM domain sequence, I identified at least two possible dimerization motifs. The first is a GXXXXA (GA<sub>4</sub>) motif, which, like the similar GXXXG (GG<sub>4</sub>) motif, is a common dimerization motif among TM helices of membrane proteins (66-69). The second is a set of two Leu(Ile) zipper motifs which also have been shown to mediate dimer formation among soluble proteins as well as some eukaryotic and viral membrane proteins (70-74). Of interest, the 40.i2 mutation that selectively disrupts T-pilus biogenesis is positioned both within the GA<sub>4</sub> and Leu(Ile) zipper motifs; accordingly, this mutation might disrupt one or both of these interaction motifs.

In this study, I designed mutations to test for the contributions of putative dimerization motifs to VirB10 function. My findings support a model that one Leu zipper motif is important for assembly of T-pili. This motif, contributes to weak self-association of VirB10 TM helices.

## **Results**

### **The GA<sub>4</sub> dimer motif is dispensable for VirB10 function**

On the basis of my MPB labeling data, I predict the VirB10 TM domain spans residues ~30-50 (SQKLIVGGVVLALSLSLIWLG). This sequence, including the GA<sub>4</sub> motif, is highly conserved among VirB10 homologs identified in other members of the *Rhizobiaceae* (Figure 4-1). In fact, additional conserved residues form GG<sub>4</sub> or GA<sub>4</sub> dimer interfaces (LIXXGVXXG/AVXXT) (66, 75). In VirB10 and its close homologs, these additional residues (33-LIVGGVVLALSLS-45) are also present (Figure 4-1). In the well-characterized glycophorin A, this extended GG<sub>4</sub> motif has been shown to promote lateral interactions between adjacent TM domains (66, 76, 77).

To evaluate the importance of the GA<sub>4</sub> motif for VirB10 function, I introduced isoleucine (Ile) residue replacements to create steric clashes in the putative TM-TM packing interface (Figure 4-2). Elsewhere, it has been shown that corresponding mutations of GG<sub>4</sub> or GA<sub>4</sub> TM domains of GpA or other dimerizing proteins abolishes dimerization (26). These mutant proteins (G37I and A41I) were subsequently tested for effects on protein accumulation, substrate transfer and T-pilus biogenesis. Both GA<sub>4</sub> mutant proteins accumulated at abundant

levels when produced in a  $\Delta virB10$  strain, suggesting that the mutations do not affect protein stability (Figure 4-2). Additionally, the corresponding mutant strains produced abundant levels of T-pili as judged by detection of VirB2 pilin on the cell surface by colony immunoblotting and in high-molecular-weight material recovered by shearing of surface proteins and structures (Figure 4-2). I further tested for effects of the mutations on T-DNA transfer to *K.*

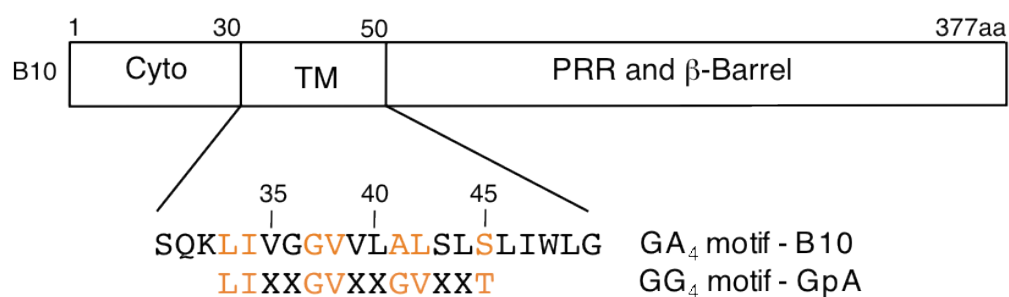
*diagremontiana* leaves with a virulence assay and conjugative transfer of a mobilizable IncQ plasmid to agrobacterial recipient cells (Figure 4-2). Overall, the mutant strains showed only a slight reduction in virulence and IncQ plasmid transfer as compared to the wild-type control strain. Given that these substitutions do not exert pronounced effects on the capacity of VirB10 to support either T-pilus production or substrate transfer, we conclude that this GA<sub>4</sub> motif is not a functionally important motif. Below, I provide additional evidence that the GA<sub>4</sub> motif does not contribute to formation of VirB10 TM-TM dimers.



**Figure 4-1 VirB10 TM aligned with GA<sub>4</sub> consensus motif and Pro Dom analysis**

- A. Diagram illustrating sequence similarity between VirB10 GA<sub>4</sub> motif and the glycoporphin A (GpA) GG<sub>4</sub> motif.
- B. Pro Dom analysis (78) (<http://prodom.prabi.fr/prodom.html>) identified sequence conservation among VirB10 homologs. Invariant residues are upper cased and red, residues of similar homology are lower cased and blue.

A



B

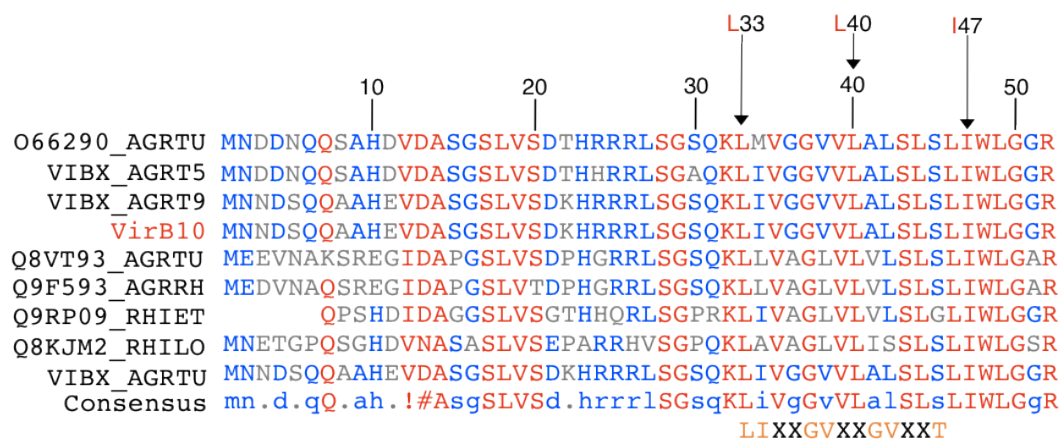
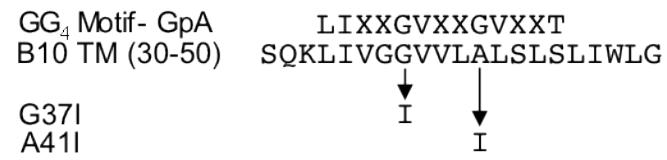


#### **Figure 4-2 Effects of GA<sub>4</sub> point mutations on protein function**

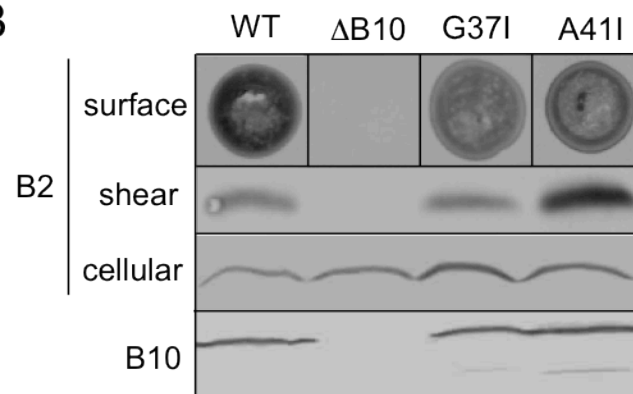
- A. Sequence alignment between the TM domain of VirB10, showing residues 30-50, and the consensus sequence for GG<sub>4</sub> motif. Downward arrows indicate residue position of isoleucine (Ile) replacements engineered in the TM domain of VirB10.
- B. From top, T-pilus production by strains producing the GA<sub>4</sub> mutant proteins. VirB2 surface blot assays, T-pilus isolation (shear) assays, total cellular levels for VirB2 and VirB10. Immunodetection was with anti-VirB2 or anti-VirB10 antibodies as indicated at left of the panel.
- C. Conjugative DNA transfer efficiencies and virulence data for infected *K. diagrammontiana* leaves are shown for listed strains. Conjugative IncQ plasmid transfer (white bars) frequencies are reported as the number of transconjugants per donor cell. Virulence (black bars) is reported in relation to WT (+++; WT virulence) and  $\Delta$ B10 ( - ; avirulent).

Strains: WT, A348;  $\Delta$ B10, PC1010; G37I and A41I, PC1010 producing VirB10 mutants with Ile substitutions at positions 37 and 41 in the TM domain.

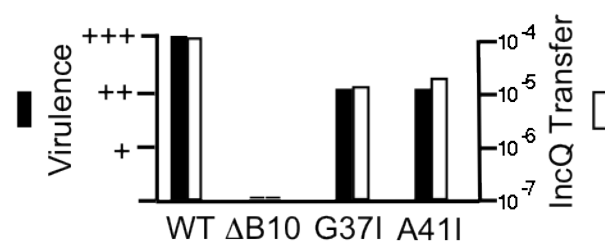
A



B



C



### **Mutations in TM leucine residues abolish T-pilus formation**

The VirB10 TM domain also has two putative Leu(Ile) zipper motifs, designated LZ1 (L33, L40, I47) and LZ2 (V35, L42, L49). Leu zippers have a characteristic Leu or Ile heptad motif  $(abcdefg)_n$  that forms an  $\alpha$ -helix TM-TM packing interface (79-81). Accordingly, a heptad wheel shows the two Leu clusters are situated on opposite faces of the  $\alpha$ -helix (Figure 4-3). In view of the pKM101 CryoEM images presenting evidence that TM domains of the VirB10-like TraF form a 14-membered ring structure at the inner membrane (16), I sought to test whether VirB10 might undergo lateral TM-TM packing interactions required for substrate transfer and/or T-pilus biogenesis.

I created single and triple Leu to Ala substitutions in the putative LZ1 and LZ2 motifs (Figure 4-4 and 4-5). All mutant proteins accumulated at abundant levels and there was little accumulation of proteolytic degradation products. Interestingly strains with LZ1 mutations elaborated reduced levels of T-pilus, as monitored by colony immunoblot and shear assays using anti-VirB2 antibodies. The L33A and L40A mutant strains accumulated detectable levels of extracellular VirB2 indicative of some T-pilus production, whereas VirB2 was barely or not detectable in the extracellular fractions from the I47A mutant and the triple Ala mutant (Figure 4-4). Together, these data indicate that the Leu residues comprising the putative LZ1 contribute in some way to T-pilus production (Figure 4-4).

In contrast to the effects of the Ala substitution mutations on T-pilus production, strains producing the L33A or L40A mutations exhibited wild-type levels of virulence on plants and interbacterial IncQ plasmid transfer (Figure 4-4). The I47A mutant strain also transferred the DNA substrates at near wild-type levels, although the triple Ala substitution mutant showed a reduction of ~2 orders of magnitude in IncQ plasmid transfer efficiencies (Figure 4-4). Even so, the triple mutant transferred DNA substrates well above background levels indicating that the putative LZ1 is not absolutely essential for assembly of a functional translocation channel.

I also tested for effects of Ala substitution mutations of the putative LZ2 motif (V35, L42, L49) (Figure 4-5). In contrast to the LZ1 analyses, the single and triple Ala substitution mutations exerted no discernible effects on VirB10 protein accumulation or the capacity of mutant strains to elaborate T-pili or transfer DNA substrates (Figure 4-5). These results indicate that the putative LZ2 motif (V35, L42, L49) does not contribute in detectable ways to VirB10 function.

**Figure 4-3 VirB10 TM aligned in a heptad repeat to identify possible Leu zippers**

Helical wheel diagram for the VirB10 TM sequence identifying two possible Leu zippers; LZ1 (L33, L40, I47; red) and LZ2 (V35, L42, L49; blue).

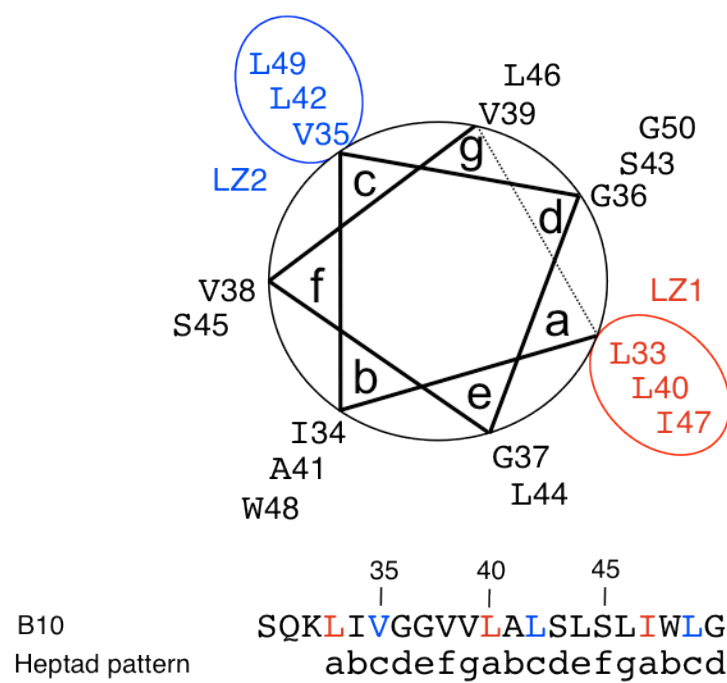


**Figure 4-4 Effects of Ala substitutions in the putative LZ1 motif (L33, L40, I47)**

- A. Sequence of the TM domain of native VirB10 from residues 30 to 50. Downward arrows indicate Ala substitutions.
- B. From top: T-pilus production by VirB2 surface and shear assays. Total cellular levels of VirB2 and VirB10. Development was with anti-VirB2 or anti-VirB10 antibodies as listed to the left of panel.
- C. DNA substrate transfer efficiencies and virulence data. Conjugative IncQ transfer (white bars) is presented as the number of transconjugants per donor cell. Virulence (black bars) is reported on a scale ranging from WT virulence (three pluses) to avirulent (minus sign).

Strains: WT, A348;  $\Delta$ B10, PC1010; PC1010 producing mutant proteins as listed.



A

Heptad pattern  
B10 TM (30-50)

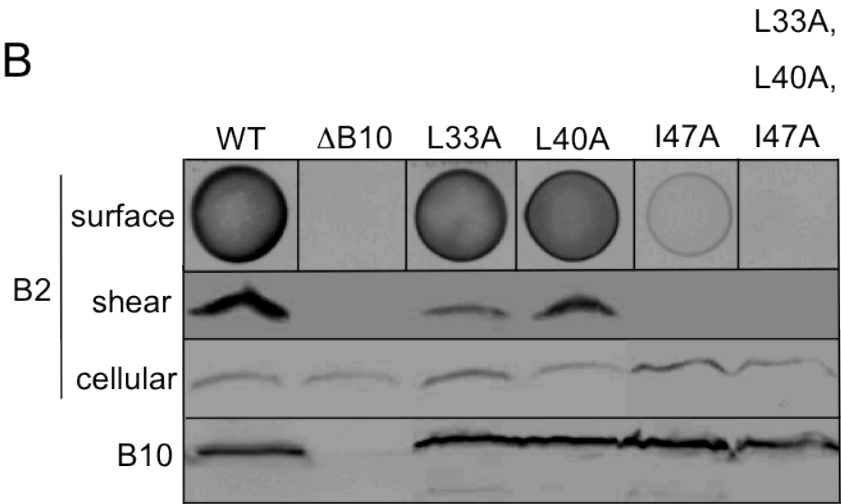
abcde f g a b c d e f g a b c d  
S Q K L I V G G V V L A L S L S L I W L G

↓ A ↓ A ↓ A

L33A  
L40A  
I47A  
L33A, L40A, I47A

A A A

B



C

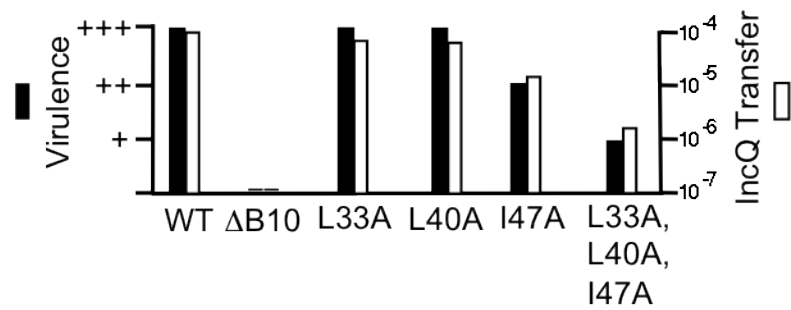
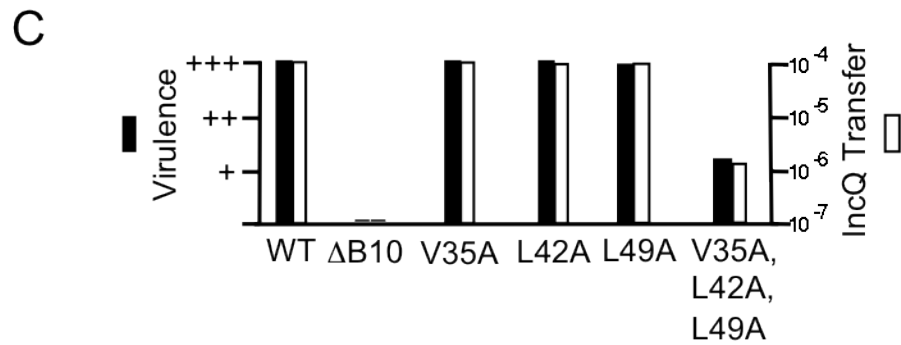
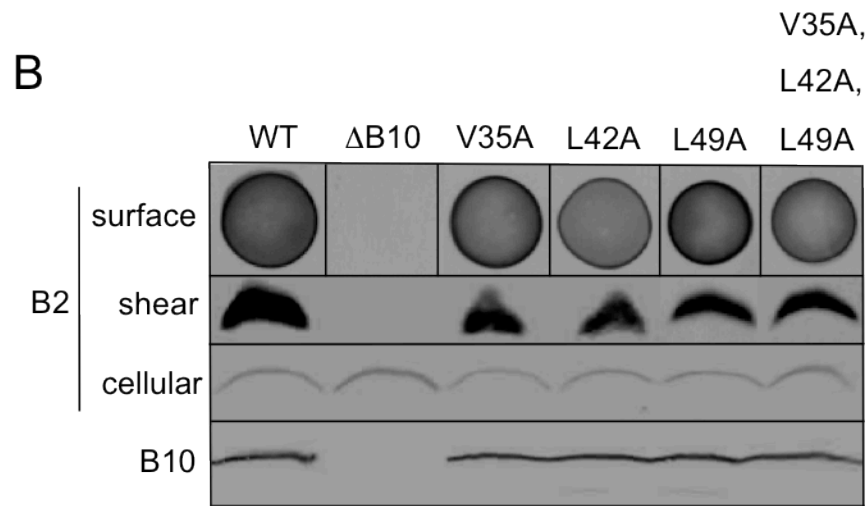
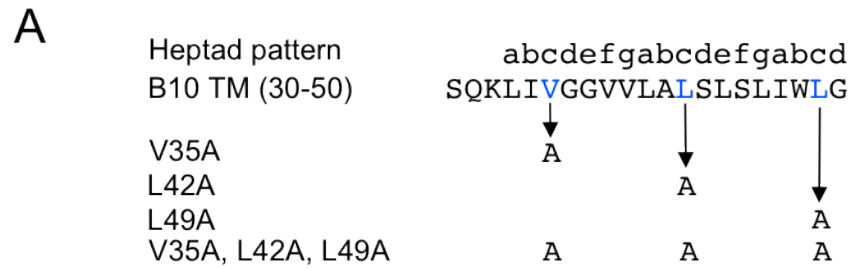


**Figure 4-5 Effects of Ala substitutions in the putative LZ2 motif (V35, L42, L49)**

- A. Sequence of the TM domain of wild type VirB10 (residues 30 to 50). Downward arrows indicate positions of Ala substitution(s)
- B. From top: T-pilus production by VirB2 surface and shear assays. Total cellular levels of VirB2 and VirB10. Immunoblots were developed with anti-VirB2 or anti-VirB10 antibodies as listed to the left of panel.
- C. DNA substrate transfer efficiencies and virulence data. Conjugative IncQ transfer (white bars) is presented as the number of transconjugants per donor cell. Virulence (black bars) is reported on a scale of three pluses for wild-type virulence to a minus sign for avirulence.

Strains: WT, A348;  $\Delta$ B10, PC1010; PC1010 producing mutant proteins as listed.



### **VirB10 TM domain substitutions: an FtsN TM domain swap**

The above findings suggest that the putative LZ1 motif, but not the GA<sub>4</sub> or LZ2 motifs, contributes to VirB10 function. The LZ1 Ala substitution mutations disrupted T-pilus biogenesis and the triple Ala mutation also conferred diminished substrate transfer. To test a model that the putative LZ1 motif might participate in assembly of TM-TM helix homo- or heterodimers required for protein function, I constructed two TM domain swaps. The first involved replacement of the VirB10 TM domain with that of a heterologous TM domain that retains a putative LZ1 zipper motif but differs in other residues. This was achieved by replacing residues 35-50 of VirB10 with the corresponding region of the bitopic protein FtsN. FtsN functions in stabilization of FtsZ and other subunits of the divisome at the site of cell division (82). FtsN derivatives bearing substitutions of its TM and N-terminal cytoplasmic domains with corresponding domains from heterologous bitopic proteins were reported to function in cell division (83), although a more recent study provided genetic evidence for the involvement of one or both FtsN domains for divisome assembly (84).

The chimeric VirB10 TM domain is composed of a putative LZ1 motif (L33, L40, L47) which as shown for native VirB10 forms a poly Leu face in a helical wheel representation (Figure 4-3). The VirB10/FtsN<sub>TM</sub> chimeric protein accumulated at abundant levels, although a proteolytic breakdown product of ~40 kDa that is occasionally detected with the native protein was also abundant (Figure 4-6). Nevertheless, the chimeric protein supported near wild-type levels of T-pilus production as monitored by both colony immunoblot and shear assays. Of, further interest, VirB10/FtsN<sub>TM</sub> also supported wild-type levels of substrate transfer as monitored by virulence on plants (Figure 4-6).

I next sought to determine if the putative LZ1 motif is responsible for the functionality of the VirB10/FtsN<sub>TM</sub> chimeric protein. Two mutant proteins were constructed, one with a Leu47Ala substitution and a second with Ala substitutions at Leu33, Leu40, and Leu47 (Figure 4-6). A poly Ala face that is unlikely to mediate TM-TM dimerization replaced the poly Leu face in the helical wheel representation. Both mutant proteins accumulated to abundant levels, but again the 40-kDa degradation product was also detected. Surprisingly, strains producing the mutant proteins elaborated T-pili and were virulent on plants (Figure 4-6). In general, the levels of T-pilus production and substrate transfer approximated levels observed with the VirB/FtsN<sub>TM</sub>-producing strain.

These findings would appear to argue against the importance of a Leu zipper motif for VirB10 function. However it is possible that the FtsN<sub>TM</sub> concurrently introduced an unidentified dimerizing element that is independent of the putative Leu zipper within the TM sequence. This might explain the observed complementation in VirB10 protein function.

Interestingly, the substitution of the entire N-terminal region of FtsN, including its short cytoplasmic domain and TM sequence, for the corresponding domains of VirB10 completely abolished protein function (Figure 4-6: panel D).

**Figure 4-6 FtsN TM domain substitutions**

- A. Helical wheel diagrams for VirB10/FtsN<sub>TM</sub> derivatives. In red are residues of the atypical leucine zipper.
- B. Sequences for both wild type VirB10 and FtsN<sub>TM</sub> derivatives.
- C. and D. VirB2 surface and T-pilus shear assays. Total cellular levels of VirB2 and VirB10 are included (Bottom panel). Virulence is indicated on a scale of three pluses for wild-type virulence to a minus sign for avirulence.







Strains: WT, A348;  $\Delta$ B10, PC1010; FtsN TM substitutions, PC1010 producing VirB10 FtsN TMs; FtsN Cyto TM substitution, PC1010 producing VirB10 FtsN Cyto TM. Cyto, cytoplasmic domain, TM, transmembrane domain.

Heptad pattern  
B10 TM (30-50)  
B10/FtsN<sub>TM</sub>

                abcde f g abcde f g abcd  
S Q K L I V G G V L L A S L S L I W L G  
S Q K L I V A A A V L V T F I G G L Y F I

                ↓                    ↓                    ↓  
B10/FtsN<sub>TM</sub> L47A   A  
B10/FtsN<sub>TM</sub> L33A, L40A, L47A           A                         A                         A

		B10/FtsN <sub>TM</sub>				
		WT	ΔB10	L33A, L40A, L47A	L47A	L47A
B2	surface					
	shear					
	cellular					
	B10					
Virulence		+++	-	++	++	++

	$\Delta$ B10	WT	B10/FtsN <sup>Cyto TM</sup>
B2 surface			
B10			
Virulence	-	+++	-

### **VirB10 TM domain substitutions: poly Leu-Ala TM domain swaps**

To complement the above approach, I devised a strategy aimed at identifying residues in the VirB10 TM domain that are required for function. I created a synthetic TM domain comprised of alternating Leu and Ala residues. Previous studies have shown that a poly-Leu/Ala (pLA) TM sequence forms a stable membrane  $\alpha$ -helix, but one that does not interact with other TM helices (85). Poly-LA TM substitutions have been used previously to define TM helix contributions to protein function (86-88). I constructed and analyzed the phenotypic consequences of pLA substitutions of VirB10 TM domain residues 27-50 and 33-50 (Figure 4-7). For the latter substitution, I also created swaps with and without Trp48. A corresponding Ala substitution of Trp48 in the TM domain of native VirB10 was also constructed. The rationale for testing the importance of Trp48 was that aromatic residues associated with TM domains tend to sit at the membrane – aqueous interface and help stabilize and orient the  $\alpha$ -helix in the membrane (89, 90). I reasoned that Trp48 might influence the functionality of the VirB10 TM domain as well as the pLA swap.

The VirB10/pLA<sub>27-50</sub> and VirB10/pLA<sub>33-50</sub> mutant proteins accumulated at abundant levels as a 48-kDa species corresponding in size to native VirB10 (Figure 4-7). A ~40-kDa degradation product also accumulated at abundant levels, suggestive of an effect of the pLA swaps on protein stability (Figure 4-7). The VirB10/pLA<sub>33-50</sub> mutant containing Trp48 accumulated almost exclusively as the 48-kDa species, further suggesting that Trp48 stabilizes the pLA mutant proteins possibly as a topogenic signal. Regardless of the presence of Trp48, however, strains producing the pLA mutant proteins failed to accumulate detectable levels of extracellular VirB2 indicative of a defect in T-pilus production (Figure 4-7). By contrast, all three mutant strains were transfer proficient, as shown by the capacity to infect plants and transfer the IncQ plasmid to agrobacterial recipients. The mutant strains transferred substrates at diminished levels in comparison to strains producing native VirB10; nevertheless, the Tra<sup>+</sup> phenotype firmly establishes that a nondimerizing pLA  $\alpha$ -helix suffices for elaboration of a functional translocation channel (Figure 4-7).

The W48A substitution in the context of the VirB10 TM domain did not disrupt protein function (Figure 4-7). The mutant protein accumulated predominantly as the 48-kDa species and the corresponding mutant strain accumulated abundant levels of extracellular VirB2 pilin indicative of T-pilus production. The W48A mutant strain also delivered DNA substrates to plants and other agrobacteria (Figure 4-7). Trp48 of native VirB10 thus appears to be dispensable for proper insertion of the native TM domain into the membrane.



**Figure 4-7 poly-LA (poly Leu-Ala) TM substitutions**

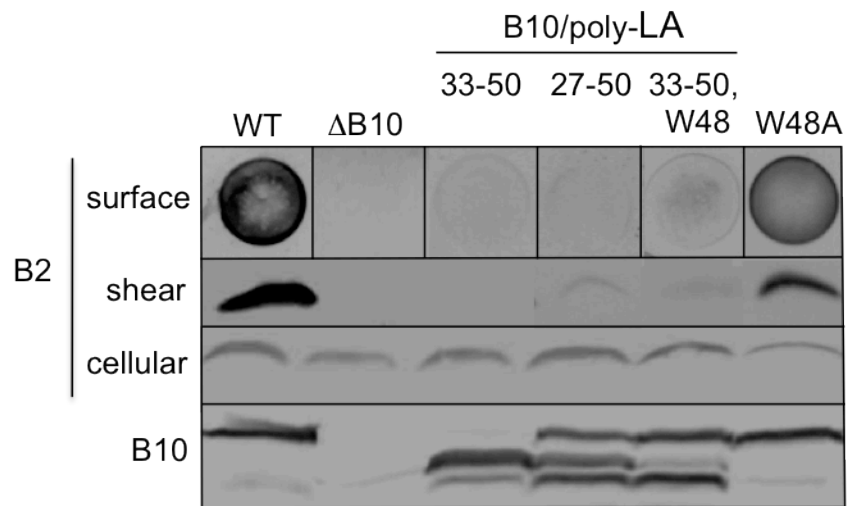
- A. Native VirB10 sequence, poly-Leu/Ala (pLA) substitutions, and W48A substitution.
- B. Extracellular VirB2 as monitored with surface and shear assays. Total cellular levels of VirB2 and VirB10 detected by SDS-PAGE and immunostaining with anti-VirB2 and anti-VirB10 antibodies.
- C. DNA substrate transfer as monitored by virulence on plants and mobilization of an IncQ plasmid to agrobacterial recipients. Conjugative IncQ transfer (white bars) is presented as the number of transconjugants per donor cell. Virulence (black bars), reported on a scale of 3 pluses (+) to a negative sign (-) for avirulence.

Strains: WT, A348;  $\Delta$ B10, PC1010; PC1010 producing VirB10/pLA TMs or W48A.

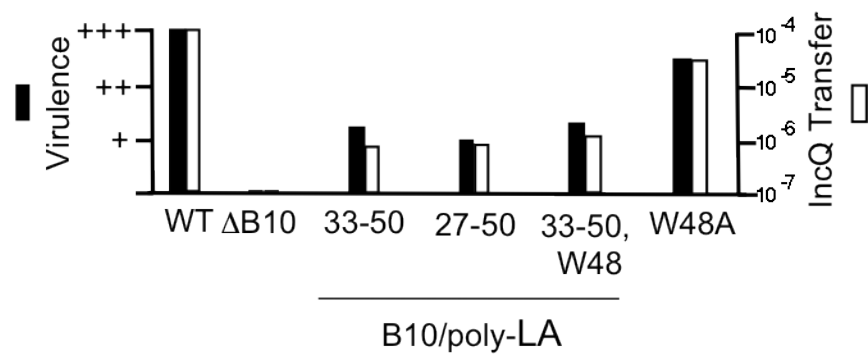
A

B10 TM (25-50)	RRLSGSQK <b>L</b> IVGGVV <b>L</b> ALSLSL <b>I</b> WLG
B10/poly-LA <sub>33-50</sub>	SQK <b>L</b> ALALALALALALAL <b>L</b> ALA
B10/poly-LA <sub>27-50</sub>	RRLALALAL <b>L</b> ALALALALALALAL <b>L</b> ALA
B10/poly-LA <sub>33-50,W48</sub>	SQK <b>L</b> ALALALALALALAL <b>L</b> WLA
W48A	SQK <b>L</b> IVGGVV <b>L</b> ALSLSL <b>I</b> ALG

B



C



## **Introduction of conserved residues in the VirB10 poly-LA TM domain restores T-pilus production**

Next, I sought to identify minimal changes in the pLA TM sequence that would restore the capacity of host cells to assemble T-pili. VirB10 subunits of T4SS elaborated by members of the *Rhizobiaceae* contain several invariant residues in their TM domains, including Val39, Leu40, Ser43, and Leu44 (Figure 4-1). Leu40 is within the putative LZ1 that might be important for T-pilus production (see Figure 4-4). Therefore, I first substituted Leu for Ala40 (bold) within the S<sub>30</sub>QKLALALALA<sub>40</sub>LALALALWLA<sub>50</sub> TM sequence. I also substituted Val39, Leu40, Ser43, and Leu44 for the Ala or Leu residues at the corresponding positions (above, underlined) of the pLA sequence.

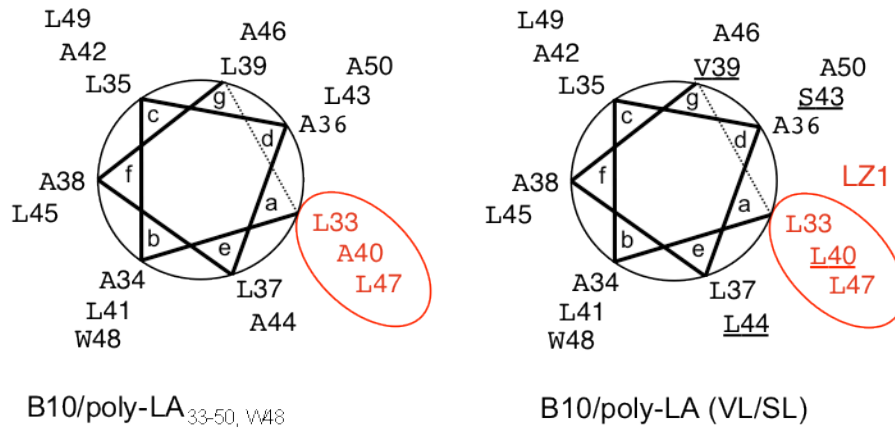
The mutant proteins bearing the pLA (L40) and pLA (VL/SL) substitutions accumulated at abundant levels and the latter mutant protein also showed appreciably lower amounts of the degradation products suggestive of enhanced protein stability (Figure 4-8). Very interestingly, strains producing either of the derivatized pLA sequences elaborated T-pilus as deduced from the detection of extracellular VirB2 pilin with colony (surface) blot and shear assays. The pLA (VL/SL) and pLA (L40) mutant proteins also supported substrate transfer at approximately the same levels as the parental pLA mutant as shown with the plant virulence assay (Figure 4-8). These findings show that the substitution of only one residue, Leu40, in the pLA TM sequence was sufficient for restoration of T-pilus formation to abundant levels.

**Figure 4-8 Introduction of conserved residues into a poly-LA TM domain restores T-pilus production**

- A. Helical wheel diagrams for VirB10/poly-LA derivatives.
- B. Schematic showing native VirB10 sequence, the pLA TM domain, and locations of residues conserved among VirB10 homologs that were introduced into the pLA sequence
- C. Extracellular VirB2 as monitored with surface and shear assays. Total cellular levels of VirB2 and VirB10 detected by SDS-PAGE and immunostaining with anti-VirB2 and anti-VirB10 antibodies. Virulence is indicated on a scale of three pluses for wild-type virulence to a minus sign for avirulence.

Strains: WT, A348;  $\Delta$ B10, PC1010; PC1010 producing VirB10/pLA TM derivatives as listed.

A



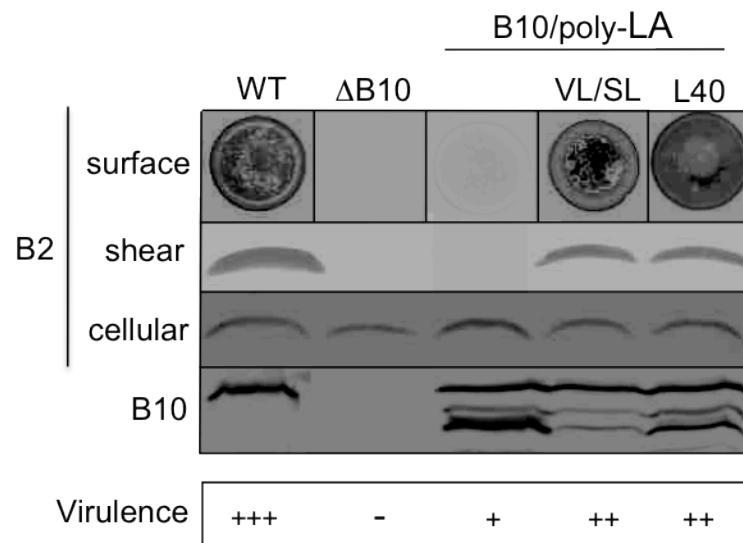
B

B10 TM (30-50)  
 B10/poly-LA<sub>33-50, W48</sub>  
 B10/poly-LA (VL/SL)  
 B10/poly-LA (L40)

SQK**L**IVGGV**V**LALSLSL**I**WL**G**  
 SQK**L**ALALALALALALAL**L**WL**A**

↓ ↓   ↓ ↓  
 VL   SL  
 L

C



## **VirB10 TM domain weakly self-associates**

The above findings suggest that a putative Leu zipper (LZ1) marked by Leu(Ile) residues at positions 33, 40, and 47 of the VirB10 TM domain contributes to assembly of T-pili. By contrast, a nondimerizing pLA TM helix suffices for elaboration of a functional translocation channel. I envisioned that the putative LZ1 motif might mediate formation of TM-TM helix homo- or heterodimers required for T-pilus biogenesis. Homomultimerization is consistent with results of early yeast two-hybrid experiments providing evidence for self-association of the N-terminal third of VirB10 (21). Additionally, as noted above, the N-terminal regions of the 14 copies of TraF in the pKM101 core complex appear to assemble as a ring as judged by CryoEM microscopy (16). Interactions among the N-terminal TM domains might serve to stabilize the core ring at the inner membrane. Alternatively – or additionally – the TM domains might interact stably or dynamically with other VirB channel subunits to promote assembly or dynamic activity of the inner membrane translocase.

I first assayed for VirB10 TM domain self-association by use of TOXCAT, a reporter assay developed for quantifying TM self-association within membranes (26). In TOXCAT, a chimeric protein is constructed in which a TM sequence of interest is introduced between cytoplasmic ToxR, which functions as a transcriptional activator only as a homodimer, and periplasmic maltose binding protein (MBP). If two fusion proteins are brought into physical juxtaposition due to self-interaction of the TM domains, the ToxR monomers assemble to form homodimers that can then activate expression from a *ctx* promoter. This promoter is engineered to direct transcription of a gene for chloramphenicol acetyltransferase (CAT) (26, 91). Therefore, quantification of CAT activity in lysates of cells expressing these fusion proteins serves in direct measure of TM self-association. Proper orientation of the fusion protein across the cytoplasmic membrane can be confirmed by assaying for growth of *E. coli* MM39 cells on maltose-containing plates (26, 91).

In setting up the TOXCAT assay, I used the glycophorin A TM domain as a positive control; this domain has been shown to strongly self-associate through the GXXXG dimerization motif (26). Additionally, the GpA TM domain bearing the G83I mutation served as a negative control as this mutation abolishes GXXXG-mediated dimerization (26). Assays were carried out in the *E. coli* *malE* mutant strain MM39 (see Materials and Methods). This strain fails to metabolize maltose in the absence of a ToxR-TM-MBP fusion protein that is properly oriented across the cytoplasmic membrane. With TOXCAT, I confirmed that cells expressing the gene for ToxR-GpA<sub>TM</sub>-MBP accumulated abundant levels of the fusion protein,

grew on maltose containing plates, and possessed high levels of CAT activity suggestive of strong dimerization (Figure 4-9 and 4-10). Cells expressing the gene for the GpA<sub>TM</sub> fusion protein bearing a G83I mutation also accumulated abundant levels of the fusion protein and grew on maltose, but possessed only very low levels of CAT activity (< 5% of that for the unmutated TM domain) suggestive of no or very weak dimerization (Figure 4-9 and 4-10).

Given that the VirB10 TM domain possesses a GA<sub>4</sub> motif as well as two potential Leu zipper motifs, I had anticipated that this TM domain would strongly self-associate. On the contrary, although cells accumulated abundant levels of the fusion protein and grew on maltose, these cells exhibited only ~20% of the activity of cells producing the GpA<sub>TM</sub> fusion protein (Figures 4-9 and 4-10). In several repetitions of these experiments, however, CAT activity levels were routinely higher in cells producing the VirB10<sub>TM</sub> versus the GpA<sub>TM</sub>(G83I) fusion proteins (Figure 4-10). The VirB10 TM domain thus appears to self-associate but only weakly compared to the GpA TM domain in the context of a TOXCAT fusion protein produced in *E. coli*.

I next sought to determine whether the possible dimerization motifs in the VirB10 TM domain promote self-association. I introduced variant TM domains bearing mutations of interest (Figure 4-10). As with the fusion protein bearing the native TM domain, proteins with mutant TM domains accumulated at abundant levels, and cells grew on maltose suggestive of proper orientation of the mutant proteins across the membrane (Figure 4-9 and 4-10). I normalized CAT activity of cells producing the VirB10<sub>TM</sub> fusion protein to 100, and reported CAT activities of cells producing the mutant derivatives as a percentage of that value (Figure 4-10). Recall that *A. tumefaciens* strains producing VirB10 mutants with i2 mutations at positions 35 and 45 in the TM domain were Tra<sup>+</sup>, Pil<sup>Att</sup>, whereas a strain with an i2 mutation at residue 40 was Tra<sup>+</sup>, Pil<sup>-</sup> (24). In *E. coli*, production of the 35.i2 or 40.i2 mutant fusion proteins yielded CAT activity at levels of 40 – 50% that of the unmutated construct (Figure 4-10). However, production of the 45.i2 mutant TM domain yielded CAT activity at WT levels. Additionally, Ala substitutions of L33, L40, and I47 also resulted in a reduction by more than 40% in CAT activity compared to the unmutated VirB10<sub>TM</sub> fusion protein (Figure 4-10). In *A. tumefaciens*, the corresponding VirB10 mutant protein failed to support T-pilus production. It is noteworthy that the 40.i2 mutation shown to abolish T-pilus production in *A. tumefaciens* would disrupt the heptad register of Leu(Ile) residues comprising the putative LZ1 motif. These correlative effects of the 40.i2 mutation and LZ1 Ala substitutions on TM dimer formation and

T-pilus production are compatible with a model that weak self-association of the VirB10 TM is important for T-pilus biogenesis.

I further examined the effects of mutations in the GA<sub>4</sub> and LZ2 motifs on TM self-association. Consistent with their lack of phenotypes in substrate transfer and T-pilus production assays in *A. tumefaciens*, the Ile substitutions of G37 and A41 in the GA<sub>4</sub> motif did not disrupt TM-TM dimerization as monitored by TOXCAT (Figure 4-10). The Ala substitutions of V35, L42, and L49 of the putative LZ2 motif also neither affected VirB10 function in *A. tumefaciens* nor TM-TM self-association in *E. coli*.

Overall, these findings suggest that VirB10 homomultimerization might be selectively important for T-pilus formation but not for substrate transfer. To further test this idea I used TOXCAT to assay for dimerization of proteins with poly Leu-Ala (pLA) TM sequences. Recall that VirB10 with a pLA TM sequence conferred a Tra<sup>+</sup>, Pil<sup>-</sup> phenotype in *A. tumefaciens*, and that substitution of Leu40 (L40) and Val39, Leu40, Ser43, and Leu44 (VL/SL) in the pLA sequence restored T-pilus production. I hypothesized that the pLA (W48) sequence lacks stable TM-TM interactions needed for multimerization and the L40 and VL/SL derivative proteins might restore T-pilus formation by concurrently restoring TM-TM self-association. To test this hypothesis, I introduced these TM sequences into TOXCAT. These proteins, like the pLA(W48) fusion protein, supported growth of MM39 on maltose minimal media confirming a correct topology (Figure 4-9). The pLA(W48) and L40 derivatives both supported abundant protein accumulation, however, the VL/SL derivative also showed significant degradation (Figure 4-11). The pLA (W48) sequence in TOXCAT yielded a very low CAT activity similar to the nondimerizing GpA(G83I) negative control (Figure 4-11). This is in agreement with a TM sequence lacking a dimerizing interaction. Poly-LA sequences containing the conserved residues L40 and VL/SL, yielded TOXCAT fusion proteins that conferred slightly higher CAT activity values relative to the nondimerizing GpA(G83I) and pLA fusion proteins (Figure 4-11). However, CAT activity levels exhibited by these pLA derivatives were still low, preventing firm conclusions regarding the role of the LZ1 motif for self-association.



**Figure 4-9 Growth of MM39 cells expressing ToxR-B10<sub>TM</sub>-MBP proteins on maltose minimal media**

MM39 (*malE*) cells expressing ToxR-B10<sub>TM</sub>-MBP were streaked on 0.4% maltose M9 minimal media plates and tested for growth at 37°C for 2 days. Cell viability indicates a topology in which the maltose-binding domain is periplasmic.

Strains: MM39, empty vector; pMal-p2 and -c2, + and – control; GpA, strong dimerizing control; GpA(G83I), nondimerizing control; B10 and listed mutations, native and mutagenized TM sequences introduced into the TOXCAT vector, pccKan, expressed in MM39.

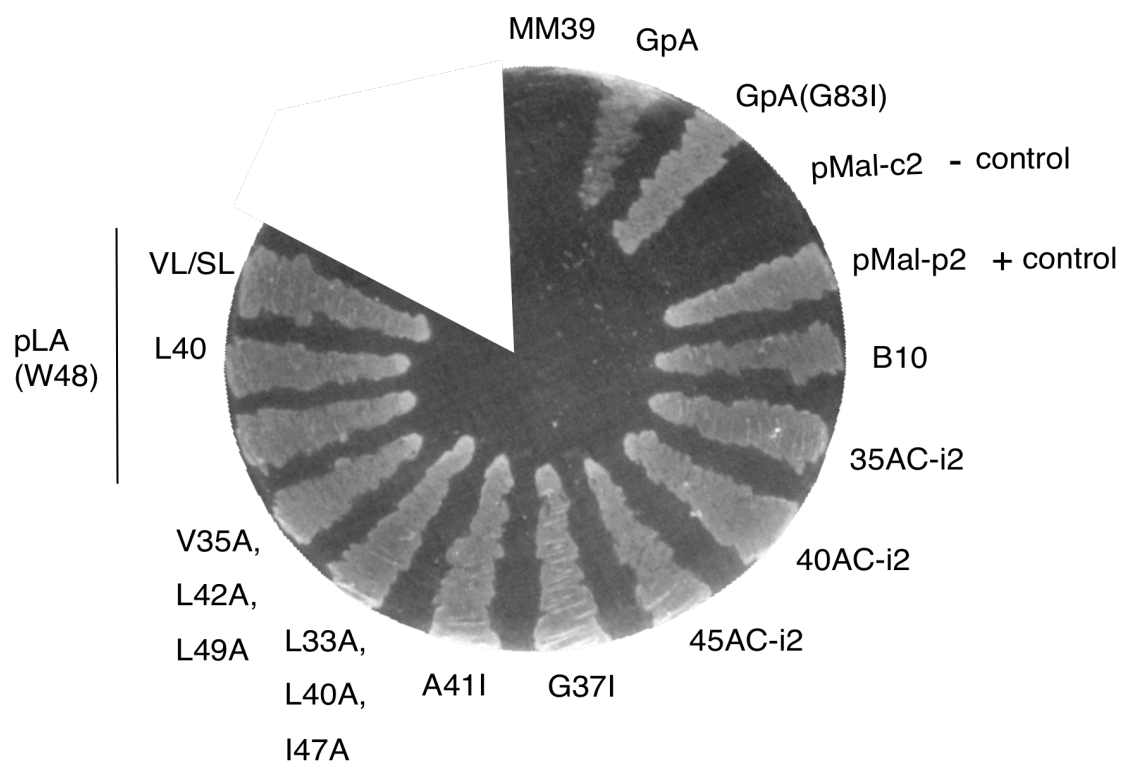
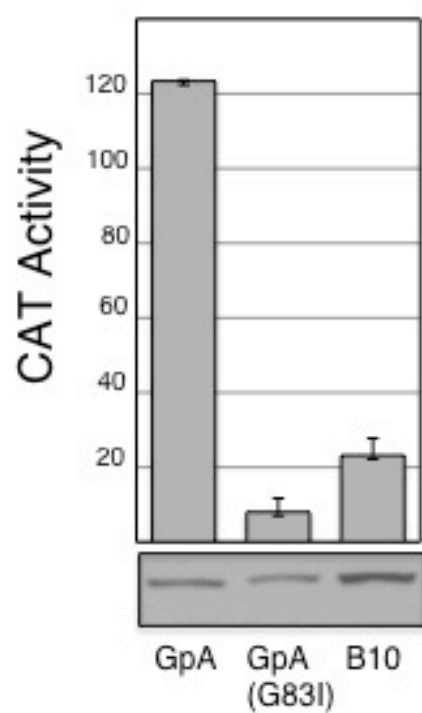


**Figure 4-10 Quantification of CAT activity from cell lysates expressing ToxR-B10<sub>TM</sub>-MBP fusion proteins**

- A. Quantification of CAT activity for cells synthesizing fusion proteins with the TM sequences of GpA, the nondimerizing GpA(G83I) mutant, and native VirB10. Bottom: western blot analysis of whole cell extracts.
- B. Quantification of CAT activity for cells synthesizing fusion proteins with native and mutant VirB10 TM sequences. CAT activities are normalized to that of cells synthesizing the TOXCAT reporter with the native VirB10 TM domain.

Strains: GpA, strong dimerizing control; GpA(G83I), nondimerizing control; *E. coli* MM39(*malE*) producing the TOXCAT reporter with native and mutant VirB10 TM sequences as listed.

A



B

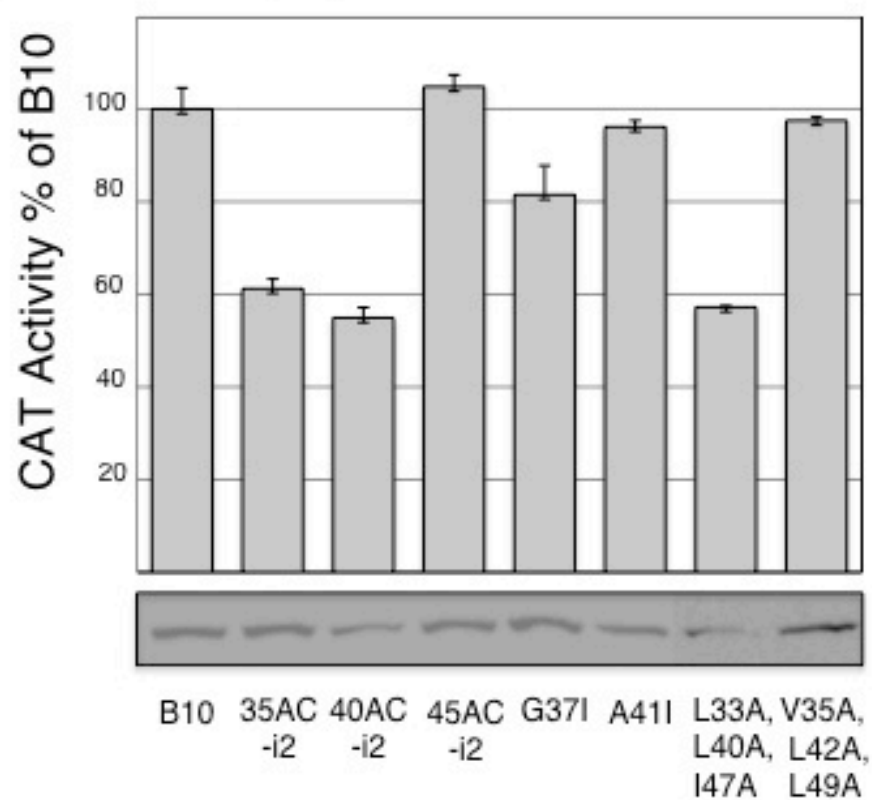
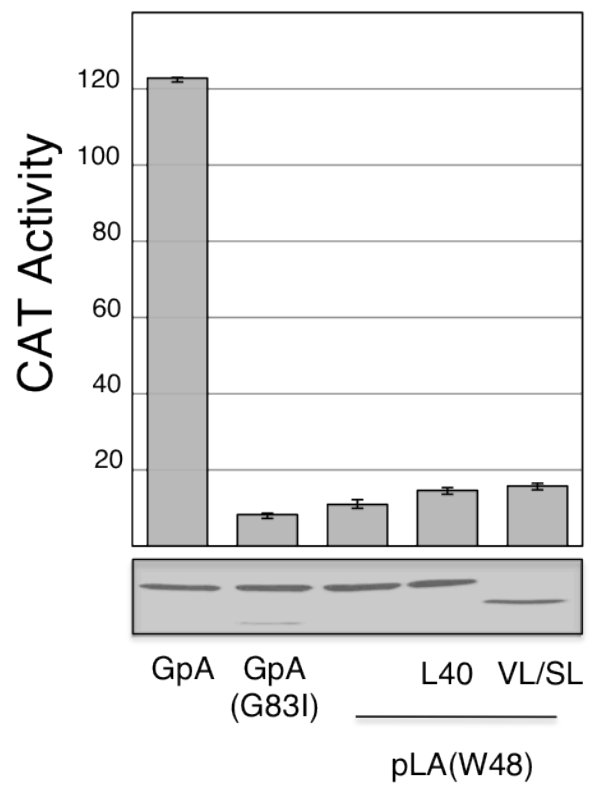


### **Figure 4-11 TOXCAT with poly-LA sequences**

Quantification of CAT activity for cells synthesizing fusion proteins with the TM sequences of GpA, the nondimerizing GpA(G83I) mutant, and various pLA sequences. Bottom: western blot analysis of whole cell extracts.

Strains: GpA, strong dimerizing control; GpA(G83I), nondimerizing control; *E.coli* MM39 (*malE*) producing the TOXCAT reporter with various pLA sequences as listed.



### **VirB10 TM domain mutations do not disrupt outer membrane channel gating**

The above findings suggest that the VirB10 TM domain self-interacts although weakly compared with the GpA TM domain. Mutations in the putative LZ1 motif diminish self-association, and this might account for the associated  $\text{Pil}^-$  phenotype in *A. tumefaciens*. However, another possible explanation for the block in T-pilus production is that the LZ1 motif mediates formation of VirB10 heterodimers with another channel subunit in *A. tumefaciens*. Candidate partner proteins include the bitopic or polytopic VirB subunits VirB2, VirB3, VirB4, VirB6, or VirB8, or the substrate receptor VirD4. Deciphering the nature of the possible heteromeric TM-TM helix interactions involving VirB10 is beyond the scope of this study. However, earlier studies in the Christie laboratory provided evidence that VirB10 regulates formation or gating of the distal portion of the translocation channel near or across the outer membrane in response to sensing of ATP energy use by the cytoplasmic membrane ATPases VirD4 and VirB11 (20). Consistent with this earlier work, recently our collaborator, Dr. L. Banta at Williams College, isolated a VirB10 mutation, G272R, that confers the nonspecific release of the VirE2 secretion substrate to the extracellular milieu. This mutation appears to lock VirB10 in an energy-activated conformation so that substrates are delivered across the outer membrane even in the absence of target cell contact. Interestingly, the G272R mutation does not affect substrate transfer to target cells, but it does block T-pilus biogenesis (L. Banta, personal communication).

I hypothesized that the TM domain mutations conferring the  $\text{Pil}^-$ ,  $\text{Tra}^+$  phenotype might phenocopy the G272R mutation in causing release of secretion substrates to the extracellular milieu. Mechanistically, this could occur if the TM domain mutations disrupt interactions with one or more of the energizing ATPases. To test this possibility, I assayed for surface display of a FLAG-epitope tagged VirE2 substrate, which was shown by the Banta laboratory to be released in the G272R mutant strain. By use of a colony immunoblot assay, Jennifer E. Kerr and I confirmed that *A. tumefaciens* producing the G272R mutant protein releases FLAG-VirE2 to the cell surface, whereas strains producing native VirB10 do not release this secretion substrate (Figure 4-12). Interestingly, strains producing the VirB10 TM mutant proteins conferring the  $\text{Tra}^+$ ,  $\text{Pil}^-$  phenotype (40.i2, triple Ala-substituted LZ1, pLA) showed no release of FLAG-VirE2 (Figure 4-12). Similarly, strains with other TM mutations (FtsN swap, triple Ala-substituted LZ2) also did not release the FLAG-VirE2 substrate at detectable levels. These findings suggest that the VirB10 TM domain mutations do not act indirectly on outer membrane channel activity or integrity, but instead block T-pilus production at an earlier step in the biogenesis pathway.

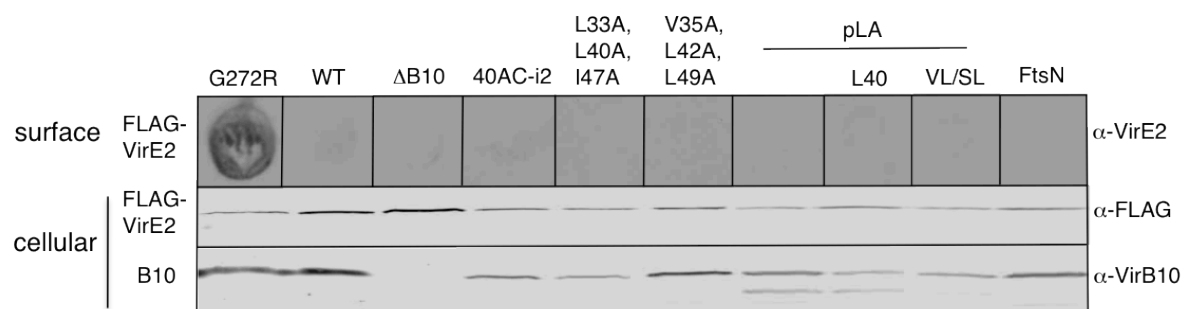
**Figure 4-12 Outer membrane gating defect assay (release of FLAG-VirE2 substrate)**

Surface colony assay monitoring the release of FLAG-VirE2. Equivalent *vir*-induced cells were spotted on ABIM inducing media plates, and allowed to grow for 3 days. Surface proteins from induced colonies were transferred to nitrocellulose membranes and incubated with an anti-VirE2 antibody (Top panel). Induced cells were also tested for cellular levels of FLAG-VirE2 and VirB10 by western blot analysis (Bottom panel).

Strains: WT, A348;  $\Delta$ B10, PC1010; VirB10 mutations, PC1010 carrying VirB10 with listed mutations.

The G272R mutation was isolated and characterized by L. Banta at Williams College.





## Discussion

In this study, I explored the contributions of putative dimerization motifs in the VirB10 transmembrane (TM) sequence for TM self-association, and T4SS channel activity and T-pilus biogenesis. One of the most interesting findings from my work is that substitutions of the TM domain for heterologous transmembrane sequences, including the FtsN TM domain and a synthetic pLA sequence, do not abolish substrate transfer. Although it is formally possible that the FtsN TM domain could mediate assembly of dimers required for VirB10 function through interactions motifs that are not defined at this time, previous findings established that the pLA TM sequence does not dimerize (86, 87, 92). On the basis of these findings, I conclude that VirB10 requires only a TM membrane anchor, not TM-mediated homo- or heteromeric contacts, for assembly of a functional translocation channel.

The lack of sequence specificity of the VirB10 TM domain for substrate transfer is of interest in view of data from the Christie laboratory and other groups that VirB10-like proteins interact with VirD4-like substrate receptors (48, 52, 53). These substrate receptors typically have two N-terminal TM domains with a short, intervening loop located in the periplasm. A crystal structure of one substrate receptor, TrwB of the plasmid R388 conjugation system, presented as a homohexameric sphere with a central channel (93, 94). The N-terminal TM domain was modeled as a stem-like projection extending from the sphere across the inner membrane (95). Two-hybrid studies localized the regions involved in the interaction between homologs of VirB10 and VirD4 to their N-terminal halves, leading to a proposal that these proteins might interact via their TM domains (52, 53). Although this has not been tested directly, a recent mutational analysis further identified mutations in the TM domains of VirB10-like and VirD4-like subunits that resulted in stronger interactions in a two-hybrid screen (96). These findings led to a proposal that substrate receptors interact with T4SS core complexes via TM-TM domain interactions (96). However, my findings that heterologous TM domains, including a monomeric pLA TM sequence, functionally substitute for the VirB10 TM domain for substrate transfer argue strongly that the TM domain does not by itself mediate the VirB10 – VirD4 interaction. It is noteworthy that I found that the substitution of the entire N-terminal region of FtsN, including its short cytoplasmic domain and the TM sequence, for the corresponding domains of VirB10 completely abolished protein function (Figure 4-6). Moreover, VirB10 deleted of both of these N-terminal domains does not form an immunoprecipitable complex with VirD4 (24). Together, these data suggest that the N-terminal cytoplasmic domain of VirB10 might mediate VirD4 partner binding and that VirB10 TM

domain acts only indirectly on VirD4 complex formation. Future studies will examine this possibility.

VirD4 is not required for T-pilus biogenesis (97). Therefore, it is not surprising that 2-residue insertion mutations in the VirB10 TM domain that selectively blocked T-pilus biogenesis did not disrupt formation of a precipitable VirB10-VirD4 complex (24). While the role of the VirB10 TM domain in T-pilus biogenesis is not completely defined, my findings did identify contributions of putative dimerization motifs. A GA<sub>4</sub> motif, like the structurally similar GG<sub>4</sub> motif, is overrepresented in transmembrane helices and mediates helix-helix interactions in membrane proteins (75, 98). The noted conservation in VirB10 of the extended version of the GG<sub>4</sub> motif (LlxxGVxxGVxxT) prompted a test of the functional importance of this motif; however, substitutions of Gly37 and Ala41 with a bulky Ile residue were phenotypically silent. For GpA, the extended GG<sub>4</sub> motif forms a homodimeric interface and, in agreement with previous findings (26), I determined that a G83I mutation completely abolishes GpA-mediated dimerization as shown with the TOXCAT assay (Figure 4-10). Interestingly, even though VirB10 carries an extended motif (LlxxGVxxALxxS) similar to that of GpA, the VirB10 TM domain only weakly dimerizes and the Ile substitution mutations do not further diminish homodimer formation as quantitated by TOXCAT (Figure 4-10). My studies do not exclude the possibility that the GA<sub>4</sub> motif mediates formation or stabilization of TM-TM heterodimers with other VirB channel subunits, but even if this were the case, results of the mutational studies establish that any GA<sub>4</sub>-mediated dimerization is completely dispensable for VirB10 function.

The extended GG<sub>4</sub> or GA<sub>4</sub> motifs conform to a repeat designated as [abcd]<sub>n</sub> where the *a* and *b* residues form a right-handed helix-helix interface (75, 77, 99). By contrast, the second type of dimerization motif identified in the VirB10 TM domain, the Leu zipper, forms dimeric contacts via a [abcdefg]<sub>n</sub> heptad repeat in which residues at the *a* and *d* positions form a left-handed helix-helix interface (100). Leu zipper-mediated dimerization is most commonly reported for soluble binding partners, but a number of eukaryotic and virus membrane proteins have been shown to form partner interactions via Leu zipper motifs in TM sequences (70-73). In bacteria, Leu-zipper mediated dimerization of TM helices has not been reported, although a Leu zipper domain of the GCN4 transcription factor was found to functionally substitute for the TM domain of the *A. tumefaciens* VirA sensor kinase (101). Leu-to-Ala substitutions disrupt Leu zipper-mediated interactions, and here I showed that Ala substitutions of the putative LZ1 motif (L33, L40, I47) block T-pilus formation. In contrast, Ala substitutions of the putative LZ2

motif (V35, L42, L49) were phenotypically silent, indicating that this Leu interface is not required for VirB10 function.

I extended my analyses of the VirB10 TM domain and the LZ1 motif by substituting heterologous TM domains for the native sequence. Introduction of the FtsN TM sequence resulted in a TM sequence that retained the LZ1 motif but little other sequence identity with the VirB10 TM sequence. The corresponding VirB10/FtsN<sub>TM</sub> mutant protein displayed WT function; however, so also did the same chimeric protein bearing Ala substitutions of the LZ1 residues. This could raise questions about the importance of the VirB10 LZ1 motif, but an alternative possibility is that the chimeric VirB10/FtsN TM sequence possesses another dimerization motif that functionally substitutes for the LZ1 motif. While further studies are needed to explore this possibility, I also tested whether substitution of a TM sequence devoid of a dimerization motif would impact VirB10 function. The poly-LA sequence is monomeric and all three swaps that I constructed (27-50, 33-50, 33-50 with W48 retained) phenocopied the Leu-to-Ala substitutions of the LZ1 motif in blocking T-pilus production and supporting substrate transfer. I also confirmed that the pLA motif does not mediate assembly of TM homodimers in the TOXCAT assay consistent with previous reports (86, 87, 92).

Starting with the monomeric pLA sequence, I next attempted to restore the capacity of cells to assemble T-pili by reintroducing residues that are conserved among VirB10 homologs. Intriguingly, substitution of a single Leu for Ala at position 40 in the TM sequence resulted in accumulation of appreciably higher levels of T-pilus, as did substitution of conserved residues Val39, Leu40, Ser43, and Leu44. The Leu40 substitution restores the LZ1 motif (L33, L40, L47), which could account for the gain-of-function phenotype with respect to T-pilus assembly. However, the pLA TM sequence and the two derivatives bearing substitutions of conserved residues showed only weak dimerization as monitored by TOXCAT. These findings suggest that the putative LZ1 motif does not mediate formation of strong TM-TM homodimers, at least in *E. coli*.

I can envision three explanations for why substitutions of conserved residues into the pLA sequence restore T-pilus production in *A. tumefaciens* but not homodimer formation as monitored by TOXCAT in *E. coli*. First, as shown for some Leu zipper motifs of soluble proteins (102, 103), the VirB10 LZ1 motif might instead mediate a heteromeric interaction required for T-pilus biogenesis. As noted above, there are several VirB channel subunits, including VirB2, VirB3, VirB4, VirB5, VirB6, or VirB8, with which VirB10 might interact for T-

pilus production. These interactions would not have been identified with our TOXCAT assay although future studies with a variant of the TOXCAT assay (104) could reveal such heteromeric TM helix-helix interactions. Alternatively, it is conceivable that LZ1 motif weakly or dynamically self-associates in *A. tumefaciens* and that this type of TM-TM self-association is essential for VirB10 to function in T-pilus assembly. A weak, or for that matter, strong TM helix-helix interaction might form in the context of the assembled VirB7/VirB9/VirB10 core complex but not the TOXCAT constructs in *E. coli*. Finally, it is possible that the VirB10 TM domain contributes indirectly to establishment of homo- or heterotypic interactions through structural effects on the adjacent cytoplasmic or Pro-rich periplasmic domains. The TM mutations shown to affect T-pilus production could exert their effects by imposing a structural change or constraint on one of both of these extramembraneous domains.

Besides considering my experimental findings, it is important to incorporate the available structural information in development of models depicting how the VirB10 TM domain might contribute to T-pilus biogenesis. On the basis of the pKM101 core complex visualized by CryoEM and X-ray crystallography, it is proposed that VirB10-like subunits, together with VirB7 and VirB9-like subunits form a ring-shaped complex that spans both membranes and the intervening periplasmic space (15, 16). This core complex serves as a scaffold upon which the translocation channel is assembled, most likely within the core's chamber. We further postulate that the core complex serves as a scaffold for T-pilus assembly. T-pili might assemble from i) an inner membrane platform within the core's chamber or ii) an outer membrane platform formed by the core complex. Although it is not possible at this time to discriminate between the inner versus outer membrane assembly models, we envision that for both models the VirB2 pilin subunit must gain access to the core chamber for T-pilin polymerization. If so, the pool of pilin monomers that accumulates within the inner membrane for use in building T-pili must translocate from their site of membrane insertion into the core chamber at an early stage of the assembly pathway. Accordingly, during translocation through the membrane, pilin monomers would encounter VirB10 TM domains configured as a 14-membered ring encircling the chamber. The nature of VirB10 TM-TM helix homo- or heterotypic interactions could thus be critical for this step of T-pilin translocation.

If I assume that the 14 VirB10 TM domains form only homotypic interactions, there are two possible TM helical arrangements (Figure 4-13). Each helix might interact with both adjacent helices forming a 14-membered ring. In this scenario, an LZ1 motif (L33, L40, L47) of one subunit might interact with the LZ2 motif (V35, L42, L49) of an adjacent subunit, making a

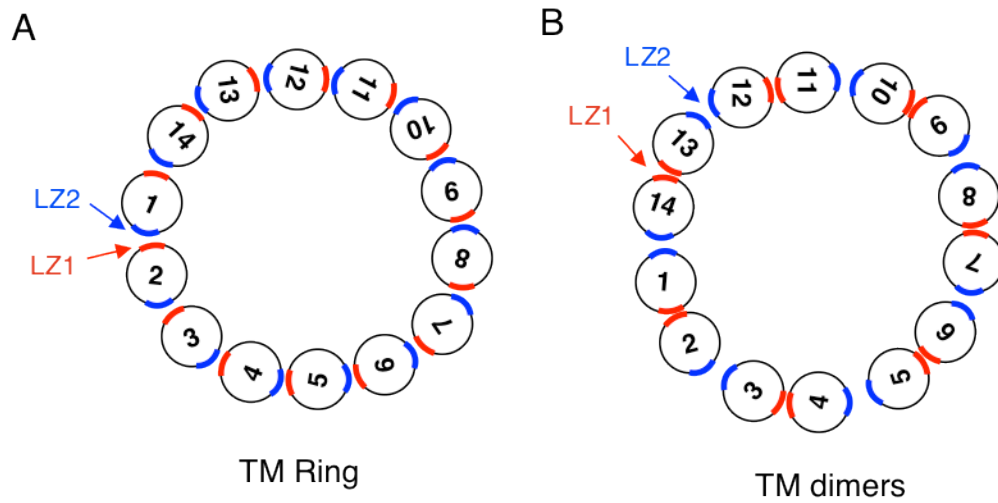
ringed complex of interacting  $\alpha$ -helices (Figure 4-13: panel A). For the pilin to translocate through such a ringed complex, transient breaks in the ringed complex would need to occur. However, arguing against such a structural arrangement, I showed that the putative LZ2 motif is completely dispensable whereas putative LZ1 motif is required for T-pilus production. Thus, an alternative structural arrangement is that an LZ1 motif of one VirB10 monomer interacts with an LZ1 motif of an adjacent monomer. The resulting structure is a 14-membered ring comprised of 7 TM-TM dimers (Figure 4-13: panel B). This model is in agreement with my data demonstrating the functional importance of the LZ1 motif and also with results of the TOXCAT assays showing that LZ1 mutations abrogate VirB10 self-association. This model would also accommodate the proposed requirement for pilin subunits to translocate across the 14-membered ring of TM helices as adjacent VirB10 dimers need not be physically associated.

As noted above, however, at this point we cannot rule out the possibility that the VirB10 TM domain forms heterotypic interactions with other channel subunits. It seems unlikely that the VirB10 TM domain would interact stably with the VirB2 pilin although a transient weak-affinity interaction might be important for guiding the pilin into the core chamber. Additionally J. Kerr in our lab recently supplied evidence that the VirB4 ATPase mediates dislocation of VirB2 pilin from the inner membrane (105). S. Jakubowski in our lab also has supplied evidence that VirB10 interacts with the VirB4 ATPase (unpublished data). In view of these findings, the VirB10 TM domain might interact with VirB4 as a means of spatially localizing pilin dislocase activity at the core complex. VirB3 has been shown to interact with VirB4 and thus represents yet another candidate interacting subunit with the VirB10 TM domain (106, 107). Other candidate subunits VirB6 and VirB8, two proteins that likely comprise part of the translocase at the inner membrane. A model depicting VirB10 TM domain heterotypic interactions is shown in Figure 4-13 panel C. Finally, it is conceivable that VirB10 participates in a mix of homotypic and heterotypic interactions - stably or dynamically - within the lipid environment of the inner membrane (Figure 4-13: panel D).

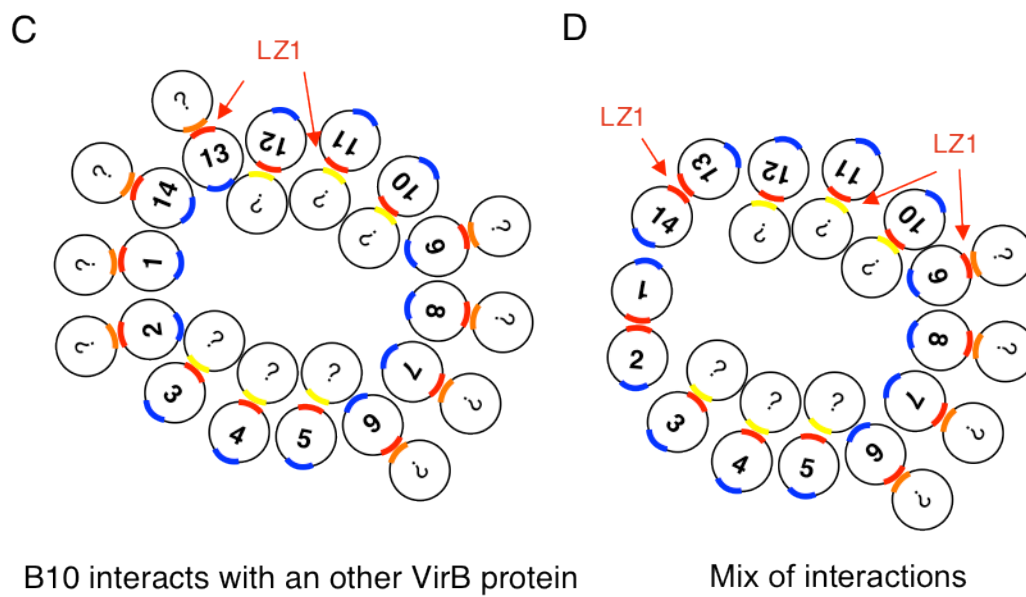
**Figure 4-13 Model depicting VirB10 helical TM packing**

- A. TM ring model where individual and adjacent TM domains interact by contacts between different Leu zipper motifs (LZ1; red and LZ2; blue).
- B. Contacts via LZ1 create TM dimers.
- C. Heterotypic interactions occur via contacts between LZ1 and another VirB protein.
- D. Model depicting a mix of homo- and heterotypic interactions.

## Homotypic Interactions



## Heterotypic Interactions





## Chapter 5. Summary and Perspectives

### Summary

Type IV secretion systems are large multiprotein complexes consisting of a dynamic network of 11 VirB proteins and the coupling protein, VirD4 (4). These systems assemble a transenvelope secretion channel that functions to transport macromolecules across cell membranes and many also assemble surface filaments or T-pili. This thesis is centered on advancing our understanding of type IV substrate secretion and T-pilus biogenesis through a mutational analysis of VirB10.

In chapter 3, I identified phenotypes associated with Ala-Cys insertions and Cys substitution mutations along the length of VirB10. In general, Ala-Cys insertions in the N-terminal cytoplasmic and TM domains had marginal effects on protein function. However, a few insertions nearly or completely blocked T-pilus biogenesis (Ala-Cys inserted at 35, 40, and 45) (24). Further analysis of these N-terminal insertion mutations along with C-terminal Cys substitutions confirmed a bitopic topology.

Phenotypic studies of proteins with Cys substitutions gave various phenotypes when assayed for effects on protein function, and ability to form high molecular weight species in nonreducing gels. Interestingly most of the Cys derivative proteins formed large molecular weight species consistent with a homodimer (~105-kDa). Thus VirB10 forms an extended protein interface with itself, which is in agreement with recent structural information of the VirB10 homolog (TraF) in the pKM101 core complex (15, 16).

In view of the X-ray crystal structure of the outer membrane layer composed of TraF, TraN, and TraO, it is possible but unproven that the AP domain of TraF/VirB10 functions as an outer membrane pore (15). Several Cys substitutions were introduced into the AP domain of VirB10. These mutant proteins were first tested for effects on protein function and then used in surface accessibility studies with an outer membrane impermeable thiol reactive compound, MPEG. In these studies, I was not able to detect reactivity with MPEG and thus unable to validate surface accessible sites along the AP domain of VirB10. One possibility could be that the AP domain is only transiently surface accessible or other surface proteins block its accessibility. By contrast, MPB labeling in different genetic backgrounds of Cys mutant proteins provided some initial evidence that the AP domain exists in different structural states in the absence versus presence of other VirB proteins. Therefore, the possibility that the AP

domain of VirB10 functions as the outer membrane pore is still a subject of debate and further study.

In chapter 4, I characterized the contributions of the TM domain to VirB10 function, specifically T-pilus formation. I described the identification of various TM dimerizing motifs and subsequently introduced mutations to characterize the contributions of these motifs to protein function. Results of these mutational studies showed that a GA<sub>4</sub> motif and LZ2 (V35, L42, L49) Leu zipper motif do not contribute to VirB10 function. In contrast, the putative LZ1 (L33, L40, I47) Leu zipper does seem to contribute to T-pilus formation. To further examine this proposal, I created and phenotypically characterized several pLA and FtsN TM domain substitutions. Proteins with pLA TM substitutions were very reduced for T-pilus formation and substrate transfer. Interestingly the introduction of conserved native residues into the pLA TM sequence restored T-pilus production. By contrast proteins with FtsN TM substitutions complemented protein function even in FtsN TM sequences containing Ala substitutions in the putative LZ1 motif.

The ability of various TM sequences to self-associate was measured using the TOXCAT assay. The TM sequence of native VirB10 was found to have a weak dimerizing affinity when compared to GpA. Most mutagenized TM sequences had similar self-association affinities to native B10, however, there were two exceptions: i) the TM carrying the 40AC insertion and ii) the TM carrying the triple Ala substitutions in LZ1 (L33, L40, I47). Both of these mutations abolished T-pilus production in *A. tumefaciens*. Therefore, mutations that block T-pilus formation also confer slight reductions in TM-TM self-association.

Mutations in the TM domain blocked or reduced T-pilus production whereas partial deletion of the AP caused release of pilin monomers into the milieu (24), indicating a defect in pilin polymerization. These results are supportive of a hypothesis that the TM and AP domain contribute to T-pilus biogenesis at distinct steps in the biosynthetic pathway. The TM domain might contribute in some way to the recruitment of pilin monomers to the core channel, whereas the AP might function as a platform for pilin polymerization or gate T-pilus extension.

I hypothesize that the VirB10 core complex functions as a structural scaffold for the assembly of the T-pilus (Figure 5-1). This working model describes VirB2 pilin subunits as accumulating in the inner membrane prior to polymerization. Next, VirB2 pilin monomers enter the core complex via lateral movement in the inner membrane through an open VirB10 TM

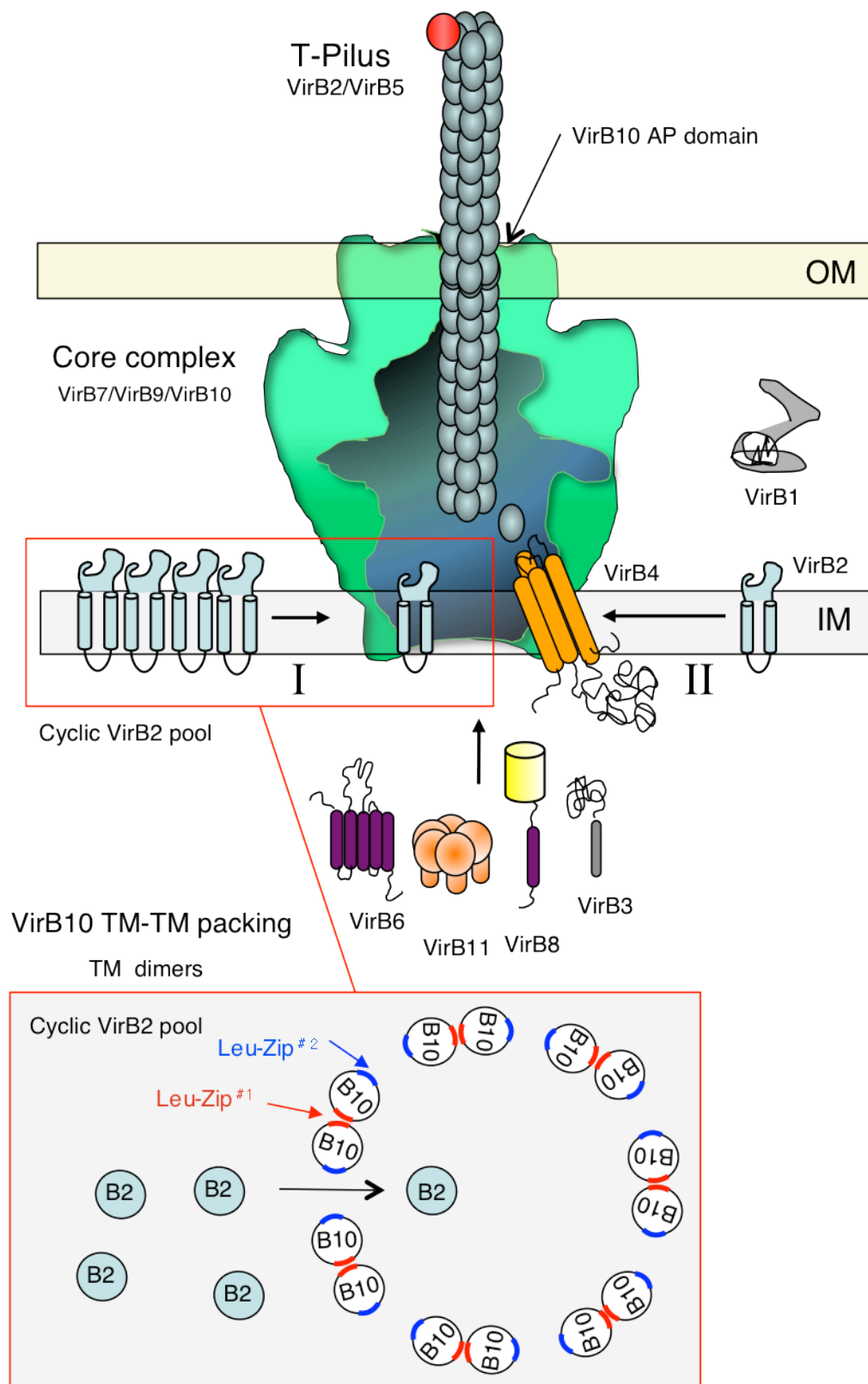
gate. One working model is that adjacent VirB10 TM's dimerize via their LZ1 (L33, L40, I47) motif. This homotypic contact between TM helices creates a space between adjacent TM dimers (Figure 5-1: I). I hypothesize that this space is used by VirB2 to enter the lumen of the core complex to then form a nascent T-pilus filament. This filament subsequently extends and protrudes out of the core channel and likely makes subunit contacts with the AP domain of VirB10 (Figure 5-1). According to this model, the AP might serve as a gate that allows passage of the T-pilus across the outer membrane. However, an alternative model is pilin subunits enter the core chamber and are transferred to the AP domain at the cell surface where the AP functions as an outer membrane platform upon which the T-pilus assembles.

At this time, we cannot exclude the possibility of heterotypic interactions involved in the recruitment and delivery of VirB2 pilin monomers into the interior of the core channel. The Christie laboratory has recently provided evidence for VirB4 dislocation of VirB2 pilin from the inner membrane (105). This process was described as necessary in the initial steps of T-pilus biogenesis. These findings coupled with studies describing the contributions of VirB10 led to a model where VirB4 might coordinate with VirB10 via TM helical interactions to dislocate and transfer VirB2 pilin to the core channel (Figure 5-1: II). Moreover, VirB2 pilin once in the core channel or during the dislocation process likely undergoes structural changes necessary for T-pilus polymerization.

**Figure 5-1 Models depicting contributions of VirB10 TM helices to entry of VirB2 pilin subunits into the core complex**

- I. VirB10 TM helical self-association contributes to entry of VirB2 pilin monomers via an open inner membrane TM gate. An inner membrane pool of VirB2 pilin accumulates and moves laterally to enter the lumen of the core complex via spaces created by VirB10 dimers. VirB2 pilin within the core complex polymerize and assemble a T-pilus filament that extends and exit the outer membrane pore composed of the AP domain of VirB10.
- II. An alternative model describing VirB2 pilin entry and transfer into the core complex is through dislocation by the ATPase VirB4. In this model VirB4 coordinates with VirB10 possibility through TM helical contacts to transfer VirB2 pilin into the interior of the core channel for subsequent pilin polymerization reactions.

VirB7, VirB9, and VirB10 form a core complex as shown through cryoelectron microscopy from homologues in the pKM101 conjugation system (16). This core complex is composed of 14 copies of each of TraF, TraN, and TraO in a 1:1:1 stoichiometric ratio (16). Here a cartoon representation of this structure is provided.



## **Future experiments**

Future experiments will be centered on testing contributions of the TM domain in mediating heterotypic contacts with other VirB proteins. Two unanswered questions will be explored: (i) does VirB10 interact with VirB2 or VirB4 via TM helical or AP contacts, (ii) is the core complex a structural scaffold for the T-pilus?

### **Do the VirB10 TM or AP domains mediate subunit contacts with VirB2 pilin?**

I rationalize that if VirB2 enters and assembles within the core complex a number of possible subunit contacts will occur. First TM-TM contacts will occur between VirB10 and VirB2 pilin as a result of lateral movement through the inner membrane. Second, the assembled T-pilus will make contact with the outer membrane pore composed of the AP domain of VirB10 as the T-pilus elongates and extends to the cell surface. Thus VirB10 makes two possible subunit contacts with VirB2 in the proposed T-pilus biogenesis process: i) in the inner membrane by TM helical interactions for pilin entry into the core, and ii) in the outer membrane pore for T-pilus extension to the cell surface.

### **Do VirB10 and VirB4 interact?**

An alternative model describing VirB2 entry and delivery into the interior of the core complex is through dislocation by the ATPase VirB4. According to this model, VirB4 dislocates VirB2 from the inner membrane and in coordination with VirB10, VirB2 is shunted into the core complex for subsequent polymerization reactions. This model suggests a stable interaction between VirB4 and VirB10 for transfer of VirB2 into the core channel.

To test for subunit contacts between VirB10, VirB2, and VirB4, I propose co-immunoprecipitation (Co-IP) and cross-linking studies as well as a two-hybrid system designed for testing heterotypic interactions between membrane proteins (104).

The goal of these Co-IP studies is to isolate complexes of VirB10, VirB2, and VirB4 with native VirB10 versus VirB10 containing TM or AP domain mutations. Chemical cross-linking will be applied to stabilize transient or weak interactions.

To define areas of subunit contacts I propose cross-linking studies with Cys derivative proteins of VirB10 and VirB2. Recall from chapter 3, several Cys residues were introduced into the AP and TM domains of VirB10. These Cys derivative proteins will be co-expressed in strains producing Cys-substituted VirB2 mutants and tested for presence of molecular weight

crosslinks between VirB10 and VirB2. Cross-linking will be done in the presence of the oxidant copper-phenanthroline.

To determine heterotypic association between TM segments of VirB10 with VirB2 and VirB4, GALLEX, a two-hybrid system for membrane proteins could be used (104). This system like TOXCAT, is a reporter system where fusion proteins are produced with altered TM sequences in *E. coli*. Association of fusion proteins is driven by heterotypic interaction between TM helices and causes the repression of a reporter gene (104). This system will be used to test for TM helical interactions between the TM segments for VirB10 with VirB2, and VirB10 with VirB4.

### **Complex isolation through the use of an N-terminal profinity-VirB10**

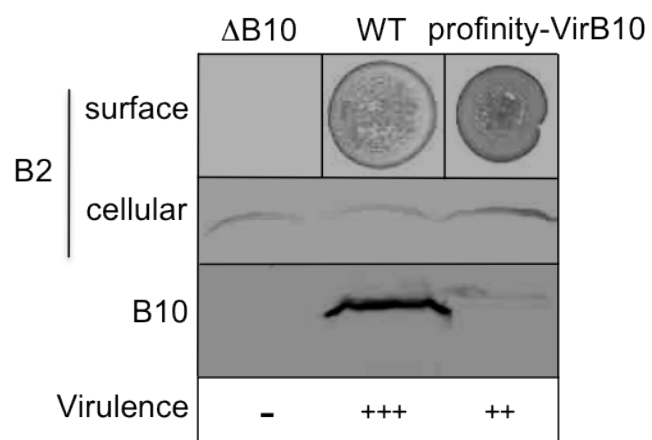
To test the hypothesis that the core channel serves as a scaffold or chaperone for the T-pilus, isolation conditions will be developed to detect and analyze assemblies of the core channel complex. I constructed an N-terminal profinity tagged VirB10 (see Materials and Methods). Protein purification using the profinity system first includes attaching the 8kDa tag to VirB10. Cell lysate containing the tagged protein is passed through a column packed with a S189 mutant subtilisin protease resin. The profinity tag contains a subtilisin recognition/cleavage sequence (EEDKLFKAL); therefore the tagged protein is bound with high affinity to the resin. The resin is washed to remove unbound proteins. Elution is achieved by triggering the S189 subtilisin to cleave the recognition/cleavage sequence via incubation in buffers of high ionic concentration. Profinity-VirB10 does accumulate however at reduced levels and supports substrate transfer and T-pilus production (Figure 5-2). Thus the N-terminal tag does not abolish protein function, and is suitable for protein purification and structural studies.

**Figure 5-2 Effects of profinity-VirB10 fusion on protein function**

From top: T-pilus production by VirB2 surface assay. Total cellular levels of VirB2 and VirB10 detected by SDS-PAGE and immunostaining with anti-VirB2 or anti-VirB10 antibodies. Virulence is reported on a scale of three pluses for wild-type virulence to a minus sign for avirulent.

Strains: WT, A348;  $\Delta$ B10, PC1010; profinity-VirB10, PC1010 producing profinity-VirB10.





## **Final Acknowledgements**

I recognize the many contributions others have made to the completion of these studies. I would like to thank the current and past members of the Christie laboratory, specifically Jennifer E. Kerr, Simon J. Jakubowski, and Vidhya Krishamoorthy. Moreover I thank Dr. Kevin Ridge for donating items critical to the profinity experiments. I also thank Dr. D. M. Engelman for providing TOXCAT vectors and materials. I am appreciative to Dr. Renhao Li for providing helpful comments concerning the TOXCAT system.

## References

1. Alvarez-Martinez, C. E., and P. J. Christie. 2009. Biological diversity of prokaryotic type IV secretion systems. *Microbiol Mol Biol Rev* 73:775-808.
2. McCullen, C. A., and A. N. Binns. 2006. *Agrobacterium tumefaciens* and plant cell interactions and activities required for interkingdom macromolecular transfer. *Annu Rev Cell Dev Biol* 22:101-127.
3. Smith, E. F., and C. O. Townsend. 1907. A Plant-Tumor of Bacterial Origin. *Science* 25:671-673.
4. Christie, P. J., K. Atmakuri, V. Krishnamoorthy, S. Jakubowski, and E. Cascales. 2005. Biogenesis, architecture, and function of bacterial type IV secretion systems. *Annu Rev Microbiol* 59:451-485.
5. Christie, P. J., and E. Cascales. 2005. Structural and dynamic properties of bacterial type IV secretion systems (review). *Mol Membr Biol* 22:51-61.
6. Rabel, C., A. M. Grahm, R. Lurz, and E. Lanka. 2003. The VirB4 family of proposed traffic nucleoside triphosphatases: common motifs in plasmid RP4 TrbE are essential for conjugation and phage adsorption. *J Bacteriol* 185:1045-1058.
7. Berger, B. R., and P. J. Christie. 1993. The *Agrobacterium tumefaciens* virB4 gene product is an essential virulence protein requiring an intact nucleoside triphosphate-binding domain. *J Bacteriol* 175:1723-1734.
8. Dang, T. A., and P. J. Christie. 1997. The VirB4 ATPase of *Agrobacterium tumefaciens* is a cytoplasmic membrane protein exposed at the periplasmic surface. *J Bacteriol* 179:453-462.
9. Rashkova, S., G. M. Spudich, and P. J. Christie. 1997. Characterization of membrane and protein interaction determinants of the *Agrobacterium tumefaciens* VirB11 ATPase. *J Bacteriol* 179:583-591.
10. Das, A., and Y. H. Xie. 1998. Construction of transposon Tn3phoA: its application in defining the membrane topology of the *Agrobacterium tumefaciens* DNA transfer proteins. *Mol Microbiol* 27:405-414.
11. Aly, K. A., and C. Baron. 2007. The VirB5 protein localizes to the T-pilus tips in *Agrobacterium tumefaciens*. *Microbiology* 153:3766-3775.
12. Cao, T. B., and M. H. Saier, Jr. 2001. Conjugal type IV macromolecular transfer systems of Gram-negative bacteria: organismal distribution, structural constraints and evolutionary conclusions. *Microbiology* 147:3201-3214.

13. Cascales, E., and P. J. Christie. 2003. The versatile bacterial type IV secretion systems. *Nat Rev Microbiol* 1:137-149.
14. Baron, C., O. C. D., and E. Lanka. 2002. Bacterial secrets of secretion: EuroConference on the biology of type IV secretion processes. *Mol Microbiol* 43:1359-1365.
15. Chandran, V., R. Fronzes, S. Duquerroy, N. Cronin, J. Navaza, and G. Waksman. 2009. Structure of the outer membrane complex of a type IV secretion system. *Nature* 462:1011-1015.
16. Fronzes, R., E. Schafer, L. Wang, H. R. Saibil, E. V. Orlova, and G. Waksman. 2009. Structure of a type IV secretion system core complex. *Science* 323:266-268.
17. Cascales, E., and P. J. Christie. 2004. Definition of a bacterial type IV secretion pathway for a DNA substrate. *Science* 304:1170-1173.
18. Terradot, L., R. Bayliss, C. Oomen, G. A. Leonard, C. Baron, and G. Waksman. 2005. Structures of two core subunits of the bacterial type IV secretion system, VirB8 from *Brucella suis* and ComB10 from *Helicobacter pylori*. *Proc Natl Acad Sci U S A* 102:4596-4601.
19. Berger, B. R., and P. J. Christie. 1994. Genetic complementation analysis of the *Agrobacterium tumefaciens* virB operon: virB2 through virB11 are essential virulence genes. *J Bacteriol* 176:3646-3660.
20. Cascales, E., and P. J. Christie. 2004. *Agrobacterium* VirB10, an ATP energy sensor required for type IV secretion. *Proc Natl Acad Sci U S A* 101:17228-17233.
21. Das, A., and Y. H. Xie. 2000. The *Agrobacterium* T-DNA transport pore proteins VirB8, VirB9, and VirB10 interact with one another. *J Bacteriol* 182:758-763.
22. Ward, D. V., O. Draper, J. R. Zupan, and P. C. Zambryski. 2002. Peptide linkage mapping of the *Agrobacterium tumefaciens* vir-encoded type IV secretion system reveals protein subassemblies. *Proc Natl Acad Sci U S A* 99:11493-11500.
23. Fronzes, R., P. J. Christie, and G. Waksman. 2009. The structural biology of type IV secretion systems. *Nat Rev Microbiol* 7:703-714.
24. Jakubowski, S. J., J. E. Kerr, I. Garza, V. Krishnamoorthy, R. Bayliss, G. Waksman, and P. J. Christie. 2009. *Agrobacterium* VirB10 domain requirements for type IV secretion and T pilus biogenesis. *Mol Microbiol* 71:779-794.
25. Bogdanov, M., W. Zhang, J. Xie, and W. Dowhan. 2005. Transmembrane protein topology mapping by the substituted cysteine accessibility method (SCAM(TM)): application to lipid-specific membrane protein topogenesis. *Methods* 36:148-171.

26. Russ, W. P., and D. M. Engelman. 1999. TOXCAT: a measure of transmembrane helix association in a biological membrane. *Proc Natl Acad Sci U S A* 96:863-868.
27. Zhu, J., P. M. Oger, B. Schrammeijer, P. J. Hooykaas, S. K. Farrand, and S. C. Winans. 2000. The bases of crown gall tumorigenesis. *J Bacteriol* 182:3885-3895.
28. Fernandez, D., T. A. Dang, G. M. Spudich, X. R. Zhou, B. R. Berger, and P. J. Christie. 1996. The *Agrobacterium tumefaciens* virB7 gene product, a proposed component of the T-complex transport apparatus, is a membrane-associated lipoprotein exposed at the periplasmic surface. *J Bacteriol* 178:3156-3167.
29. Zhou, X. R., and P. J. Christie. 1999. Mutagenesis of the *Agrobacterium* VirE2 single-stranded DNA-binding protein identifies regions required for self-association and interaction with VirE1 and a permissive site for hybrid protein construction. *J Bacteriol* 181:4342-4352.
30. Fernandez, D., G. M. Spudich, X. R. Zhou, and P. J. Christie. 1996. The *Agrobacterium tumefaciens* VirB7 lipoprotein is required for stabilization of VirB proteins during assembly of the T-complex transport apparatus. *J Bacteriol* 178:3168-3176.
31. Christie, P. J., J. E. Ward, Jr., M. P. Gordon, and E. W. Nester. 1989. A gene required for transfer of T-DNA to plants encodes an ATPase with autophosphorylating activity. *Proc Natl Acad Sci U S A* 86:9677-9681.
32. Christie, P. J., J. E. Ward, S. C. Winans, and E. W. Nester. 1988. The *Agrobacterium tumefaciens* virE2 gene product is a single-stranded-DNA-binding protein that associates with T-DNA. *J Bacteriol* 170:2659-2667.
33. Kunkel, T. A., K. Bebenek, and J. McClary. 1991. Efficient site-directed mutagenesis using uracil-containing DNA. *Methods Enzymol* 204:125-139.
34. Chen, C. Y., and S. C. Winans. 1991. Controlled expression of the transcriptional activator gene virG in *Agrobacterium tumefaciens* by using the *Escherichia coli* lac promoter. *J Bacteriol* 173:1139-1144.
35. Zhao, Z., E. Sagulenko, Z. Ding, and P. J. Christie. 2001. Activities of virE1 and the VirE1 secretion chaperone in export of the multifunctional VirE2 effector via an *Agrobacterium* type IV secretion pathway. *J Bacteriol* 183:3855-3865.
36. Cangelosi, G. A., E. A. Best, G. Martinetti, and E. W. Nester. 1991. Genetic analysis of *Agrobacterium*. *Methods Enzymol* 204:384-397.
37. Manoil, C. 1991. Analysis of membrane protein topology using alkaline phosphatase and beta-galactosidase gene fusions. *Methods Cell Biol* 34:61-75.

38. Sagulenko, E., V. Sagulenko, J. Chen, and P. J. Christie. 2001. Role of *Agrobacterium* VirB11 ATPase in T-pilus assembly and substrate selection. *J Bacteriol* 183:5813-5825.
39. Bohne, J., A. Yim, and A. N. Binns. 1998. The Ti plasmid increases the efficiency of *Agrobacterium tumefaciens* as a recipient in virB-mediated conjugal transfer of an IncQ plasmid. *Proc Natl Acad Sci U S A* 95:7057-7062.
40. Garfinkel, D. J., R. B. Simpson, L. W. Ream, F. F. White, M. P. Gordon, and E. W. Nester. 1981. Genetic analysis of crown gall: fine structure map of the T-DNA by site-directed mutagenesis. *Cell* 27:143-153.
41. Fullner, K. J. 1998. Role of *Agrobacterium* virB genes in transfer of T complexes and RSF1010. *J Bacteriol* 180:430-434.
42. Sagulenko, V., E. Sagulenko, S. Jakubowski, E. Spudich, and P. J. Christie. 2001. VirB7 lipoprotein is exocellular and associates with the *Agrobacterium tumefaciens* T pilus. *J Bacteriol* 183:3642-3651.
43. Jin, S. G., T. Komari, M. P. Gordon, and E. W. Nester. 1987. Genes responsible for the supervirulence phenotype of *Agrobacterium tumefaciens* A281. *J Bacteriol* 169:4417-4425.
44. Shaw, W. V. 1975. Chloramphenicol acetyltransferase from chloramphenicol-resistant bacteria. *Methods Enzymol* 43:737-755.
45. Christie, P. J. 2001. Type IV secretion: intercellular transfer of macromolecules by systems ancestrally related to conjugation machines. *Mol Microbiol* 40:294-305.
46. Lai, E. M., R. Eisenbrandt, M. Kalkum, E. Lanka, and C. I. Kado. 2002. Biogenesis of T pili in *Agrobacterium tumefaciens* requires precise VirB2 propilin cleavage and cyclization. *J Bacteriol* 184:327-330.
47. Lai, E. M., and C. I. Kado. 1998. Processed VirB2 is the major subunit of the promiscuous pilus of *Agrobacterium tumefaciens*. *J Bacteriol* 180:2711-2717.
48. Atmakuri, K., E. Cascales, and P. J. Christie. 2004. Energetic components VirD4, VirB11 and VirB4 mediate early DNA transfer reactions required for bacterial type IV secretion. *Mol Microbiol* 54:1199-1211.
49. Dong, C., K. Beis, J. Nesper, A. L. Brunkan-Lamontagne, B. R. Clarke, C. Whitfield, and J. H. Naismith. 2006. Wza the translocon for *E. coli* capsular polysaccharides defines a new class of membrane protein. *Nature* 444:226-229.

50. Beaupre, C. E., J. Bohne, E. M. Dale, and A. N. Binns. 1997. Interactions between VirB9 and VirB10 membrane proteins involved in movement of DNA from *Agrobacterium tumefaciens* into plant cells. *J Bacteriol* 179:78-89.
51. Jakubowski, S. J., V. Krishnamoorthy, and P. J. Christie. 2003. *Agrobacterium tumefaciens* VirB6 protein participates in formation of VirB7 and VirB9 complexes required for type IV secretion. *J Bacteriol* 185:2867-2878.
52. Gilmour, M. W., J. E. Gunton, T. D. Lawley, and D. E. Taylor. 2003. Interaction between the IncHI1 plasmid R27 coupling protein and type IV secretion system: TraG associates with the coiled-coil mating pair formation protein TrhB. *Mol Microbiol* 49:105-116.
53. Llosa, M., S. Zunzunegui, and F. de la Cruz. 2003. Conjugative coupling proteins interact with cognate and heterologous VirB10-like proteins while exhibiting specificity for cognate relaxosomes. *Proc Natl Acad Sci U S A* 100:10465-10470.
54. Larsen, R. A., T. E. Letain, and K. Postle. 2003. In vivo evidence of TonB shuttling between the cytoplasmic and outer membrane in *Escherichia coli*. *Mol Microbiol* 49:211-218.
55. Williamson, M. P. 1994. The structure and function of proline-rich regions in proteins. *Biochem J* 297 ( Pt 2):249-260.
56. Bayliss, R., R. Harris, L. Coutte, A. Monier, R. Fronzes, P. J. Christie, P. C. Driscoll, and G. Waksman. 2007. NMR structure of a complex between the VirB9/VirB7 interaction domains of the pKM101 type IV secretion system. *Proc Natl Acad Sci U S A* 104:1673-1678.
57. Lu, J., and C. Deutsch. 2001. Pegylation: a method for assessing topological accessibilities in Kv1.3. *Biochemistry* 40:13288-13301.
58. Zhou, X. R., and P. J. Christie. 1997. Suppression of mutant phenotypes of the *Agrobacterium tumefaciens* VirB11 ATPase by overproduction of VirB proteins. *J Bacteriol* 179:5835-5842.
59. Jakubowski, S. J., V. Krishnamoorthy, E. Cascales, and P. J. Christie. 2004. *Agrobacterium tumefaciens* VirB6 domains direct the ordered export of a DNA substrate through a type IV secretion System. *J Mol Biol* 341:961-977.
60. Jakubowski, S. J., E. Cascales, V. Krishnamoorthy, and P. J. Christie. 2005. *Agrobacterium tumefaciens* VirB9, an outer-membrane-associated component of a type IV secretion system, regulates substrate selection and T-pilus biogenesis. *J Bacteriol* 187:3486-3495.

61. Eisenbrandt, R., M. Kalkum, R. Lurz, and E. Lanka. 2000. Maturation of IncP pilin precursors resembles the catalytic Dyad-like mechanism of leader peptidases. *J Bacteriol* 182:6751-6761.
62. Postle, K. 2007. TonB system, in vivo assays and characterization. *Methods Enzymol* 422:245-269.
63. Evans, J. S., B. A. Levine, I. P. Trayer, C. J. Dorman, and C. F. Higgins. 1986. Sequence-imposed structural constraints in the TonB protein of *E. coli*. *FEBS Lett* 208:211-216.
64. Adzhubei, A. A., and M. J. Sternberg. 1993. Left-handed polyproline II helices commonly occur in globular proteins. *J Mol Biol* 229:472-493.
65. Kay, B. K., M. P. Williamson, and M. Sudol. 2000. The importance of being proline: the interaction of proline-rich motifs in signaling proteins with their cognate domains. *FASEB J* 14:231-241.
66. Arkin, I. T. 2002. Structural aspects of oligomerization taking place between the transmembrane alpha-helices of bitopic membrane proteins. *Biochim Biophys Acta* 1565:347-363.
67. Russ, W. P., and D. M. Engelman. 2000. The GxxxG motif: a framework for transmembrane helix-helix association. *J Mol Biol* 296:911-919.
68. Lin, Z., K. Witschas, T. Garcia, R. S. Chen, J. P. Hansen, Z. M. Sellers, E. Kuzmenkina, S. Herzig, and P. M. Best. 2008. A critical GxxxA motif in the gamma6 calcium channel subunit mediates its inhibitory effect on Cav3.1 calcium current. *J Physiol* 586:5349-5366.
69. Zvilning, M., U. Kochva, and I. T. Arkin. 2007. How important are transmembrane helices of bitopic membrane proteins? *Biochim Biophys Acta* 1768:387-392.
70. Noordeen, N. A., F. Carafoli, E. Hohenester, M. A. Horton, and B. Leitinger. 2006. A transmembrane leucine zipper is required for activation of the dimeric receptor tyrosine kinase DDR1. *J Biol Chem* 281:22744-22751.
71. Reinke, A. W., G. Grigoryan, and A. E. Keating. Identification of bZIP interaction partners of viral proteins HBZ, MEQ, BZLF1, and K-bZIP using coiled-coil arrays. *Biochemistry* 49:1985-1997.
72. Pinto, L. H., G. R. Dieckmann, C. S. Gandhi, C. G. Papworth, J. Braman, M. A. Shaughnessy, J. D. Lear, R. A. Lamb, and W. F. DeGrado. 1997. A functionally defined model for the M2 proton channel of influenza A virus suggests a mechanism for its ion selectivity. *Proc Natl Acad Sci U S A* 94:11301-11306.



73. Oxenoid, K., and J. J. Chou. 2005. The structure of phospholamban pentamer reveals a channel-like architecture in membranes. *Proc Natl Acad Sci U S A* 102:10870-10875.
74. Rodrigues-Pousada, C., R. A. Menezes, and C. Pimentel. The Yap family and its role in stress response. *Yeast* 27:245-258.
75. Curran, A. R., and D. M. Engelman. 2003. Sequence motifs, polar interactions and conformational changes in helical membrane proteins. *Curr Opin Struct Biol* 13:412-417.
76. MacKenzie, K. R., and K. G. Fleming. 2008. Association energetics of membrane spanning alpha-helices. *Curr Opin Struct Biol* 18:412-419.
77. MacKenzie, K. R., J. H. Prestegard, and D. M. Engelman. 1997. A transmembrane helix dimer: structure and implications. *Science* 276:131-133.
78. Servant, F., C. Bru, S. Carrere, E. Courcelle, J. Gouzy, D. Peyruc, and D. Kahn. 2002. ProDom: automated clustering of homologous domains. *Brief Bioinform* 3:246-251.
79. Langosch, D., and J. Heringa. 1998. Interaction of transmembrane helices by a knobs-into-holes packing characteristic of soluble coiled coils. *Proteins* 31:150-159.
80. Mackenzie, K. R. 2006. Folding and stability of alpha-helical integral membrane proteins. *Chem Rev* 106:1931-1977.
81. Lupas, A. 1996. Coiled coils: new structures and new functions. *Trends Biochem Sci* 21:375-382.
82. Rico, A. I., M. Garcia-Ovalle, P. Palacios, M. Casanova, and M. Vicente. Role of *Escherichia coli* FtsN protein in the assembly and stability of the cell division ring. *Mol Microbiol* 76:760-771.
83. Dai, K., Y. Xu, and J. Lutkenhaus. 1996. Topological characterization of the essential *Escherichia coli* cell division protein FtsN. *J Bacteriol* 178:1328-1334.
84. Goehring, N. W., C. Robichon, and J. Beckwith. 2007. Role for the nonessential N terminus of FtsN in divisome assembly. *J Bacteriol* 189:646-649.
85. de Planque, M. R., E. Goormaghtigh, D. V. Greathouse, R. E. Koeppe, 2nd, J. A. Kruijtzter, R. M. Liskamp, B. de Kruijff, and J. A. Killian. 2001. Sensitivity of single membrane-spanning alpha-helical peptides to hydrophobic mismatch with a lipid bilayer: effects on backbone structure, orientation, and extent of membrane incorporation. *Biochemistry* 40:5000-5010.
86. Gurezka, R., R. Laage, B. Brosig, and D. Langosch. 1999. A heptad motif of leucine residues found in membrane proteins can drive self-assembly of artificial transmembrane segments. *J Biol Chem* 274:9265-9270.

87. Mo, X., N. Lu, A. Padilla, J. A. Lopez, and R. Li. 2006. The transmembrane domain of glycoprotein Ibbeta is critical to efficient expression of glycoprotein Ib-IX complex in the plasma membrane. *J Biol Chem* 281:23050-23059.
88. Luo, S. Z., X. Mo, J. A. Lopez, and R. Li. 2007. Role of the transmembrane domain of glycoprotein IX in assembly of the glycoprotein Ib-IX complex. *J Thromb Haemost* 5:2494-2502.
89. Granseth, E., G. von Heijne, and A. Elofsson. 2005. A study of the membrane-water interface region of membrane proteins. *J Mol Biol* 346:377-385.
90. Killian, J. A., and G. von Heijne. 2000. How proteins adapt to a membrane-water interface. *Trends Biochem Sci* 25:429-434.
91. Sulistijo, E. S., T. M. Jaszewski, and K. R. MacKenzie. 2003. Sequence-specific dimerization of the transmembrane domain of the "BH3-only" protein BNIP3 in membranes and detergent. *J Biol Chem* 278:51950-51956.
92. Zhou, F. X., M. J. Cocco, W. P. Russ, A. T. Brunger, and D. M. Engelman. 2000. Interhelical hydrogen bonding drives strong interactions in membrane proteins. *Nat Struct Biol* 7:154-160.
93. Gomis-Ruth, F. X., and M. Coll. 2001. Structure of TrwB, a gatekeeper in bacterial conjugation. *Int J Biochem Cell Biol* 33:839-843.
94. Gomis-Ruth, F. X., G. Moncalian, R. Perez-Luque, A. Gonzalez, E. Cabezon, F. de la Cruz, and M. Coll. 2001. The bacterial conjugation protein TrwB resembles ring helicases and F1-ATPase. *Nature* 409:637-641.
95. Gomis-Ruth, F. X., F. de la Cruz, and M. Coll. 2002. Structure and role of coupling proteins in conjugal DNA transfer. *Res Microbiol* 153:199-204.
96. de Paz, H. D., D. Larrea, S. Zunzunegui, C. Dehio, F. de la Cruz, and M. Llosa. Functional dissection of the conjugative coupling protein TrwB. *J Bacteriol* 192:2655-2669.
97. Lai, E. M., O. Chesnokova, L. M. Banta, and C. I. Kado. 2000. Genetic and environmental factors affecting T-pilin export and T-pilus biogenesis in relation to flagellation of *Agrobacterium tumefaciens*. *J Bacteriol* 182:3705-3716.
98. Senes, A., M. Gerstein, and D. M. Engelman. 2000. Statistical analysis of amino acid patterns in transmembrane helices: the GxxxG motif occurs frequently and in association with beta-branched residues at neighboring positions. *J Mol Biol* 296:921-936.

99. Lemmon, M. A., J. M. Flanagan, H. R. Treutlein, J. Zhang, and D. M. Engelman. 1992. Sequence specificity in the dimerization of transmembrane alpha-helices. *Biochemistry* 31:12719-12725.
100. Mason, J. M., and K. M. Arndt. 2004. Coiled coil domains: stability, specificity, and biological implications. *ChemBiochem* 5:170-176.
101. Wang, Y., R. Gao, and D. G. Lynn. 2002. Ratcheting up vir gene expression in *Agrobacterium tumefaciens*: coiled coils in histidine kinase signal transduction. *ChemBiochem* 3:311-317.
102. van Dam, H., and M. Castellazzi. 2001. Distinct roles of Jun : Fos and Jun : ATF dimers in oncogenesis. *Oncogene* 20:2453-2464.
103. Miller, M. 2009. The importance of being flexible: the case of basic region leucine zipper transcriptional regulators. *Curr Protein Pept Sci* 10:244-269.
104. Schneider, D., and D. M. Engelman. 2003. GALLEX, a measurement of heterologous association of transmembrane helices in a biological membrane. *J Biol Chem* 278:3105-3111.
105. Kerr, J. E., and P. J. Christie. Evidence for VirB4-mediated dislocation of membrane-integrated VirB2 pilin during biogenesis of the *Agrobacterium* VirB/VirD4 type IV secretion system. *J Bacteriol* 192:4923-4934.
106. Jones, A. L., K. Shirasu, and C. I. Kado. 1994. The product of the virB4 gene of *Agrobacterium tumefaciens* promotes accumulation of VirB3 protein. *J Bacteriol* 176:5255-5261.
107. Yuan, Q., A. Carle, C. Gao, D. Sivanesan, K. A. Aly, C. Hoppner, L. Krall, N. Domke, and C. Baron. 2005. Identification of the VirB4-VirB8-VirB5-VirB2 pilus assembly sequence of type IV secretion systems. *J Biol Chem* 280:26349-26359.

## **Vita**

Isaac Garza was born in Houston, Texas on June 1, 1984, the son of Irma Villa Tristan, and Tiberio Garza. Isaac grew up in San Antonio, Texas and advanced through the Harlandale Independent public school system. Next he studied at Texas A&M University in College Station, Texas and received a Bachelor of Science in his major Biochemistry as well as received a minor in Business. After his undergraduate studies, Isaac entered the Graduate School of Biomedical Sciences (GSBS) at the University of Texas Health Science Center in Houston. Here he joined the Microbiology and Molecular Genetics (MMG) department and devoted much attention to studying bacterial secretion systems in the laboratory of Dr. Peter J. Christie.

Permanent address: 634 Mebane, San Antonio, Texas 78223